THE UNIVERSITY
of EDINBURGH

Design and simulation of pressure swing adsorption cycles for CO_2 capture

Gabriel D. Oreggioni

For the degree of Dr. of Philosophy. School of Engineering. The University of Edinburgh.

2014

Declaration

I, Gabriel David Oreggioni, declare that this thesis titled, “Design and Simulation of pressure swing adsorption cycles for CO_2 capture” and the work presented in it are my own. I confirm that :

- The thesis has been composed by me.
- The work is my own.
- This work has not been submitted for any other degree or professional qualification except as specified.
- This work was done wholly or mainly while in candidature for a research degree at this University.
- Where I have consulted the published work of others, this is always clearly attributed.
- Where I have quoted from the work of others, the source is always given.

Signed :

Dated: 13/10/2015

Lay summary

The decarbonisation of the energy industries play a key role in the abatement of climate change. Latest studies carried out by the Intergovernmental Panel on Climate Change reported that carbon capture processes were the most economically viable technology to reduce the CO_2 emissions of this sector.

Post combustion amines based configuration is the most mature carbon capture processes however its high energy consumption has motivated to carry out research to explore the feasibility of other gas separation technologies in the role of CO_2 capture units. Pressure swing adsorption (PSA) cycles exhibited promising results when applied at lab scale allowing the same separation targets (CO_2 recovery= 90% and CO_2 purity= 95%) but with lower energy consumption than conventional absorptive processes thus promoting studies to upscale the adsorptive units and analyse the influence of power plant restrictions in the performance of integrated PSA cycles.

The design of PSA cycles requires robust simulation tools that enable modelling the adsorptive gas separation processes by employing few experimentally determined input parameters as well as allowing a quick convergence to cycle steady. In this thesis, this objective was accomplished by developing a generic PSA cycle solver able to simulate multi transition systems that can be used for pre-selecting high separation efficiency configurations to be further studied and optimised employing full governing equation routines.

As part of this thesis, a technical feasibility analysis of the incorporation of adsorptive units in a 10 MW input biomass gasification CHP was also undertaken. A two stage Skarmstrom cycle adsorptive unit was designed and optimised in order to be applied in the role of pre-combustion technology in the afore mentioned energy plant. It was proved based on the results of accurate and detailed process simulations that integrated PSA cycles had a better performance than MEA post combustion configurations in term of the energy penalty associated with the capture process and associated unit operations. It could be then concluded that for the range of capacity under study, adsorptive carbon capture units could be a more competitive technology than post combustion solvent based processes . Results presented in this thesis are expected to encourage the deployment of this technology as a tool for the low carbonisation of the energy industries

Abstract

Carbon capture and storage technologies (CCS) are expected to play a key role in the future energy matrix. Different gas separation processes are under investigation with the purpose of becoming a more economical alternative than solvent based post combustion configurations. Previous works have proved that pressure swing adsorption (PSA) cycles manage to reach similar carbon capture targets than conventional amine process but with approx. a 50% lower specific energy consumption when they are applied at lab scale. These encouraging results suggest that research must be undertaken to study the feasibility of this technology at a low to medium power plant scale.

The simulation of PSA cycles is a computationally challenging and time consuming task that requires as well a large set of experimentally measured data as input parameters. The assumption of Equilibrium Theory reduces the amount of empirically determined input variables that are necessary for modelling adsorption dynamics as well as enabling a simpler code implementation for the simulators. As part of this work, an Equilibrium Theory PSA cycle solver (Esim) was developed, the novel tool enables the quantification of the thermodynamic limit for a given PSA cycle allowing as well a pre-selection of promising operating conditions and configurations (high separation efficiency) for further investigation by using full governing equation based software The tool presented in this thesis is able to simulate multi-transition adsorption systems that obey any kind of equilibrium isotherm function without modifying its main code.

The second part of this work is devoted to the design, simulation and optimisation of two stage two bed Skarmstrom PSA cycles to be applied as a pre-combustion process in a biomass gasification CHP plant. Simulations were carried out employing an in house software (CySim) in which full governing equations have been implemented. An accurate analysis of the operating conditions and cycle configurations was undertaken in order to improve the performance of the carbon capture unit. It was estimated that the energy penalty associated with the incorporation of the adsorptive pre combustion process was lower for a conventional post combustion solvent unit, leading as well to lower specific energy consumption per unit of captured CO_2 and higher overall efficiencies for the CHP plant with installed pre-combustion PSA cycles.

This work is pioneer in its kind as far as modelling, simulation, optimisation and integration of PSA units in energy industries is concerned and its results are expected to contribute to the deployment of this technology in the future energy matrix.

Acknowledgments

Sometimes when I am asked about my PhD experience or if I advise to do a PhD degree, my answer is that it is a challenging experience not just at academic but mainly at personal level but at the end as every challenge we must face in our life it is useful and makes us wiser people. Going through this not easy road would not have been possible without the help and support of a lot of people. In this occasion, I would like to express my gratitude towards my family specially to my mum and my grandparents whom I owe all I am and that have always encouraged me to pursue my dreams understanding my moods and trying to make me feel better in those days in which I felt I could not cope with the difficulties.

I would also like to thank Dr. Daniel Friedrich for his help in the development of the Equilibrium Theory simulator. His constant support and interest in my research was very motivating and it was good to know that he was always there to guide me when the code did not work.

Having shared office with Mauro, Davide, Zoe, Francisco, Enzo and Zhiling has been a pleasure. We were not just work colleagues but friends or in some cases as close as siblings. Their patience and tolerance towards my constant complains when my code did not produce the expected results is admirable as admirable as their behavior in some difficult moments, I am really grateful to them. I would also like to mention other friends whose presence has also been very important: Neil Dorans, Greet Maenhout, Maria Sanchez del Rio, Leigh Murray, Sue Simpson and I hope I am not forgetting anyone.

Finally but not least important, I would like to acknowledge my supervisors that had to deal with me during these years, understanding my complicated way of solving easy problems and my not very practical and engineering mind. I would like to express my gratitude towards Dr. Ahn for tolerating my non easy personality and always being relatively calm trying to make me understand what was wrong in what I was doing. I would also like to thank Professor Brandani, his broad knowledge in the field of Chemical Engineering was always a reassurance in those moments in which maybe results seemed to be strange or had no sense. His critics towards my work were always useful and encouraging for further improvements.

Contents

Chapter 1: The role of carbon capture and storage (CCS) technologies in the low-carbonisation of the global energy matrix

Introduction

The evidence of climate change associated with the greenhouse effect has prompted the international community to take actions in order to reduce the carbon footprint of the economy. Technological options that both satisfy the future energy demand and keep atmospheric greenhouse gas concentrations at a sustainable level are currently being researched. Such options include more efficient conventional fossil fuelled energy plants, the incorporation of carbon capture and storage (CCS) processes and the use of renewable sources. These technologies can sometimes be combined, as in the case of a biomass-fuelled plant integrated with CCS, which leads to carbon negative emission energy generation. In this chapter, the influence of the energy industries on global CO_2 emissions as well as the potential of CCS as a way to reach their low-carbonisation will be discussed. Those technologies that are part of the CCS portfolio and exhibit higher level of maturity will be presented, highlighting the role of post-combustion absorption and pre-combustion adsorption processes that will be further analysed in a case study in Chapter 6.

1.1 Greenhouse effect, climate change and CO_2 anthropogenic emissions

The natural greenhouse effect consists of the heating of the lowest layers of the atmosphere due to the presence of gases that transmit the Sun's visible light, absorb and re-emit the Earth's infrared thermal radiation (Jacob, 1999). These "greenhouse gases" are: CO_2, CH_4, N_2O, ozone (O_3) and water vapour (Jacob, 1999). Without the natural greenhouse effect, the temperature on Earth would be approximately 255K and the life would not be possible (Jacob, 1999). The variation in atmospheric greenhouse gas and aerosol concentrations influences the balance of the absorption and reflection of the Sun's energy arriving at the Earth. The exponential growth of the anthropogenic greenhouse gas emissions since 1750 has led to

an increase of the global temperature. If this trend persists through the next decades, global warming effects would intensify to the extent of causing catastrophic consequences in the global climate (IPCC, 2005).

The International Panel on Climate Change (IPCC, 2005) and Mastandrea and Sneider (Mastandrea and Sneider, 2005) estimated that a global temperature increase of 2°C would be dangerous and could cause rising sea levels, detrimental changes to ecosystems and biodiversity losses. The European Union adopted 2°C above the pre-industrial global temperature as a goal to be achieved by decreasing anthropogenic CO_2 emissions (European Council, 2005). Other authors have considered lower temperature increases in their CO_2 atmospheric concentration scenarios (1.7°C in the case of Hansen et al., 2007 and 1.5°C, Azar et al., 2013) since also a global temperature rise up of this magnitude would lead to damages in the ecosystems. These limits can be reached if the CO_2 concentration in atmosphere is in the range of 350 to 450 ppm (Azar et al., 2013 and Hansen et al., 2007). Decreasing the CO_2 emissions originating from the energy sector would help meet this target; different technological alternatives are thus being considered to accomplish this objective.

1.2 Global CO_2 emissions from fossil fuel use by sector

Electricity generation is one of the sectors that contributes most to GHG emissions (**Figure 1.1**). In fact, it has, on average, accounted for 36% of global CO_2 emissions in the last three decades (Janssens-Maenhout et al., 2012). Despite a transition from coal to natural gas that has taken place in this sector, an exponential growth in CO_2 emissions is still observed due to increased thermal fossil electricity generation (**Figure 1.2)** in both developed and developing economies (Janssens-Maenhout et al., 2012).

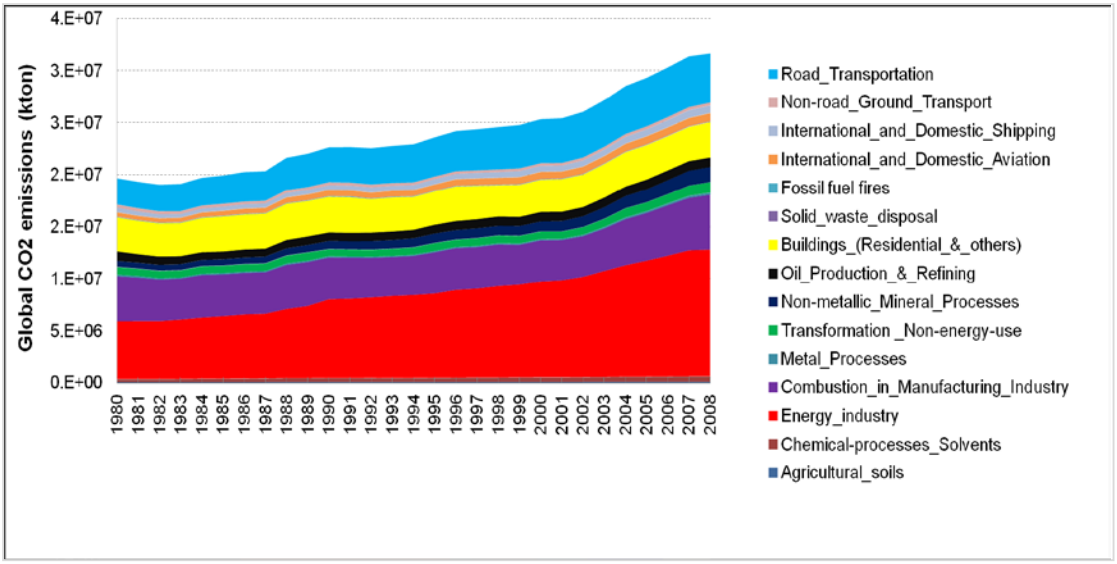

Figure 1.1: Global CO2 emissions by sector for the period 1980-2005 (EDGAR database)

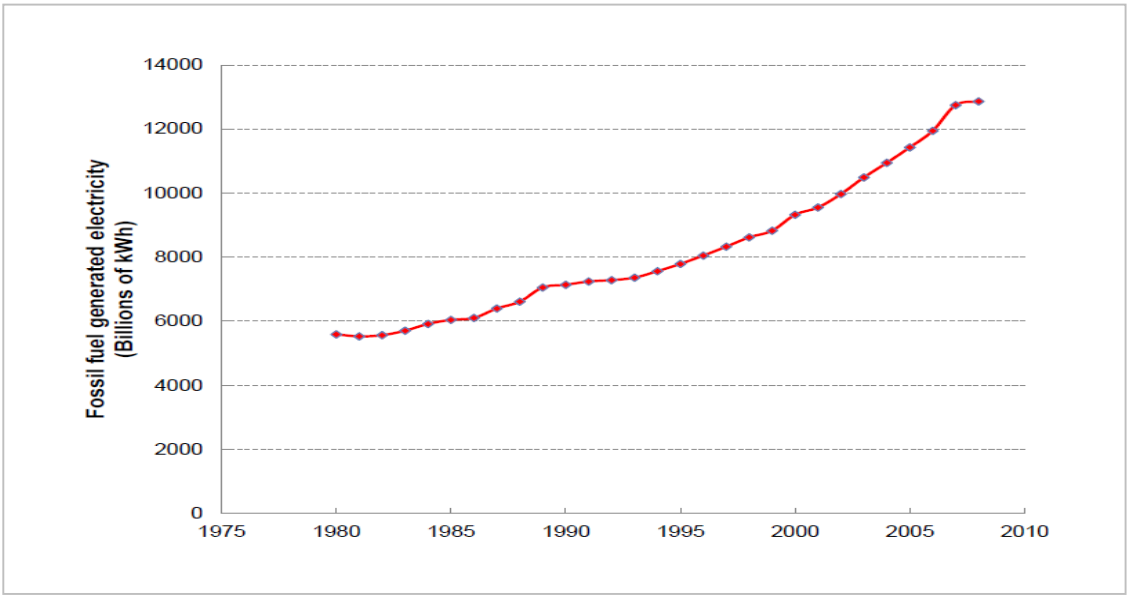

Figure 1.2: Global fossil fuel-generated electricity 1980-2008 (EIA, 2010)

Electricity demand is expected to rise up to 45 PWh in 2050 (IEA, 2010). Less carbon-intense technologies must thus be introduced in order to generate the required electricity without affecting the CO_2 levels in atmosphere. Prospective energy technology studies carried out by the International Energy Agency (IEA, 2010) claim that if no CO_2 emissions reduction strategies were implemented, total CO_2 emissions would reach 67 Gt (business as usual scenario). The IEA has also presented a cost effective portfolio (BLUE Map scenario) that

would decrease CO_2 emissions to half of 2005 levels by 2050. In this technology mix, CCS processes are expected to play a key role since they are forecasted to contribute to 20% of the emission reduction (**Figure 1.3).** Research, development and improvements are currently being undertaken in the field of designing carbon capture processes with the intention of reducing the energy penalty associated with their introduction in energy plants **(**Markewitz et al., 2012 and Webley, 2014)

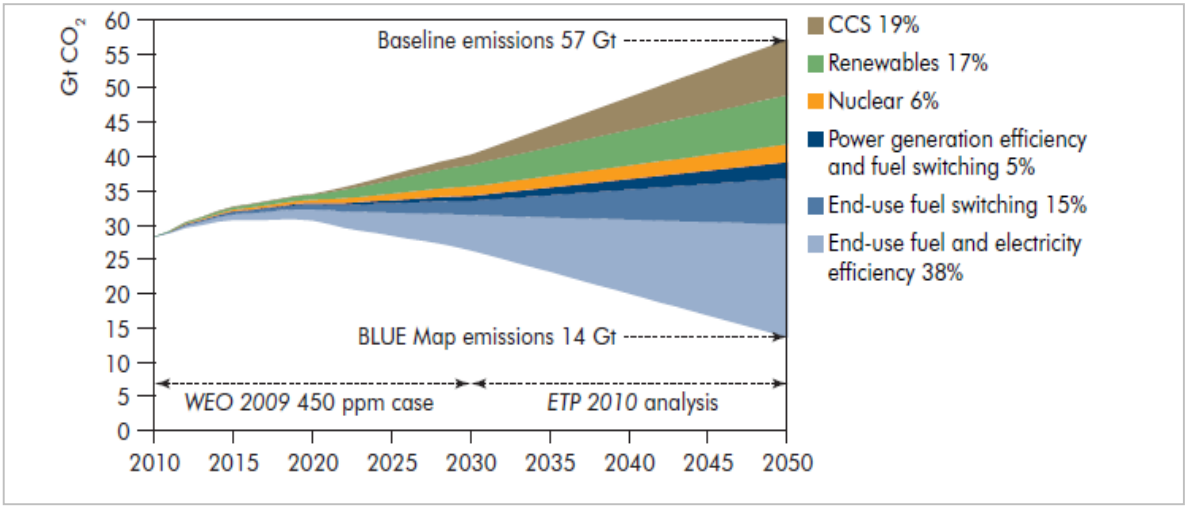

Figure 1.3: Contribution of different technologies to reduce the carbon intensity of the energy matrix (IEA, 2010)

1.3 Carbon capture technologies

Carbon capture technologies can be defined as processes or unit operations that separate CO_2 from gas mixtures to produce a CO_2-rich stream to be subsequently stored or utilised (IPCC,2005). The CO_2 separation or enrichment unit may be incorporated downstream (post-combustion) or upstream (pre-combustion) of the combustor device (IPCC, 2005) A CO_2-rich stream can also be produced when the combustion occurs in the absence of N_2, such as in the cases of cryogenic oxy-fuel process, chemical looping, Graz cycles for gas turbines, advanced zero emissions power plants (AZEP) and solid oxide fuel cells. For post- and pre-combustion configurations, the CO_2 recovery may be driven by a chemical reaction (e.g., solvent based configurations, calcium looping and enzymes) or by a physical processes (e.g., adsorption or membrane processes). Advanced configurations may involve the combination of both

mechanisms (e.g., enhanced and membrane water gas shift reactions) **Figure 1.4** illustrates the three main three types of CCS processes.

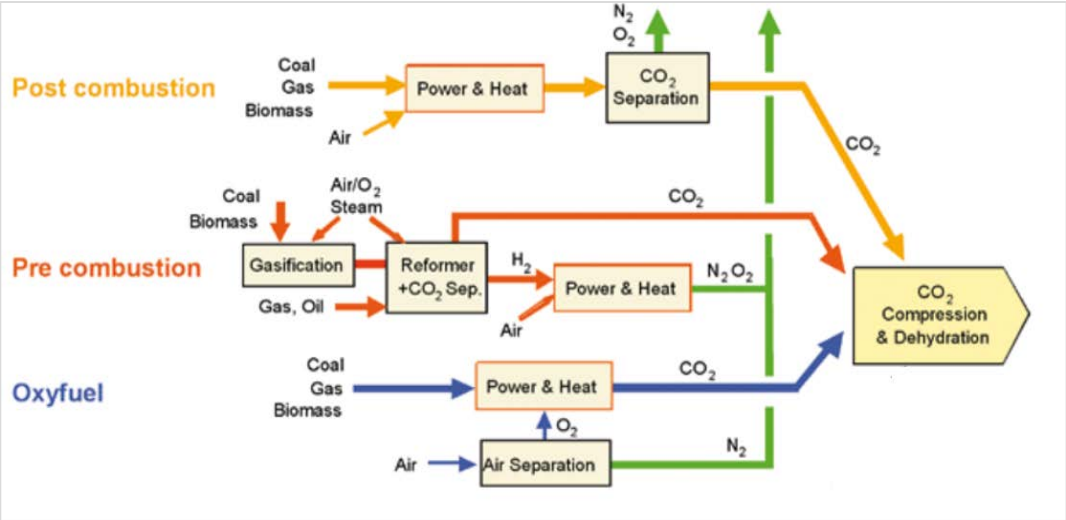

Figure 1.4: Classification and generic schematics for carbon capture processes (IPCC, 2005)

It can be found in literature (Folger, 2010, Florin and Fennel, 2010, Kuramochi and Ramirez, 2011, NETL, 2012) that the maturity of the different CCS technologies can be scored by employing TRL (technological readiness level) indices. Higher values for this index mean that the process configuration is closer to large scale implementation. In this thesis, it was decided to describe those technologies that present the highest values for this index according to the previously cited studies. The different sources agree on the fact that post combustion MEA is the most mature CCS process. Lower but still high TRL values are reported for carbonate looping and membrane configurations when applied in the role of post combustion carbon capture units. Physical absorption (using Selexol or Rectisol), cryogenic oxy-fuel and chemical looping configurations exhibit the largest TRL values when applied as pre-combustion and oxy-fuel processes respectively.

1.3.1. Post-combustion technologies

1.3.1.1. Chemical absorption

Gas separation using chemical absorption is the most widely employed carbon capture technology. Special amine-based processes have been largely employed in industries for this purpose. Several configurations may be found in literature like the one patented by Kerr McGee/ABB Lummus Crest (Barchas and Davis, 1992), the Fluor Daniel® ECONAMINE™ (Sander and Mariz, 1992, Chapel et al., 1999) and the Kansai Electric Power Co., Mitsubishi Heavy Industries, Ltd., KEPCO/MHI (Mimura et al., 1999) processes. In the case of the Kerr McGee/ABB Lummus Crest configuration, CO_2 is recovered from a coal-fired boiler power plant by employing a 15-20% by weight aqueous MEA solution and is subsequently used to produce soda ash and liquid CO_2. The second referred process is a MEA-based reaction (30% by weight aqueous solution) with an inhibitor to avoid carbon steel corrosion and specifically tailored for oxygen-containing gas stream. The carbon capture unit recovers CO_2 for beverage and urea production. The third mentioned patent describes a sterically hindered amines (KS-1, KS-2 and KS-3) process that has the advantage of reducing amine losses reporting as well lower solvent degradation without the need of employing inhibitors or additives.

When amine-based configurations are applied to power plants for carbon capture, the flue gas requires further upstream cleaning than in conventional energy plants (**Figure 1.5)** since SO_x, NO_x, and PM may affect adversely the performance of the separation unit. SO_x and NO_x react with the amine, leading to the formation of heat stable salts in the absorption column (Rao and Rubin, 2002). This reaction results in the increased loss of amine solvents during operation thus increases solvent consumption required to meet the same carbon capture targets (Rao and Rubin, 2002). Even inexpensive solvents like MEA, with a price around 1.8 USD/kg (ICIS, 2014) requires SO_x and NOx concentration levels lower than 10 ppm and 20 ppm respectively to make up costs at reasonable values (IPCC, 2005, Rao and Rubin, 2002) which often means that additional NOx (DeNOx) and SOx (DeSOx) removal processes are needed.

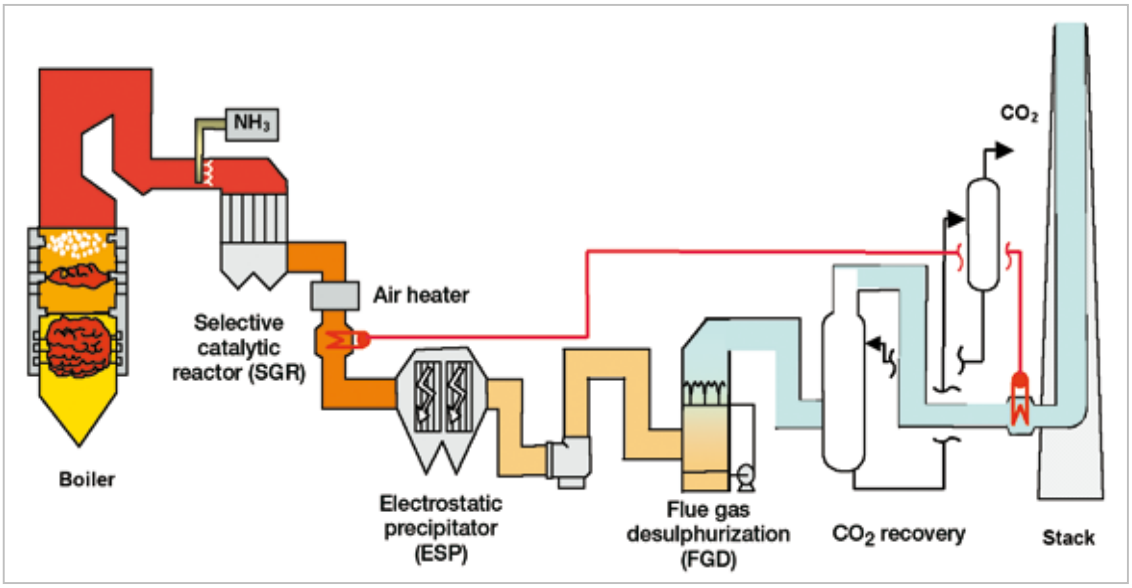

Figure 1.5: Carbon capture and pre-treatment unit operations for a coal-fired power plant (IPCC, 2005)

The cleaned effluent, containing mainly CO_2, N_2 and O_2, is then compressed using a blower in order to overcome the pressure drop through the absorber and cooled to 40-60°C (Ahn et al. 2013). The solvent used is a 30% weight MEA in water (IPCC, 2005, Sander and Mariz, 1992, Chapel et al., 1999 and Ahn et al., 2013). The CO_2-rich amine that leaves the absorber is pressurised to 3 bar and heated to 100-120°C. A temperature exceeding 120°C would result in the thermal degradation of the amines. In the stripper, higher temperatures favour the reverse reaction; CO_2 is desorbed due to contact with the steam coming from the reboiler and in the condenser a mixture of CO_2 and steam can be obtained that then it is cooled down in order to obtain a stream of high purity CO_2 (>95% molar; IPCC, 2005) to be stored. The main energy consumption of the process takes place in the reboiler of the stripper and it is approximately 150 kJ_t/mol of captured CO_2 at a recovery rate close to 90% (Ahn et al. 2013 and IPCC, 2005). A flow sheet of the amine process is shown in **Figure 1.6.**

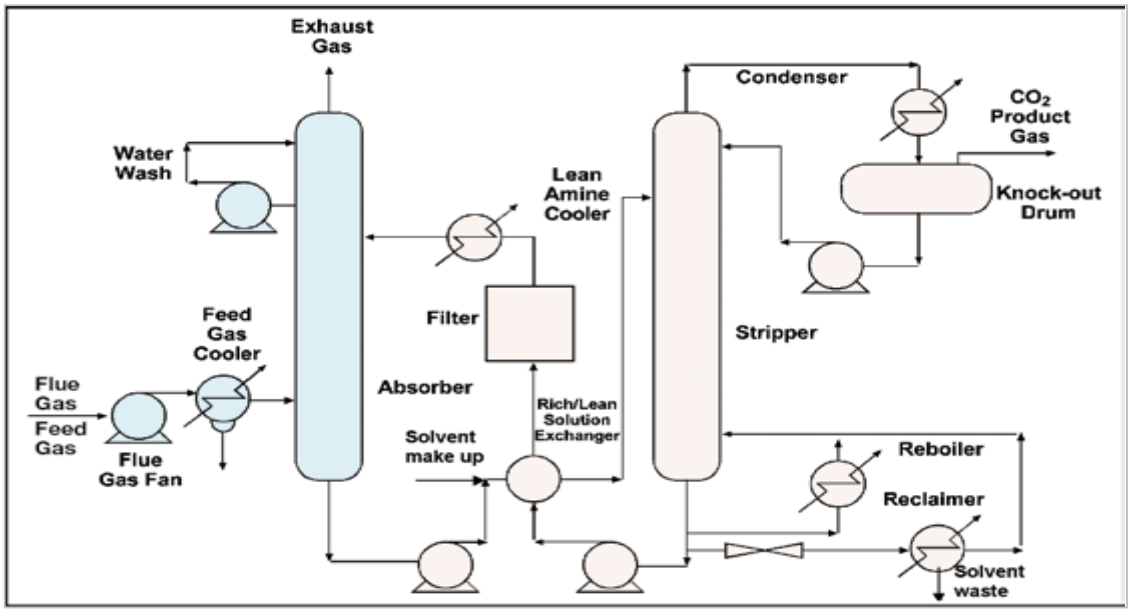

Figure 1.6: Schematics for the conventional amine process (IPCC, 2005)

Absorptive MEA post-combustion carbon capture processes offer the advantage of being a proven technology that can be incorporated into the plant with fewer modifications in comparison with other CCS technologies. MEA has high CO_2 reactivity and capacity, thereby allowing the processing of low partial pressure CO_2 flue gases; it also exhibits reasonable thermal stability and low degradation rates being as well a relatively cheap solvent (IEA Clean Coal, 2007). Disadvantages of a MEA capture process include extensive flue gas cleaning upstream of the carbon capture unit ,use of a corrosive solvent, possible issues and concerns regarding solvent toxicity and mainly a very high energy consumption for solvent regeneration.

Research is currently being undertaken in the development of novel solvents. This research aims to find a solvent that has superior performance to MEA when applied as separation agent in carbon capture unit. Solvents with lower heat regeneration requirements are of particular interest (Sanchez Fernandez et al., 2014). Blended primary, secondary and tertiary amines with additives are being studied at lab or pilot scale (Artanto et al., 2014) and in process simulations. Preliminary results show reductions in regeneration energy demand that reaches values close to 2.9 MJ/kg of CO_2 (127 kJ_{th}/mol CO_2) (Manzolini et al., 2014). However, given the fact that these solvents are costly and are still in the development phase, they have not yet been scaled up to the industrial scale. Different novel process configurations using MEA have also been analysed with the intention of reducing the reboiler duty in the stripper such as

intercooling absorption or multi-pressure stripping. These novel amine process configurations exhibit reboiler duty in the range of 110-130 kJ_t/mol of captured CO_2 (Ahn et al., 2013).

Other gas separation technologies are currently being investigated and optimised with the purpose of becoming a more economical alternative for post-combustion capture than MEA-based configurations. CO_2 capture employing membranes and calcium looping processes will be further explained in the next sub sections while a detailed description of pressure swing adsorption (PSA) cycles in the role of CCS technology will be presented in section 1.3.4.

1.3.1.3. Membranes

In the field of membrane science, a synthetic membrane behaves as a thin barrier between two phases through which differential transport can occur. Driving forces that facilitate this transport are pressure, concentration, and electrical potential across the medium (Koros et al., 1996). The transport itself is a non-equilibrium process and the separation of the species results from differences in transport rates through the membrane. Large-scale membrane gas separation emerged as a commercial process during the 1980s due to the development of synthetic polymeric membranes. These membranes are currently applied in different industrial processes such as oxygen production, natural gas dehydration and sweetening, H_2 refinery gas recovery and NH_3 purge, among others (Abedini and Nezhadmoghadam, 2010).

The first feasibility studies for CO_2 capture by employing membranes were published in the late 80s (Hendricks et al., 1989). Subsequent research has been undertaken to develop new membranes with improved CO_2/N_2 selectivity and CO_2 permeability. However, the treatment of flue gas emitted at substantial flow rates requires a very large membrane area and consequently increases the cost of this capture technology. Another drawback is the need for very large, expensive and energy-consuming compression equipment since the difference in partial pressure is the driving force for the separation. This limits the maximum pressure ratio attainable by feed compression and/or permeate vacuum to about 10. Merkel (Merkel et al., 2010) developed membranes in collaboration with the United States Department of Energy with CO_2 permeances ten times higher than commercial CO_2 membranes and CO_2/N_2

selectivity of 50 at 30°C. These authors considered the increase of membrane permeance an important step for reducing the costs of separation. Merkel et al., 2010 and Bocciardo et al. (2013) have also analysed the possibility of performing gas separation with different stages and flow patterns such as co-current, countercurrent and sweep membrane modules (**Figure 1.7**). The novel process configurations using multi-stage membrane units allowed meeting the carbon capture targets (CO_2 recovery of 90% and CO_2 purity higher than 95%) for the flue gas from a coal-fired power plant with an specific energy consumption in the range of 90 kJ_{th}/mol of captured CO_2.

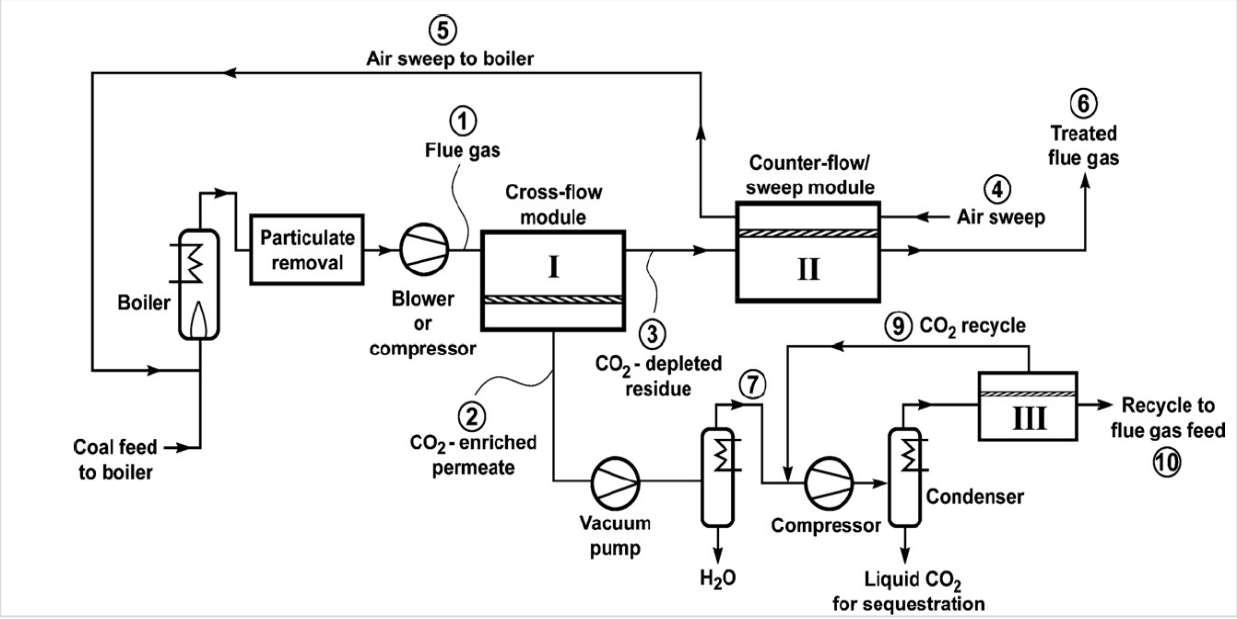

Figure 1.7: Multistage membrane process based configurations (Merkel et al., 2010)

1.3.1.4. Calcium looping

Calcium looping (CaL) is a novel CCS process that employs limestone (inexpensive cement production raw material) as CO_2 sorbent precursor according to the reversible CaO carbonation reaction (IPCC, 2005) (**Figure 1.8**).

$$CaO(s) + CO_2(g) \longrightarrow CaCO3(s)$$

Figure 1.8: Carbonation of CaO

This technology was first proposed as post combustion technology by Shimizu (Schimizu et al.,1999) and vast research has been undertaken in the last decade at lab scale in Spain, Canada, Germany and China. Currently, a 2 MW calcium looping capture unit is being tested in La Parada in Spain (Hurst et al., 2012). **Figure 1.9** displays a simple flow sheet for a CaL CCS process.

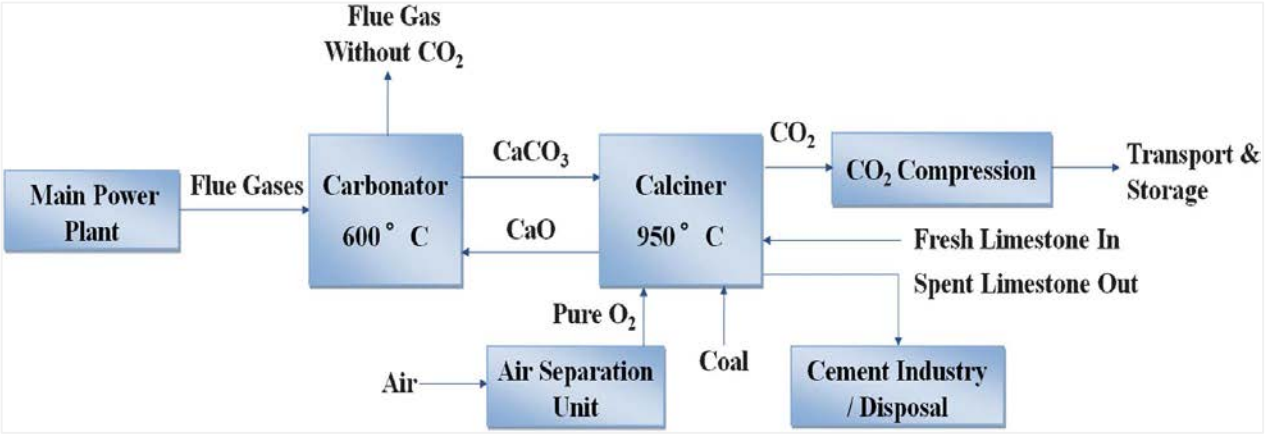

Figure 1.9: CaL post combustion process (Hurst et al., 2012)

In a conventional CaL configuration, twin fluidised bed reactors are connected by solid transportation lines.$CaCO_3$ is heated in the calciner, driving off CO_2 to produce CaO that it is recirculated to the carbonator. In the carbonator, the recirculated CaO reacts with the CO_2 from the flue gas, producing $CaCO_3$ and a CO_2-free flue gas stream. In order to achieve the calciner operating temperature of approximately 950°C (Hurst et al., 2012), extra fuel in the form of coal must be burned in an O_2-rich atmosphere. The CO_2 from the calciner is compressed and sent to storage. The O_2-rich stream is produced in an air separation unit; the electricity required for this process and for CO_2 compression is generated by the steam that can be produced employing part of the heat associated to the exothermic carbonation reaction. As it was previously underlined, additional heat input is required for the calciner; a conventional, non-optimised configuration requires a 50% increase in fuel input (Schimizu et al.,1999). However,

there are studies indicating that heat integration in the system between the hot CO_2 stream and the carbonated solids flowing in the calciner may reduce the extra fuel input by up to 10% (Abanades et al., 2005 and Martinez et al., 2012) indicating that further integration of the heat nets in the plant is of great relevance for the deployment of the technology.

1.3.2. Pre-combustion processes (gasification plants with CCS)

Pre-combustion technologies aim to lower the carbon intensity of the fuel fed to the combustion device. This objective is reached due to the incorporation of a carbon capture unit downstream the plant gasifier. In a gasification process, a solid primary feedstock such as biomass or coal is converted into a H_2-rich gaseous fuel (syngas). The gasification reaction is a partial oxidation of carbonaceous solids; fixed bed, fluidized bed or entrained flow gasifiers can be employed. Design parameters for the gasifier include reactor type, oxidant species (steam, air or O_2), operating temperature (up to 1350°C), pressure (0.1-7 MPa), feed system, and syngas cooling method. These design parameters dictate the syngas compositions and low heating value as well as the capital and operating cost of the plant. The gasifier output contains CO, H_2, CO_2, H_2O and impurities such as N_2, COS, H_2S, HCN, NH_3 and volatile trace (IPCC, 2005).

Downstream of the gasifier, water-gas shift reactors (WGSR) increase CO_2 partial pressure (higher mole fraction) by converting CO into CO_2 and H_2. The water-gas shift reaction is an exothermic catalytic process; in the presence of iron-chromium catalysts, the reaction takes place between 400-500°C and the final CO molar fraction is around 0.2 to 0.3 %. If copper-based catalysts are used, the reaction temperature can be reduced to between 180-250°C, resulting in CO molar fractions that range between 0.2 to 1% at the reactor outlet (IPCC, 2005).

The presence of sulphur compounds in the CO_2 product is rigorously regulated as H_2S is highly corrosive. An acid gas removal unit for removing H_2S must therefore be considered. The recovered H_2S is sent to a Claus plant in which the reduction of H_2S to elemental sulphur takes place. Then nearly free H_2S stream is then processed in the capture unit. A schematic diagram of an integrated gasification combined cycle (IGCC) power plant with CO_2 capture is shown in **Figure 1.10.**

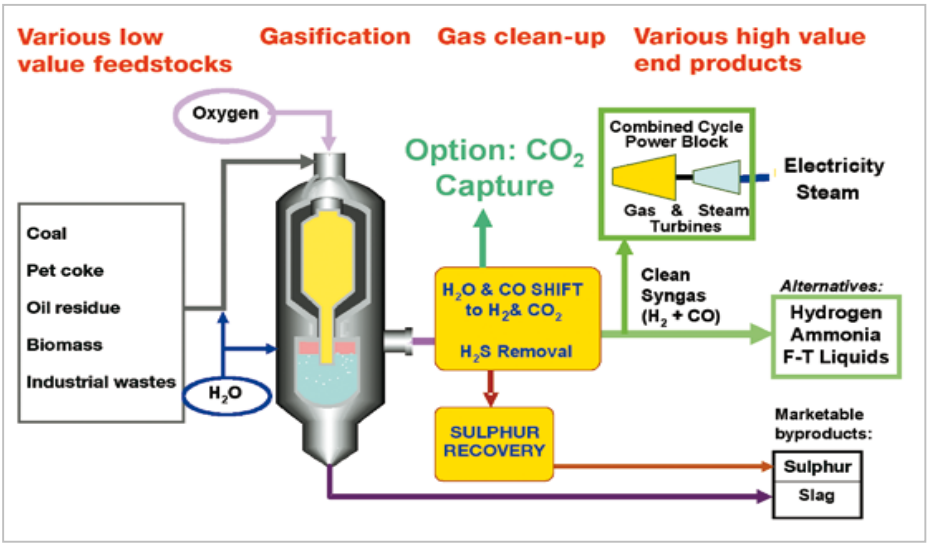

Figure 1.10: A schematic diagram of an IGCC power plant with CCS (IPCC, 2005)

An absorption process using physical solvents (e.g., Selexol) may perform CO_2 capture downstream of the WGSR system, as reported in the DOE report (NETL, 2007). As the gasifier operates at a pressure approaching 40 bar, high CO_2 solubility in physical solvent are observed enabling the separation of the gas mixture. Energy consumption for this technology is mainly associated with the solvent pumping and refrigeration since the absorptive unit requires the Selexol temperature to be approx. 5°C (DeCarbit, 2011). Drawbacks related to the implementation of this technology are based on the fact that it requires being implemented in gasification plants that exhibit higher investment costs than combustion plants (NETL, 2007 a)

PSA cycles and membranes may also be applied as separation technology for pre-combustion carbon capture (IPCC, 2005). Works like the one carried out by Scholes (Scholes et al., 2010) suggest the design of membrane water gas shift reactor in which CO_2 is being captured from the syngas In the case of PSA cycles, they can be employed instead of the absorptive unit (in attempt to avoid the energy consumption for the Selexol pumping and cooling). The use of polybed PSA cycles to purify H_2 has been intensively studied and are currently employed at industrial scale. These polybed systems achieve high H_2 recovery and purities close to 99.99% (Sircar et al., 2001; Ribeiro et al., 2008 and Luberti et al., 2013). In the previously cited studies, the adsorption process has been designed to produce H_2 that is the least adsorbing species of the mixture. In contrast, the adsorption process for carbon capture processes must be designed such that CO_2 is the strongest adsorbing species. The CO_2 capture

PSA cycles must therefore be different from the H_2 production adsorption process. Further details regarding the PSA configurations for carbon capture can be found in section 1.3.4.

1.3.3. Oxyfuel technologies

1.3.3.1. Cryogenic oxyfuel

In oxyfuel combustion processes, fuel is burned using oxygen instead of air in order to reduce the energy penalty associated with the CO_2 recovery from the flue gas (Dillon et al., 2005). In cryogenic oxyfuel configurations, O_2 is obtained in an air separation unit (ASU) upstream the boiler (**Figure 1.11).**

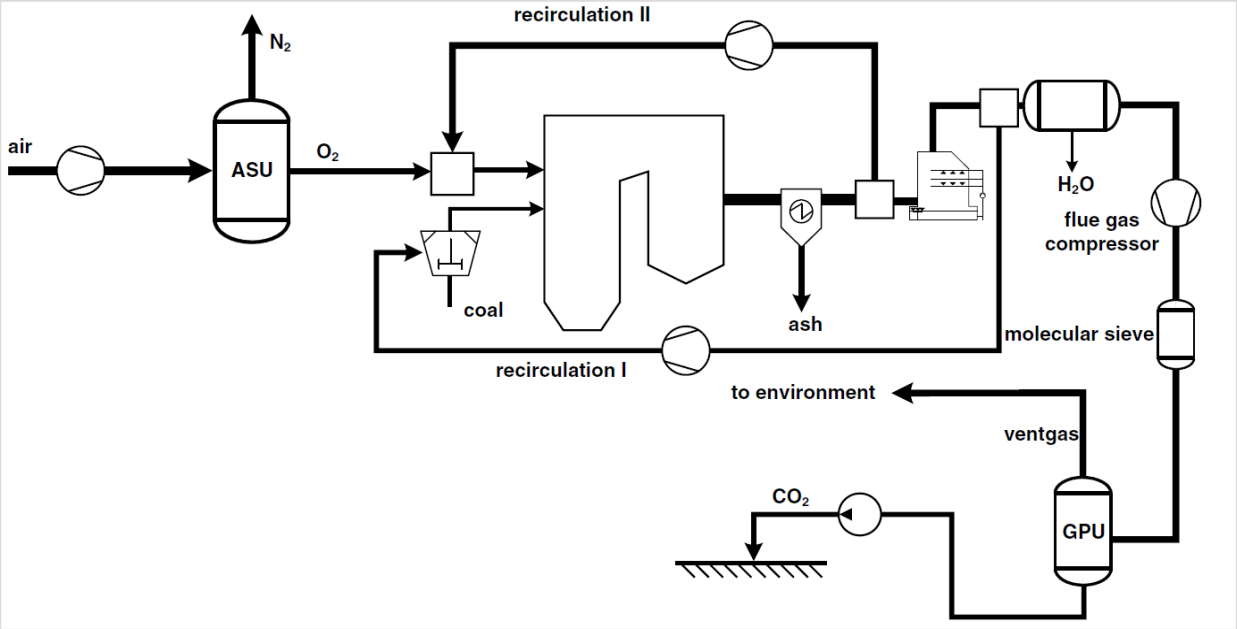

Figure 1.11: Oxyfuel combustion process with GPU (Dickimes and Kather, 2014)

The fuel (coal or natural gas) is burned using O_2 and recycled flue gas. The flue gas recycle is necessary to keep the temperatures inside the boiler within tolerances of used boiler material (IPCC, 2005). The generated flue gas has a CO_2 concentration of about 81vol.-% (dry), if an air ingress into the process of 2% is considered (Dickiness and Kather, 2014). The remaining 19 vol.-% (dry) are impurities consisting of NO_x, SO_x, O_2, N_2 and Ar. Downstream of the boiler, fly ash is reduced in an electrostatic precipitator (ESP) and downstream of the recycle, SOx is reduced in a flue gas desulphurisation (FGD) unit before being dried in the flue gas condenser. The flue gas is then compressed and passes through a molecular sieve

adsorption column aimed to remove possible trace of water . The compressed flue gas is cooled and partially liquefied in the "cold" gas processing unit. The condensing of CO_2 has a carbon capture recovery of about 90% and separates other gases from the liquid stream, which exhibits purity exceeding 96% (White, 2004 and Ritter et al., 2009). Some works, such as Dickness and Kather (Dickness and Kather, 2014), suggest the use of polymeric membranes to recover CO_2 from the vented gases.

The main advantages of this technology are associated with the fact that it can readily be applied to new coal power plants and that the key process principles, including air separation and flue gas recycle, have been proven (NETL, 2007 b). The modifications related to the oxyfuel process configuration also reduce NO_x emissions as N_2 is not present in the combustor, thereby avoiding extra flue gas cleaning required to meet the regulations for NOx emissions (NETL, 2007b and Dillon et al., 2005). The main drawbacks of the cryogenic oxyfuel combustion process are based on the high capital and operating cost. The latter is associated with the electricity consumption for the air separation unit and the parasitic load associated with the flue gas recirculation to reduce the boiler flame temperature due to the oxy combustion process (NETL, 2007 b). Estimates by the DOE (NETL, 2007 b) have quantified the efficiency of a supercritical plant using cryogenic oxyfuel as a carbon capture technology is reduced by approximately 10 percentage points (original plant=39%, plant with oxyfuel combustion =29%). By comparison, a conventional post-combustion amine process reduces efficiency by 11 percentage points.

1.3.3.2 Chemical looping

The chemical looping (CLC) technology is based on the splitting of the combustion of a hydrocarbon or carbonaceous fuel into separate oxidation and reduction reactions by introducing a suitable metal oxide as an oxygen carrier to circulate between two reactors (Adanez et al., 2012) (**Figure 1.12**). This novel technology can be applied to coal- or natural gas-fired power plants and in the production of syngas (chemical looping reforming)

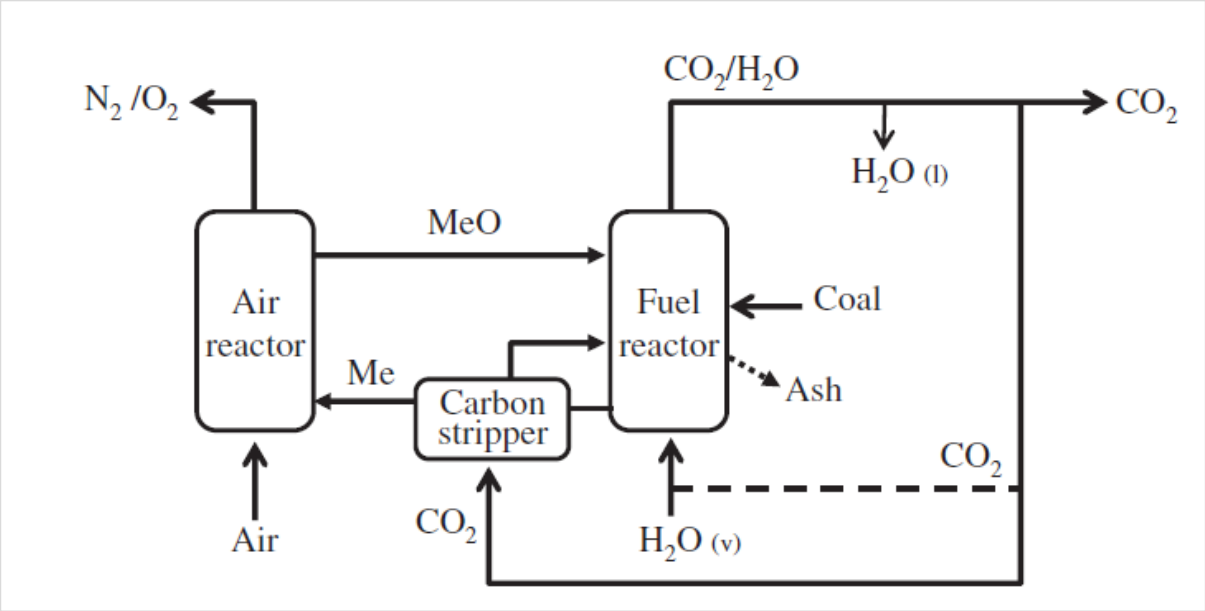

Figure 1.12: Chemical looping combustion process configuration (Adanez et al.,2012)

In the marked contrast to the oxyfuel process technology, there is no need of air separation. The reaction between fuel and oxygen occurs in a second reactor by the release of oxygen from the metal oxide in a reducing atmosphere caused by the presence of a hydrocarbon or carbonaceous fuel. The recycle rate of the solid material between the two reactors and the average solids residence time in each reactor control the heat balance and the temperature levels in each reactor. The fact that the combustion takes place in two reactors compared to conventional combustion in a single stage is that the CO_2 is not diluted with nitrogen gas, but it is almost pure after separating CO_2 from water, without requiring any extra energy demand and costly additional equipment for CO_2 separation (IPCC, 2005).

Pioneer works in this field have been reported by Richter and Knoche (Richter and Knoche, 1983) and Ishida and Jin (Ishida and Jin, 1994).In the last decades, several pilot plants with capacity up to 120 kW have been in operation in Austria and Sweden (Adanez et al., 2012), while in Germany, a 1 MW capacity plant was built at the Technical University of Darmstadt and the novel technology was scaled up in a plant with 2 MW installed capacity in Hunosa, Spain (Fan et al., 2012).

The oxides of some transition state metals such as Fe, Ni, Cu and Mn can be used as oxidising agents (Zafar et al., 2005). Reactor temperatures may be in the range of 800-1200°C (IPCC, 2005); at these temperatures, NO_x formation is low and the fuel conversion in the reduction reactor may not be complete (Cho et al., 2002). In the case of a gas turbine cycle, the oxidation reactor replaces the combustion chamber and the exothermic oxidation reaction provides the heat for increasing the air temperature entering the downstream gas turbine. Another option is to generate steam using heat transfer surfaces in the oxidation reactor. Process simulation studies claim efficiencies in the range of 37-39% for coal fired power plants (IEA Clean Coal, 2010) with CLC combustion and in the range of 45-53% for natural gas combined cycle with CLC (IEA Clean Coal, 2010 and Brandvoll and Bolland (2004)) for a CO_2 recovery rate close to 90%. The technology seems to be very promising, thus promoting further research in upscaling the pilot plants and analysing the loss of reactivity of the solid metal oxides (Adanez et al., 2012).

1.3.4. Adsorption technologies

The separation and purification of gas mixtures using adsorption is largely employed in the chemical, petrochemical, environmental and medical industry (Keller, 1986 and Sircar, 2001). The gas separation is based on the selective retention of one or several of the components of the mixture by the pores and on the surface of the adsorbent. This retention may be a consequence of the chemical similarity between the sorbate and the sorbent or of the size restriction associated with the ratio between the pore diameters and the mean free path of the molecules (Ruthven, 1984). Gas separation processes using adsorption are designed to obtain a high purity of the component of interest in the gas stream and allow the regeneration of the sorbent material.

Industrial applications for adsorption can be divided broadly into two categories: removal of trace or dilute impurities and bulk separation. Two generic cycle concepts known as temperature swing adsorption (TSA) and pressure swing adsorption (PSA) are employed to carry out the essential adsorption and desorption steps in conjunction with a variety of other complimentary steps (Ruthven, 1994). Gas purification primarily uses TSA cycles (with the exception of gas drying) in which adsorption occurs at colder temperatures than the desorption.

PSA based processes use cyclic pressure changes as the driving force for separation and are used for bulk gas separation (Sircar, 2001). Different configurations for these two kind of processes can be designed according to the product specifications (pressure, purity and recovery from feed), the energy of separation, the number of products from the feed gas, the sequence and mode of operation of the steps in the overall cyclic process, the operating conditions, the type of adsorbents as well whether the component of interest is a weak or strongly adsorbing species (Sircar, 2001).

The first commercial use of PSA cycles dates from the late 1960s with the patents by Guerrin de Montgareuil (French patent No 1233261) and Skarstrom (US Patent No 2944627). Today, PSA systems are widely used for the separation of N_2 and O_2 from air. In the zeolite process, O_2 can be obtained in high purity since N_2 is preferentially adsorbed over O_2 in the zeolites (US Patent No 3717974; Sircar, 2002; US Patent 4756723). Another adsorption process for air separation using carbon molecular sieves (CMS) was developed for the production of high purity N_2 from air since CMS adsorb O_2 faster than N_2 as a result of the kinetics of N_2 and O_2 diffusion into adsorbent pores (Ruthven, 1984). PSA cycles can also be used for high purity H_2 production from syngas originating in steam methane reforming, coal gasification processes or coke oven gases in steel industries (Lee et al 1999 and Sircar 2002).

The most basic PSA configuration is the Skarstrom cycle. In most industrial applications, the component to be recovered from the feed is the least adsorbing species. However, in the case of carbon capture processes, CO_2 is the most strongly adsorbed species in the feed (Kikkinides et al. 1993 and Webley, 2014). The configuration and operating conditions of conventional PSA processes designed to recover the least absorbing gas are therefore different from those for carbon capture, where the aim is to remove the strongest sorbate (CO_2) from the feed (Liu et al, 2011 and Reynolds et al., 2005). The conventional Skarstrom cycle consists of a sequence of four steps:

1. Pressurisation
2. Feed/Adsorption
3. Blowdown
4. Low pressure purge

In the case of the Skarstrom PSA cycle for carbon capture, pressurisation is carried out by using the feed stream (Liu et al., 2011; Wang et al., 2013, Shen et al., 2012;

Kikkinides et al, 1993). During the adsorption step, the feed is introduced into the column at a constant flow rate and the column pressure (in the range of 1.1 -1.5 bar) is kept relatively constant by back pressure regulators; nearly CO_2-depleted gas leaves the column and part of this stream is used for purging the other column. A counter-current blowdown step is employed to decrease the pressure in the column, causing the desorption of the less strongly adsorbing species thus increasing the CO_2 mole fraction of the gas in the column so that at the end of the blowdown the gas leaving the column will be quite rich in CO_2. The sorbent is partially regenerated during the purge step that must be carried out at very low pressure (between 0.1 and 0.05 bar in the case of post-combustion PSA units). **Figure 1.13** displays a schematics of a PSA cycle configuration in the role of carbon capture technology.

Three key parameters are used for evaluating the performance of PSA cycles applied for carbon capture: CO_2 recovery (Eq. (1.1)), CO_2 purity (Eq. (1.2)) and specific energy consumption associated with the separation (Eq. (1.3)). The CO_2 recovery is the ratio between the total mass of CO_2 leaving the column during the blowdown and purge steps and the mass of CO_2 that entered the column during the adsorption and pressurisation steps. The CO_2 purity is the average CO_2 molar fraction that leaves the column during the blowdown and purge steps. The energy consumption is calculated by summing the power consumed in the blower and in the vacuum pump.

$$CO_{2_{recovery}} = \frac{\int_0^{t_{blow}} c_{CO_2} v(z=0)dt + \int_0^{t_{purge}} c_{CO_2} v(z=0)dt}{\int_0^{t_{feed+press}} c_{CO_2} v(z=0)dt} \tag{1.1}$$

$$CO_{2_{purity}} = \frac{\int_0^{t_{blow}} c_{CO_2} v(z=0)dt + \int_0^{t_{purge}} c_{CO_2} v(z=0)dt}{\int_0^{t_{blow}} C\, v(z=0)dt + \int_0^{t_{purge}} C\, v(z=0)dt} \tag{1.2}$$

$$PSA\ Specfic\ power = \frac{\int_0^{t_{feed+press}} power_{blower}\, dt + \int_0^{t_{blow+purge}} power_{vacuum} dt}{\int_0^{t_{blow}} c_{CO_2} v(z=0) dt + \int_0^{t_{purge}} c_{CO_2} v(z=0) dt} \quad (1.3)$$

$$power_{blower} = \frac{\frac{\gamma}{\gamma - 1} RT_{feed} \left[\left(\frac{P_{feed}}{P_{atm}}\right)^{\frac{\gamma-1}{\gamma}} - 1 \right] mole\ flow_{\ fed\ to\ the\ column}}{\eta_{Blower}} \quad (1.4)$$

$$power_{vacuum} = \frac{\frac{\gamma}{\gamma - 1} RT_{blow} \left[\left(\frac{P_{atm}}{P_{blow}}\right)^{\frac{\gamma-1}{\gamma}} - 1 \right] mole\ flow_{\ leaving\ the\ column}}{\eta_{Vacuum\ pump}} \quad (1.5)$$

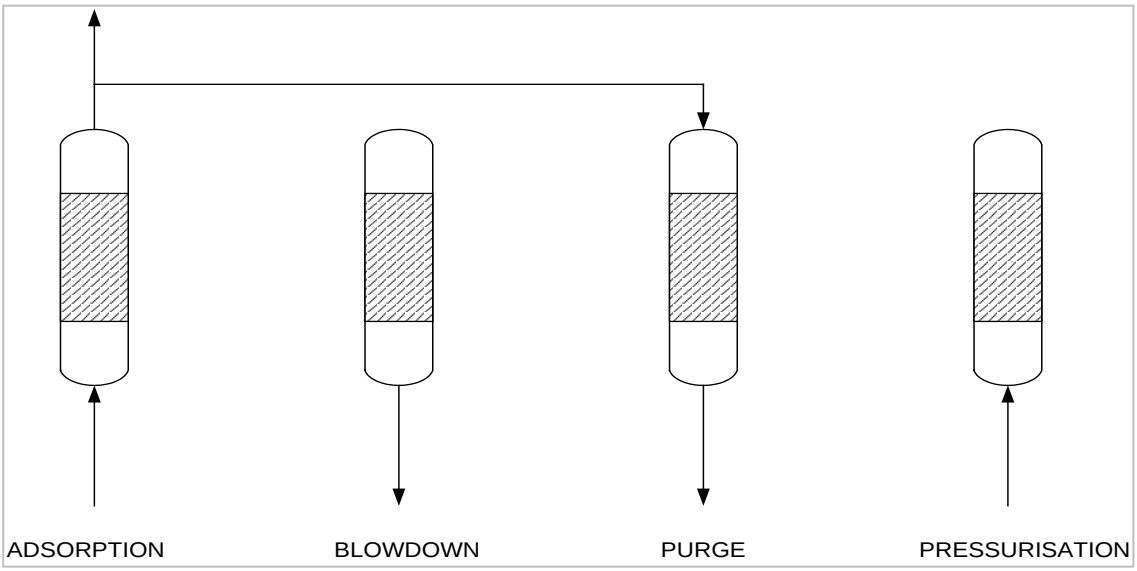

Figure 1.13: Skarstrom cycle applied to CCS

The energy penalty associated with the separation can be reduced by using pressure equalisations (PE) (**Figure 1.14**). In general, pressure equalisation takes place after the adsorption step; part of the effluent leaving the high-pressure column is employed to increase the pressure of the other column that was previously purged (Shen et al., 2012).

Different configurations, including pressure equalisations, can be implemented such as top end-to-top end, top end-to-bottom end and bottom end-to-bottom end. A schematic of a PSA cycle with a top end-to-top end pressure equalisation step is illustrated. The inclusion of top end-to-top end PE in PSA cycles using zeolite 5A in post-combustion CCS applications decreased specific energy consumption by approximately 8%, increased CO_2 purity but reduced CO_2 recovery (Liu et al., 2011). The differences in CO_2 recovery and purity can be explained due to the fact that the gas stream leaving the high-pressure column and used to pressurise the other bed is rich in the least adsorbing species (taking as well a fraction of the CO_2 that has been fed). Thus, once the high-pressure column is depressurised during blowdown, a larger CO_2 mole fraction will be obtained but at a lower CO_2 recovery.

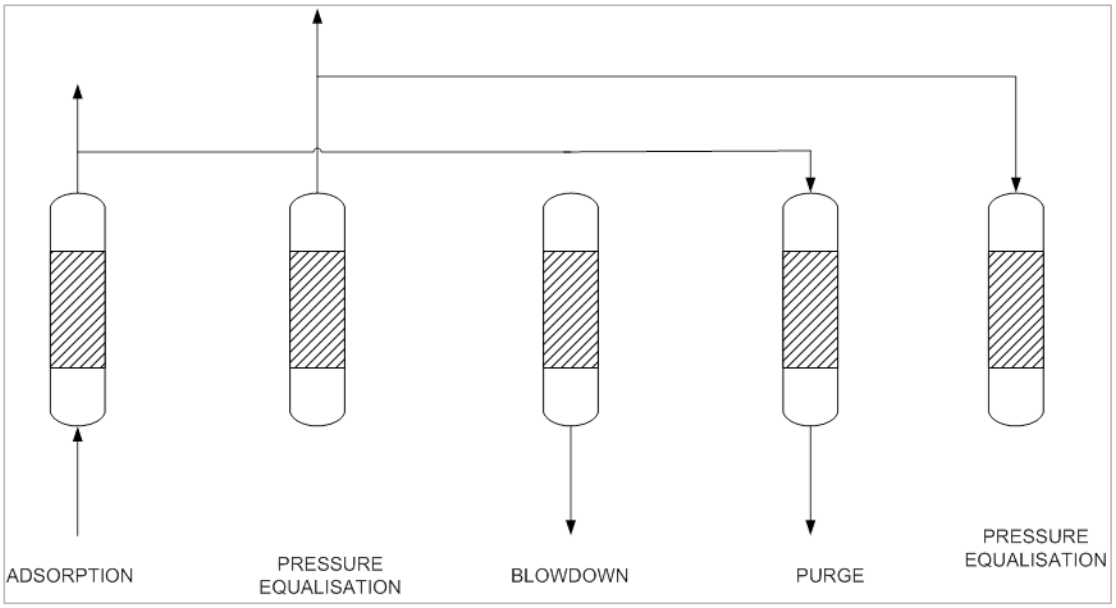

Figure 1.14: Skarstrom cycle with top end-top end pressure equalisation

Several studies have assessed the feasibility and performance of PSA cycles in the role of carbon capture technology (Xiao et al., 2008, Liu et al., 2011 and 2012, Shen et al., 2012 and Wang et al., 2013), these articles present simulations and pilot-scale research that treat streams emulating the flue gas from a coal fired power plant (downstream of the cleaning processes to reduce NO_x, SO_x and PM emissions). The influence of different operating conditions such as purge pressure, purge and feed ratio as well as different time duration for the steps has been studied with the purpose of optimising energy consumption while meeting CO_2 capture targets (90% recovery and 95% purity). Several of the cited works present research that has been undertaken on the design of two stages PSA Skarmstrom cycle carbon capture units. The first stage aims to reach CO_2 recovery in the range of 90% while the second stage fulfils the CO_2 purity target. In the previous referred works, the mechanical specific energy consumption was approximately 30 kJ_e/mol of captured CO_2, which is equivalent to 90 kJ_t/mol of captured CO_2 (using a conversion factor of 0.33 for coal fired power plant). This indicates that the PSA carbon capture process has a 40% lower specific energy consumption than the amine process (Ahn et al., 2013; IPCC, 2005).

It must be noted, however, that the previously mentioned studies are quite optimistic regarding the performance of the PSA unit since they do not address the issue of integrating the batch unit into a continuous plant. Such an integration could involve restrictions to the

cycle configuration and step time duration; the flows that are being processed in these studies are quite small and problems may arise as far as column sizing and cycle configuration when scaling up the system. The purge pressure used in the above mentioned works is quite low and in some cases (when purge pressure is lower than 25 kPa), costly multiple stages should be employed (Webley 2014). A comparison of PSA performance to a conventional post-combustion amine unit should therefore be carried out for the same baseline energy plant. Care should be taken such that the modelled adsorption unit is integrated to the plant by accounting for the identified restrictions related to scaling up and the vacuum generation system. This thesis is intended to explore these aspects as it will be further detailed in the next section.

1.4 Research objectives and thesis structure

The purpose of this work is to analyse the feasibility of PSA cycles as CCS technologies in the energy sector, to quantify the energy penalty associated with the capture process and to compare these values with mature CCS technologies in industry or in medium- to large-scale demonstration plants. In this study, an adsorptive CC unit will be designed to minimise the energy required to reach the carbon capture target (90% of the CO_2 in the feed and 95% CO_2 purity). The CC unit will be integrated into an electricity generation plant and the resulting decrease in overall efficiency will be quantified considering both upstream and downstream processes. Research undertaken in this thesis involves:

- Developing and testing of different PSA cycle solvers.

- Studying how different simplifying assumptions regarding mass and energy transfer mechanisms between the two phases influence on the mathematical formulation of the adsorption dynamics (complexity of the code of the PSA cycle solver versus the accuracy of the adsorption unit performance parameters). These simplifications will be employed to build a simulator that enables a quick scan of operating conditions discarding configurations with poor performance and selecting those ones that appear to be promising for further analysis and optimisation.

- Carrying out a sensitivity analysis accounting for cycle configurations and operating conditions with the purpose of reducing or minimising the energy consumption for the adsorptive carbon capture units by using rigorous simulation tools.

- Modelling the upstream and downstream processes of the carbon capture unit integrated to the power plant.

- Benchmarking the specific energy penalty and the net capture rate of the adsorptive unit against a conventional post-combustion amine plant.

These issues will be analysed in the different chapters of this work. Chapter 2 focuses on the modelling of adsorption dynamics, including a summary of the different mass transfer mechanisms between the phases and their influence oin the formulation of the mass and energy balances. The role of the Equilibrium Theory assumption and the associated simplifications in the development of a cycle solver are highlighted as well as possible advantages of a novel tool of this kind.

The development of an Equilibrium Theory PSA cycle solver (Esim) is the core of Chapters 3 and 4. Chapter 3 is aimed to introduce the Riemann Cauchy problem for the adsorption dynamics; a discussion regarding the application of exact and approximate Riemann solvers for the solution of the adsorption dynamics is also held, underlining advantages and drawbacks of the numerical schemes. Chapter 4 provides a detailed description of Esim numerical implementation. Result validation of the novel software for breakthrough and cycle simulations is also illustrated in this chapter using the example of the first stage of a post-combustion adsorptive unit.

The application of PSA cycles as pre-combustion technology and its comparison to an absorptive post-combustion configuration is discussed in the second part of this thesis. Chapter 5 describes the example energy plant that is selected as a base case (biomass gasification CHP with a gas engine) and how the key unit operations or processes were simulated using Unisim process simulation software.

Details regarding the design and modelling of the two different carbon capture technologies applied to the base case are introduced in Chapter 6. An extensive discussion about the influence of different operating conditions on CO_2 recovery, CO_2 purity and specific electricity consumption associated with a pre-combustion, two-stage Skarstrom two-bed with pressure equalisation PSA cycle is held. The consequent loss of efficiency in the energy plant is quantified using process simulations. The performance of the CHP plant with adsorptive CC unit is compared to a conventional post-combustion amine configuration that was specially designed to be incorporated downstream of the gas engine.

The main results of the first part of this thesis have been included in a draft that has been submitted to Computers and Chemical Engineering Journal with the next title: "Development of an Equilibrium Theory solver applied to Pressure Swing Adsorption cycles used in carbon capture processes" meanwhile the results associated with the design, optimisation and incorporation of adsorptive units in biomass gasification plants have been presented in the next peer reviewed and conference papers:

- Oreggioni G, Brandani S, Luberti M, Baykan Y, Friedrich D, Ahn H. CO_2 Capture from Syngas by an Adsorption Process at a Biomass Gasification CHP Plant: Its Comparison with Amine-based CO_2 Capture. Int. J. Greenh. Gas Control. 2015; 35:71-81.
- Ahn H, Luberti M, Oreggioni G. A Post-Combustion CO_2 Capture Rapid Pressure/Vacuum Swing Adsorption Process and Its Application for Decarbonizing a Coal-Fired Power Plant. AichE Proceedings.2014
- Oreggioni G, Friedrich D, Brandani, S, Ahn, H. Techno-economic study of adsorption processes for pre-combustion carbon capture at a biomass CHP plant. Energy Procedia. 2014; 63: 6738–6744.

This PhD thesis is one of the few works in which an optimised adsorptive carbon capture unit has been designed for incorporation in a power plant and for which operating conditions and cycle configuration were chosen in order to allow continuous operation of the energy generation plant with installed PSA cycles. The energy penalty for the carbon capture unit has been estimated taking into consideration the contributions associated with upstream and downstream processes. This feasibility study has been carried out using an in house PSA cycle solver (CySim) that enables the simulation of the adsorption units accounting for the kinetic and dispersive effects, pressure drop and heat transfer with the surroundings.

Considering that the simulation of PSA cycles requires long execution time and a large set of experimentally determined parameters, research has also been undertaken in order to develop a generic Equilibrium Theory PSA cycle solver (Esim). The new tool, with a simpler code implementation, enables the estimation of the thermodynamic limiting performance that an adsorption unit could reach (since kinetic and dispersive effects are neglected) and a pre-selection of operating conditions and adsorbents by just requiring the equilibrium isotherm function as input data. Promising configurations will be further investigated by employing full governing equation routines for which kinetic parameters must be provided as input data. The pre-selection effectuated by employing Esim allows a reduction in the number of experiments by just focussing on the operating conditions for the high separation efficiency configurations. The novel software has been tested in the simulation of multi transition systems. In these tests, the solver shows its capacity to track shock and smooth solutions without the need of implementing a shock tracking algorithm enabling the modelling of gas mixtures which components obey any kind of isotherm function. Esim is the first Equilibrium Theory solver that presents these capabilities.

Conclusions

The energy sector must take action in order to reduce its carbon footprint. CCS processes could contribute to a less carbon-intense energy matrix, however, the introduction of CCS technologies in power plants will involve a large energy penalty that reduces their net electrical efficiency. For this reason, the development of novel carbon capture technologies or the optimisation of already existing technologies must be undertaken. Post- and pre-combustion technologies are under investigation, as are oxyfuel and chemical looping combustion. Although the MEA-based process is the most common carbon capture technology in industries, it has a very large specific energy consumption (approximately 130 to 160 kJ_t/mol of captured CO_2). . Several works have proved that pressure swing adsorption cycles may reduce the energy consumption to values in the range of 70 till 90 kJ_t/mol of captured CO_2 when applied at lab scale to treat streams which compositions are analogous to the flue gas from coal fired power plants. In the case of PSA cycles, the energy consumption is expected to be lower if the feed gas is enriched with CO_2. The implementation of adsorptive units in the role of pre-combustion carbon capture would thus lower energy consumption since the syngas stream downstream of water gas shift reactor is approximately 30 mol % CO_2. Research in the

development and optimisation in PSA technology could therefore lead to the development of more economical carbon capture processes and will be analysed in this thesis.

References

Abanades JC, Anthony E., J. Wang and J. Oakey, Fluidized Bed Combustion Systems Integrating CO_2 Capture with CaO, Environ.Sci. Technol., 2005, 39, 2861–2866

Abedini R, Nezhadmoghadam A. Application of membrane in gas separation processes: Its suitability and mechanisms. Petroleum & Coal 2010;52:69-80.

Adanez J, Abad A, Garcia Labiano F, Gayan P, De Diego L F. Progress in Chemical-Looping Combustion and Reforming technologies. Prog. Energ. Combust. 2012:38;215-282.

Ahn H, Luberti M, Liu Z, Brandani S. Process configuration studies of the amine capture process for coal-fired power plants. Int. J. Greenh. Gas. Con. 2013; 16: 29-40.

Argawal A, Biegler L T, Zitney S.E. Superstructure-Based Optimal Synthesis of Pressure Swing Adsorption Cycles for Precombustion CO_2 capture. Ind. Chem. Res. 2010; 49: 5066-5979.

Arnold D, Barret D A, Isom R H. CO_2 can be produced from flue gas. Oil and Gas Journal. 1982; 130-136.

Artanto Y, Jansen J, Pearson P, Puxty G, Cottrell A, Meulleman E, Feron P. Pilot-scale evaluation of AMP/PZ to capture CO2 from flue gas of an Australian brown coal–fired power station. Int. J. Greenh. Gas. Con. 2014; 20: 189-195.

Azar C, Johanson D J A, Mattson N. Meeting global temperature targets-the role of bioenergy with carbon capture and storage. Environm Res Lett. 2013:8:1-8

Barchas R, Davis R. The Kerr-McGee / ABB Lummus Crest Technology for the Recovery of CO_2 from Stack Gases. Energ Conv Manage. 1992: 33; 333-340

Bata L. Selective adsorption process for air separation. US 3717974. 1973

Bocciardo D, Ferrrari MC, Brandani S. Modelling and Multi-stage Design of Membrane Processes Applied to Carbon Capture in Coal-fired Power Plants. Energy Procedia. 2013; 37: 932-940.

Brandvoll Ø, Bolland O. Inherent CO_2 capture using chemical looping combustion in a natural gas fired power cycle. ASME Journal of Engineering for Gas Turbines and Power. 2004;126: 316-321.

Chapel D G, Mariz C L, Ernest J. Recovery of CO2 from flue gases: commercial trends, paper No. 340 at the Annual Meeting of the Canadian Society of Chemical Engineering, Saskatoon, Canada, October.

Cho, P, Mattison T, Lyngfelt A. Reactivity of iron oxide with methane in a laboratory fluidised bed – application of chemical-looping combustion. 7th International Conference on Circulating Fluidised Beds. 2002.

DECARBit.Enabling advanced pre-combustion capture techniques and plants.European best practice guidelines for assessment of CO_2 capture technologies. European Benchmarking Task Force. 2011.

Dickmeis J, Kather A. The coal-fired Oxyfuel-process with additional gas treatment of the ventgas for increased capture rates. Energy Procedia.2013;37: 1490 – 1499

Dillon, D J, Panesar R S, Wall A, Allam R J, White V, Gibbins J, Haines M R. Oxy-combustion processes for CO_2capture from advanced supercritical PF and NGCC power plant. Proceedings of 7th International Conference on Greenhouse Gas Control Technologies. 2005. Volume I: Peer Reviewed Papers and Overviews, Elsevier Science, Oxford, UK, 211-220.

Dunsmore H E. A Geological Perspective on Global Warming and the Possibility of Carbon Dioxide Removal as Calcium Carbonate Mineral. Energy Convers. Mgmgt.. 1992; 33: 565-572.

EDGAR database. CO_2 global sectorial emissions. (Access with permission).

EIA. Global fossil fuel electricity generationhttp://www.eia.gov/cfapps/ipdbproject/IEDIndex3.cfm?tid=44&pid=44&aid=2

European Council. Winning the battle against global climate change. Official Journal C 125 . 2005.

Fan L S, Zeng L, Wang W, Luo S. Chemical looping processes for CO2 capture and carbonaceous fuel conversion – prospect and opportunity. Energy Environ. Sci.2012;5,:7254-7280.

Florin N, Fennnell P. Carbon capture technology: future fossil use and mitigating climate change. Grantham Institute for Climate Change, Briefing Paper 3. 2010

Folger P. Carbon Capture: A Technology Assessment. Congressional Research Service. 2010.

NETL. Pathway for readying the next generation of affordable clean energy technology—Carbon Capture, Utilization, and Storage (CCUS). 2012

Guerrin de Montgareuil P and Domine D. French Patent 1223261. 1957

Hansen J, Sato M, Kharecha P, Russel G, Lea D, Sidall M. Climate Change and trace gases. Phil. Trans. R. Soc. A. 2007: 365, 1925–1954

Hurst T F, Cockerill T T, Florin N H. Life cycle greenhouse gas assessment of a coal-fired power station with calcium looping CO_2 capture and offshore geological storage. Energy Environ. Sci. 2012;5: 7132-7150.

ICIS, Report on MEA costs. 2014 (information provided via e-mail)

IEA Clean Coal Centre. Post-combustion carbon capture from coal fired plants – solvent scrubbing. 2007

IEA Clean Coal Centre. Chemical looping combustion of coal. 210

IEA. Energy Technology Prospective. 2010

IPCC. Special Report on Carbon Dioxide Capture and Storage. 2005.

Ishida M and Jim H. A. New Advanced Power-Generation System Using Chemical-Looping Combustion. Energy. 1994 ;19: 415-422.

Jacob D . Introduction to Atmospheric Chemistry. Princeton University Press:Princeton;1999

Janssens-Maenhout G, Dentener F, Van Aardenne J, Monni S, Pagliari V, Orlandini L, Klimont Z, Kurokawa J, Akimoto H, Ohara, T, Wankmueller R, Battye B, Grano D; Zuber A, Keating T. EDGAR-HTAP: a Harmonized Gridded Air Pollution Emission Dataset Based on National Inventories. Ispra (Italy): European Commission Publications Office; 2012. JRC68434, EUR report No EUR 25 299 - 2012, ISBN 978-92-79-23122-0, ISSN 1831-9424

Jericha H, Sanz W, Gottlich E, Neumayer F. Design Deatils of a 600 MW Graz Cycle Thermal Power Plant for CO_2 capture. ASME Turbo Expo 2008. Berlin, Germany.

Keller G E, Anderson R A and Yon C M. Handbook of Separation Process Technology. 1986. New York. John Willey and Sons.

Kikkinides E S, Yang R T, Cho S H. Concentration and Recovery of CO2 from Flue Gas by Pressure Swing Adsorption. Ind. Eng. Chem. Res 1993; 32: 2714-2720.

Ko D, Siriwardane R, Lorenz T, Biegler .Optimization of a Pressure Swing Adsorption Process Using Zeolite 13X for CO2 Sequestration. Ind. Eng. Chem. Res. 2003; 42: 339-348.

Koros W J, Ma Y H, Shimidzu T. Technology for membranes and membrane processes. IUPAC recommendations, 1996.

Kuramochi T. Ramirez A. 2011. Presentation capture technologies. Utrecht University. The Netherlands.

Lee C H, Yang J, Ahn H. Effects of carbon to zeolite ratio on layered bed H2 PSA for coke oven gas. AichE J. 1999; 45: 535-545.

Liu Z, Grande C, Li P, Yu J,Rodrigues A. Multi-bed Vacuum Pressure Swing Adsorption for carbon dioxide capture from flue gas. Sep. Purif. Tecnol 2011; 81: 307-317.

Luberti M, Friedrich D, Brandani S, Ahn H. Design of H_2 PSA for cogeneration of ultrapure hydrogen and power at an advanced integrated gasification combined cycle with pre-combustion capture. Adsorption Journal. 2013.

Manzolini G, Sanchez Fernandez E, Rezvani S, Macchi E, Goether E L V, Vlugt T J H. Economic assessment of novel amine based CO2 capture technologies integrated in power plants based on European Benchmarking Task Force methodology. Applied Energy.2015;138:546-558.

Markewitz P, Kuckshinrichs W, Leitner W,Linssen J, Zapp P, Bongartz R, Schreiber A , Muller T. Worldwide innovations in the development of carbon capture technologies and the utilization of CO_2. Energy Environ. Sci. 2012:5:7281-7305

Martinez, A Lara,Y, Lisbona P, Romeo L. Energy penalty reduction in the calcium looping cycle, Int. J. Greenhouse Gas Control, 2012, 7, 74–81.

Mastandrea, M.D. and S.H. Schneider. 'Probabilistic Assessment of "Dangerous" Climate Change and Emissions Scenarios', International Symposium on Stabilisation of Greenhouse Gases, Exeter, February 1-3 2005.

Meerman J C, Hamborg E S, Van Kuele T, Ramirez A, Turkenburg W C, Fajai A P C. Techno-economic assessment of CO_2 capture at steam methane reforming facilities using commercially available technology. . Int. J. Greenh. Gas. Con. 2012; 9:160-171.

Merkel T., Lin H, Wei X, Baker R. Power plant post-combustion carbon dioxide capture: An opportunity for membranes. J. Membr. Sci. 2010; 359:126-139.

Mimura N, Takahara I, Saito M, Hattori T, Ohkuma K, Ando M. Dehydrogenation of ethylbenzene over iron oxide-based catalyst in the presence of carbon dioxide", Advances in Chemical Conversions for Mitigating Carbon Dioxide, Studies in Surface Science and Catalysis. 1998:114; 415-418.

Mimura T, Satsumi S, Iijiima M, Mitsuoka S. Development on Energy Saving Technology for Flue Gas Carbon Doxide Recovery by Chemical Absorption Method and Steam System in Power Plant. Greenhouse Gas Control Technologies.1999

Moller B F, Torisson T, Assadi M. AZEP Gas Turbine Cycle Power Plants—Thermo.economic Analysis. Int J of Themodynamics. 2006; 9:21-28

NETL. Pulverized Coal Oxycombustion Power Plants. US Department of Energy.2007.a

NETL. Cost and Performance baseline for fossil energy plants , US Department of Energy 2007 b .

Rao A B and Rubin E S. A technical, economic and environmental assessment of amine based CO_2 capture technology for power plant greenhouse gas control. Environ. Sci. Technol. 2002: 36; 4467-4475.

Reynolds S P, Ebner A D, Ritter J A. New Pressure Swing Adsorption Cycles for Carbon Dioxide Sequestration. Adsorption. 2005; 531-536

Ribieiro AM, Grande C A, Lopes F V S, Loureriro J M, Rodrigues A E. A parametric study of layered PSA for hydrogen purification. Chem. Eng. Sci. 2008: 63; 5258-5273.

Richter H J, Knoche K.. Reversibility of Combustion processes, Efficiency and Costing - Second Law Analysis of Processes, ACS Symposium. 1983;235: 71-85.

Ritter, R., A. Kutzschbach, and T. Stoffregen. "Energetic evaluation of a CO2 purification and compression plant for the Oxyfuel process." *1st Oxyfuel Combustion Conference*. 2009.

Sanchez Fernandez E, Goether ELV, Manzolini G, Macchi E, Rezvani S, Vlugt T J H. Thermodynamic assessment of amine based CO2 capture technologies in power plants based on European Benchmarking Task Force methodology.Fuel. 2014:129:318-329.

Sander M T and Mariz C L. The Fluor Daniel® Econamine™ FG Process: Past Experience and Present Day Focus.1992: 33; 341-348

Scholes C A, Smith K H, Kentish E, Streven G W. CO2 capture from pre-combustion processes- Strategies from membrane gas separation. Int. J. Greenh. Gas. Con. 2010; 4: 739-755

Shen C, Liu Z, Li P, Yu J. Two-Stage VPSA Process for CO_2 Capture from Flue Gas Using Activated Carbon Beads. Ind. Chem. Res. 2012; 51: 7947-7955.

Shimuzi T, Hirama T, Hosoda H, Kitano K, Inagaki M, Tejima K. A twin A twin fluid-bed reactor for removal of CO_2 from combustion processes, Trans IChemE, Vol 77, Part A, January1999, pp. 62–68.

Sircar S. Applications of Gas Separation by Adsorption for the Future. Adsorpt. Sci. Technol. 2001; 19: 347-366.

Sircar S. Pressure Swing Adsorption. Ind. Chem.Res. 2002; 41: 1389-1392.

Sircar. Preparation of high purity oxygen. US 475672.1987

Skarmstrom CW. Method and apparatus for fractionating gaseous mixtures by adsorption. US 2944627. 1960

Strohle J, Galloy A, Epple B. Feasibility Study on the Carbonate Looping Process for Post-Combustion CO_2 Capture from Coal-Fired Power Plants, Energy Proc., 2009, 1, 1313–1320

Wang L, Yang Y, Shen W, Kong X, Li P, Yu J, Rodrigues A E. CO2 Capture from Flue Gas in an Existing Coal-Fired Power Plant by Two Successive Pilot-Scale VPSA Units. Ind.Eng.Chem.Res. 2012.; 52: 7947-7955.

Webley P.A. Adsorption technology for CO_2 separation and capture: a perspective. Adsorption. 2014

White V, Wright A, Tappe S, Yan J. The Air Products Vattenfall Oxyfuel CO_2 Compression and Purification Pilot Plant at Schwarze Pumpe. Energy Procedia. 2013;37:1490-1499.

Xiao P, Wilson S, Xiao G, Singh R, Webley P. Novel adsorption processes for carbon-dioxide capture with an IGCC process. Energy Procedia. 2009; 1: 631-638.

Zafar Q, Mattison T, Gevert B. Integrated Hydrogen and Power Production with CO_2 Capture Using Chemical-Looping Reforming-Redox Reactivity of Particles of CuO, Mn_2O_3, NiO,and Fe_2O_3 Using SiO_2 as a Support. Ind. Chem. Res. 2005; 44: 3485-34

Chapter 2: Adsorption Equilibrium and dynamic

Introduction

As it was underlined in Chapter 1, several previous works have assessed the feasibility and performance of PSA cycles in the role of carbon capture technology at lab scale. In these works, it was concluded that adsorption technology exhibited a lower specific energy consumption than post combustion MEA process when applied to treat streams which compositions emulated the flue gas from coal fired power plants. The deployment of PSA cycles requires to undertake research in the field of sorbent and process design. The development of accurate and robust simulation tools is crucial in order to select and optimise adsorptive units. Simplifications associated with the modelling of the mass and energy transfer mechanisms between the phases like the Linear Driving Force (LDF) and the Equilibrium Theory (ET) assumptions enable the simulation of the adsorption dynamics by employing fewer empirically determined input parameters (ET) and fewer partial differential equations (ET and LDF). This chapter is intended to analyse how these simplifications influence on the mathematical formulation of the mass and energy balances for an adsorption column and to discuss their advantages and limitations for the development of a generic PSA cycle solver.

2.1 Adsorbents widely employed at industrial level

The use of adsorption as a separation unit operation is based on the selective retention of the gas molecules in the pores of the adsorbent (Ruthven, 1984); this selective retention may be caused by differences in the adsorption equilibrium or in kinetic rates. The molecules of a gas mixture in the neighbourhood of a solid will experience a reduction in their potential energy due to the interaction forces between the atoms of the solid and the gaseous molecules thus the gas molecules will tend to concentrate in this region leading to larger density in comparison with the free gas phase zone. The nature of surface forces will depend on the adsorbent and the

sorbates. If the interaction between the adsorbent and the sorbates are Van der Waals forces or dipole fields, the phenomena can be classified as physisorption. In the case that transference of electrons between the gas and solid phases takes place, a chemisorption phenomenon will occur (Ruthven, 1984).

The role of the adsorbents will be to provide the surface area for the selective sorption to take place. The specific selectivity and the adsorption capacity are important factors that must be taken into account to choose the sorbent as well as the operating conditions for the gas separation. The selectivity can be consequence of "chemical similarity" (equilibrium driven sorbents) between the surface of the solid and the sorbate or by steric restriction (kinetically driven sorbents).

Activated carbon, zeolites, carbon molecular sieves (CMS) are the most used adsorbents for large scale industrial applications like H_2 production/ purification and air separation. Activated carbon is produced in several forms that lead to different pore size distribution and surface polarity; the nature of the final product depends on both the starting material and the activation procedure. For liquid-phase adsorption, a relatively large pore size is required and such materials can be obtained by both thermal and chemical activation procedures from a wide range of carbonaceous starting material meanwhile the activated carbons used in gas adsorption generally have much smaller pores with a substantial fraction of the total porosity in the micropore range (Ruthven, 1994).

In contrast to AC, activated alumina and CMS, zeolites are crystalline structures; the micropores are intra crystalline channel with dimensions precisely determined by the crystal structure. Practically there is no pore size distribution and these adsorbents show well defined size selective molecular sieve properties that enables excluding the molecules that are larger than a certain critical pore size and provoking strong steric restriction of diffusion for molecules of which the diameters are close to the micropore critical size (Ruthven, 1984).

The framework of the zeolites consists of tetrahedral connected assemblages of SiO_2 and AlO_2 units. These tetrahedrons are the basic building blocks for zeolites A and X (**Figure 2.1)**. Due to the presence of alumina, the zeolites exhibit a negatively charged framework, which is counter-balanced by positive cations resulting in a strong electrostatic field on the internal surface. These cations can be exchanged to fine-tune the pore size or the adsorption characteristics. For instance, the sodium form of zeolite A has a pore opening of approximately

4Å (**Figure 2.2**) called 4A molecular sieve. If the sodium ion is exchanged with the larger potassium ion, the pore opening is reduced to approximately 3Å (3A molecular sieve). If one calcium ion replaces two sodium cations, the pore opening increases to approximately 5Å (5A molecular sieve). Ion exchange with other cations is sometimes used for particular separation purposes (Ruthven, 1984).

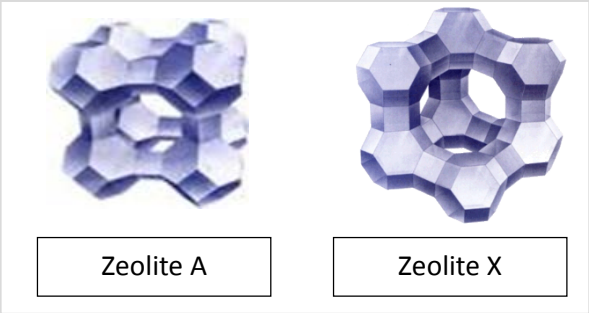

Figure 2.1: Frameworks for zeolite A and X (Huiying, 2014)

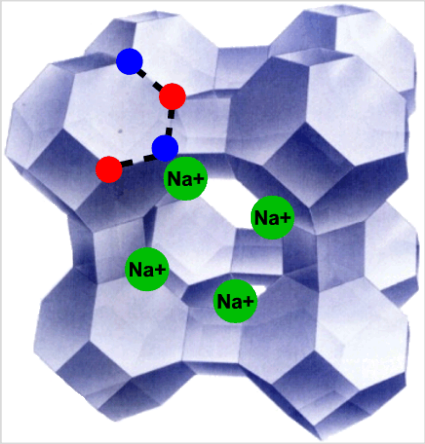

Figure 2.2: Framework for zeolite 4A (Huiying, 2014)

2.2 Adsorption Equilibrium

The isotherm equilibrium functions quantify the relationship between the mass of one of the species in the absorbed phase with the concentration or partial pressure of that specie or others in the bulk gas phase. The equilibrium functions can be based either on theoretical

models or on mathematical correlations that best fit experimental data (Ruthven, 1984). IUPAC (IUPAC, 1985) has divided the isotherms for physical adsorption into five classes as illustrated in **Figure 2.3.**

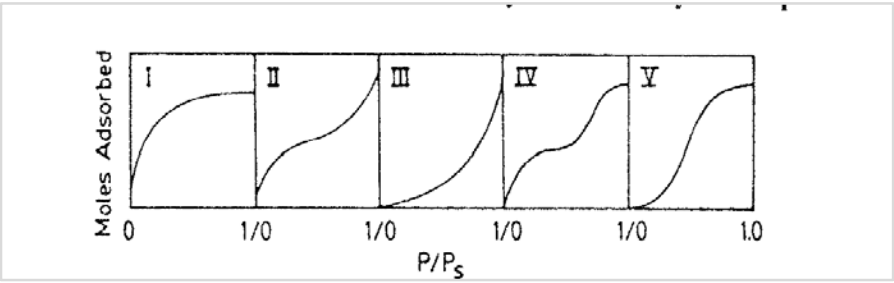

Figure 2.3: Classification of isotherm equilibrium function according to IUPAC (IUPAC,1985)

The type I equilibrium isotherm functions corresponds to true microporous adsorbents for which the pore size is not very much greater than the molecular diameter; for those adsorbents, there is a definite saturation limit that is associated with the complete filling of the micropores. The type V isotherm may be observed in systems in which there are large intermolecular attractions like in the sorption of phosphorus vapour on NaX (Ruthven, 1984). An isotherm of type IV suggests the formation of two surface layers either on a plane surface or on the wall of a pore being very much wider than the molecular diameter of the sorbate. The types II and III isotherms are generally observed only in those adsorbents for which there is a wide range of pore sizes; in such systems there is a continuous progression with increasing loading from monolayer to multilayer adsorption and then to capillarity condensation when the pressure of the gas mixture is raised. (Ruthven, 1994)

When the dynamics of adsorption systems is under study, it is useful to define the concept of favourable, linear, and non-favourable adsorption isotherms. This concept is based on the plot (x, y) shown in **Figure 2.4 .** The definitions for x and y are presented in the axes of the plot.

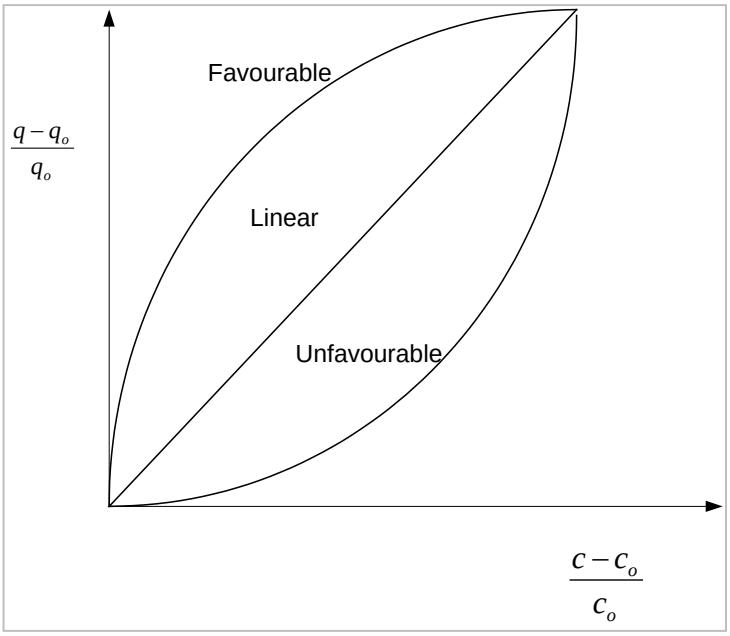

Figure 2.4: Favourable isotherm equilibrium function

Most of the adsorbents used for carbon capture applications present a Type I (favourable isotherm) (Webley, 2014). The observed behaviour for these adsorbents may be explained by the application of the Langmuir model which basic premises are:

- The molecules are adsorbed at a fixed number of well-defined localized sites.
- Each site can hold one adsorbate molecule.
- All sites are energetically equivalent.
- There is no interaction between the molecules adsorbed on neighbouring sites.

The expression for the Langmuir isotherm can be obtained by considering that when equilibrium is reached , the adsorption (Eq. (2.1)) and the desorption (Eq. (2.2**)**) rates are equal.

$$Adsorption\ rate = k_a p(1-\theta) \quad (2.1)$$

$$Desorption\ rate = k_d \theta \quad (2.2)$$

θ can be defined as the fraction of the available sites occupied as shown in Eq. (2.3), qs is the saturation capacity and it corresponds to the total available sites for adsorption.

$$\theta = \frac{q}{qs} \tag{2.3}$$

By setting that Eq. (2.1) and Eq. (2.2) are equal, it is possible to obtain Eq. (2.4). Replacing θ by its definition (Eq. (2.3)), Eq. (2.4) becomes Eq. (2.5) that it is the mathematical expression for the monosite Langmuir isotherm.

$$\frac{\theta}{1-\theta} = \frac{k_a}{k_d} p = bp \tag{2.4}$$

$$q = \frac{q_s bp}{(1+bp)} \tag{2.5}$$

2.3 Adsorption kinetics

A proper understanding of the kinetic effects in PSA systems requires analysing the mechanisms for mass transfer in the macropores and the micropores (**Figure 2.5)**. For some of the most commercially employed adsorptive gas separations, prevailing mass transfers between the phases are relatively known however when novel adsorbents or systems are being considered, uptake experiments must be undertaken aimed to identify the dominant mechanism as well as the value for the respectively diffusion coefficients. A brief discussion about these mechanisms will be held in this section.

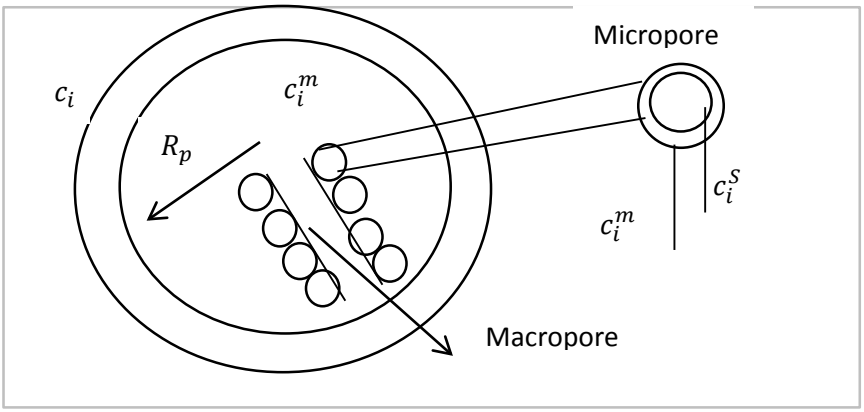

Figure 2.5: Pores and concentrations in the pellet of an adsorbent

2.3.1 Diffusion in mesopores and macropores

There are four distinguishable mechanisms that contribute to the mass transfer in the case of the mesopores and the macropores. These mechanisms are:

- Bulk diffusion
- Knudsen flow
- Poiseuille flow
- Surface diffusion

The bulk diffusion becomes dominant when the pore diameter is larger than the mean free path of the molecule (the distance that the molecule can travel without having collisions with other molecules). Eq. (2.6) shows the influence of pressure and temperature in the molecular diffusivity (Ruthven, 1994).

$$D_{i,j}^{m} = 1.6\ 10^{-7} \frac{\sqrt{T^3}}{P\sigma_{ij}^2\sqrt{M}\omega_{ij}} \tag{2.6}$$

M refers to the mean molecular mass defined as shown in Eq. (2.7) meanwhile σ_{ij} is the collision diameter from the Lennard-Jones potential and ω_{ij} is a function depending on the Lennard-Jones force constant and temperature (Ruthven, 1994). For the case of multicomponent systems, the molecular diffusivity is a function of concentrations (Ruthven, 1994) and it can be estimated by using Eq. (2.8).

$$\frac{1}{M} = \frac{1}{M_i} + \frac{1}{M_j} \tag{2.7}$$

$$D_i^m = \sum_{i=1}^{n} \frac{y_i\,(1 - y_i\,)}{\sum_{j=1, j\neq i}^{n} \frac{y_j}{D_{ij}}} \tag{2.8}$$

The Knudsen diffusivity becomes relevant at low pressure or in those adsorbents in which the pore diameters are lower than the molecular mean free path since this mass transfer mechanism is consequence of the collisions between the diffusing molecules and the pore wall (Ruthven, 1984). The value for the Knudsen diffusivity coefficient can be estimated by using Eq.(2.9)

$$D_i^K = 97 r_{pore} \sqrt{T/M} \tag{2.9}$$

In the transition region between the two mechanisms, it is valid to say that the two diffusivities can be summed up as two resistances in parallel as shown in Eq. (2.10)

$$\frac{1}{D_i^p} = \frac{1}{D_i^m} + \frac{1}{D_i^K} \tag{2.10}$$

It is clear that at higher pressures D tends to D_m meanwhile at lower pressure and small pore radius, D tends to D_K. For those systems in which just a single gas component diffuses into the adsorbent, there may also be a contribution related to the flux from forced flow (Poiseuille flow). The equivalent Poiseuille diffusivity is given by Eq. (2.11).

$$D^V = \frac{P {r_{pore}}^2}{8\mu} \tag{2.11}$$

The influence of Poiseuille diffusivity is important for sorbents with relatively large pores and high pressures; it may be important during the pressurisation step in PSA cycles. The contribution of the Poiseuille diffusivity is directly additive to the one arising from the combination of the Knudsen and molecular mechanisms (Ruthven, 1984).

The effect of surface diffusivity through the adsorbed layer is significant when the adsorbed phase is mobile and the adsorbed phase concentration is sufficiently high. It is an activated process (Eq. (2.12)) similar to the micropore diffusion that will be further discussed in the next sub-session.

$$D_i^S = \frac{1-\varepsilon_p}{\varepsilon_p} K\, D_i^{So} \exp(-\frac{E}{R\,T}) \tag{2.12}$$

The value for the overall macropore diffusivity coefficient can be quantified by using Eq. (2.13)

$$D_i^p = \frac{\varepsilon_p}{\tau}\left[\left(\frac{1}{D_i^m}+\frac{1}{D_i^K}\right)^{-1} + D_i^S + D^V\right] \tag{2.13}$$

2.3.2 Diffusion in micropores

Micropore diffusion becomes relevant when the pore sizes are comparable with the diameter of the diffusing specie thus the diffusing molecules never escape from the force field of the pore wall. The micropore diffusion mechanism is as an activated process (with a strong temperature dependency under the Arrhenius form) for which the activation energy is largely determined by the size of the diffusing molecules relative to the smallest free diameter of the pores (Ruthven, 1994).

2.4 Mass and Energy balances for an adsorption bed

2.4.1 Mass and energy balances in adsorption columns

As it was previously pointed out, according to the level of details in the assumptions regarding the mass and heat transfer mechanisms between the phases, pressure drop along the column and heat transfer to the column wall, different forms of partial differential equations (PDEs) may arise. **Figure 2.6** shows a model hierarchy for adsorption columns. The model hierarchy can be traversed from left to right and in each stage one model can be chosen (Friedrich et al., 2013). Before starting a deep analysis about the different modelling

simplification and assumptions, it is important to define several column and sorbent dimensions (**Table 2.1)** that will be present in the equations**.** A list of the abbreviations and the corresponding variables displayed in the table as well as in the equations can be found in **Annex I.**

Table2.1: Column dimension and definitions of densities and porosities

Sign	Explanation	Formula		Explanation	Formula
$A_{c,a}$	Column axial surface area	$A_{c,a} = \pi R_c^2$	ρ_{bulk}	Bulk density	$\rho_{bulk} = \frac{\mathrm{m_p}}{V_c}$
$A_{c,l}$	Column lateral surface area	$A_{c,l} = 2\pi R_c L_c$	ρ_p	Pellet density	$\rho_p = \frac{\mathrm{m_p}}{V_p}$
A_c	Column area	$A_c = 2A_{c,a} + A_{c,l}$	ρ_{cry}	Crystal density	$\rho_{cry} = \frac{\mathrm{m}_c}{V_{cry}}$
V_c	Column Volume	$V_c = \pi R_c^2 L_c$	ρ_{skel}	Skeletal density	$\rho_{skeletal} = \frac{\mathrm{m}_p}{V_{skeletal}}$
V_w	Wall Volume	$V_w = \pi \delta_w 2R_c L_w$	ε	Inter-particle void fraction	$\varepsilon = 1 - \frac{\rho_{bulk}}{\rho_p}$
A_p	Pellet surface area	$A_p = \frac{4\pi R_p^2}{\varphi}$	ε_p	Pellet void fraction	$\varepsilon_p = 1 - \frac{\rho_p}{\rho_{cry}}$
V_p	Pellet volume (Sphere)	$V_p = \frac{4}{3}\pi R_p^3$	ε_{cry}	Crystal void fraction	$\varepsilon_{cry} = 1 - \frac{\rho_{cry}}{\rho_{skel}}$

The mass balance for the gas phase is described by the axial dispersion plug flow model with an adsorption term as shown in Eq.(2.14). From a mathematical point of view, it can be classified as a dispersive advection equation with a“ reaction term”.

$$\frac{\partial c_i}{\partial t} + \frac{\partial (v c_i)}{\partial z} + \frac{\partial J_i}{\partial z} + \frac{1-\varepsilon}{\varepsilon}\frac{\partial \widetilde{Q}_\iota}{\partial t} = 0 \tag{2.14}$$

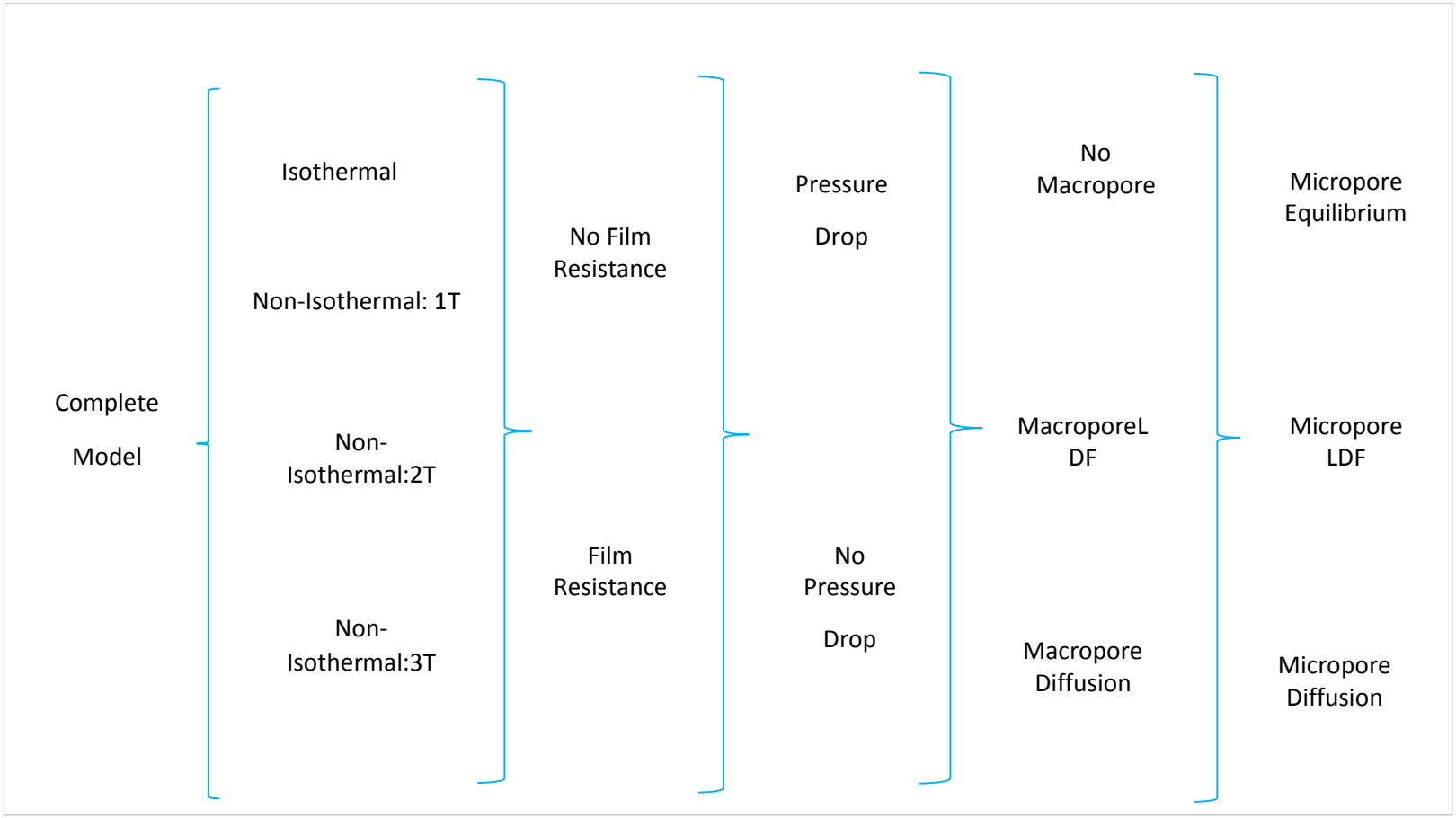

Figure 2.6: Model hierarchy for the simulation of adsorption dynamics

$\widetilde{Q_\iota}$ refers to the average concentration of the adsorbing species in the adsorbent pellet that will account for the molecules present in the macropores (c_i^m) and for the sorbate concentration ($\widetilde{q_\iota}$) as displayed in Eq. (2.15), Eq. (2.16) and Eq.(2.17).

$$Q_i = \varepsilon_p c_i^m + (1-\varepsilon_p)\widetilde{q_\iota} \tag{2.15}$$

$$\widetilde{q_\iota} = \frac{3}{{r_p}^3}\int_o^{r_p} q_i\, r^2 dr \tag{2.16}$$

$$\widetilde{Q_\iota} = \frac{3}{{R_p}^3}\int_o^{R_p} Q_i\, {r_p}^2 dr \tag{2.17}$$

In the case of considering the diffusion mechanism in the macropores, c_i^m will be determined by solving Eq. (2.18).

$$\varepsilon_p \frac{\partial c_i^m}{\partial t} + \left(1-\varepsilon_p\right)\frac{\partial \widetilde{q_\iota}}{\partial t} + \frac{1}{r^2}\frac{\partial}{\partial r}\left(-D_i^p r^2 \frac{\partial c_i^m}{\partial r}\right) = 0 \tag{2.18}$$

The adsorbed concentration in the micropores is governed by Eq. (2.19).

$$\frac{\partial q_i}{\partial t} + \frac{1}{r^2}\frac{\partial}{\partial r}(-D_i^\mu r^2 \frac{\partial q_i}{\partial r}) = 0 \tag{2.19}$$

The most rigorous definition for the energy balance considers that the temporal changes in the internal energy for the gas phase ($\widetilde{U_f}$) and for the solid phase ($\widetilde{U_p}$) are caused by the gradients of the convective ($v\widetilde{H_f}$), the axial thermal dispersion (J_T) and the enthalpy (due to axial diffusion,$(J_i\widetilde{H_\iota})$) fluxes as well as by the heat transfer between the column and the surroundings as expressed by Eq. (2.20).

$$0 = \varepsilon \frac{\partial \widetilde{U_f}}{\partial t} + (1-\varepsilon)\frac{\partial \widetilde{U_p}}{\partial t} + \varepsilon \frac{\partial (v\widetilde{H_f})}{\partial z} + \frac{\partial J_T}{\partial z} + \sum_{i=1}^{N_c} \frac{\partial (J_i \widetilde{H_\iota})}{\partial z} + h_w \frac{A_c}{V_c}(T_f - T_w) \tag{2.20}$$

The temporal change for the internal energy in the pellet can be described by Eq. (2.21)

$$0 = \frac{\partial \widetilde{U_p}}{\partial t} + \frac{1}{r}\frac{\partial}{\partial r}(-r^2 l_p^p \frac{\partial T_p}{\partial r}) \tag{2.21}$$

The constitutive equations for the terms mentioned in the energy balances for both phases (Eq. (2.20) and Eq. (2.21) are displayed bellow:

$$\widetilde{U_f} = c_T \widetilde{U_{f,ref}} + c_T \int_{T_{ref}}^{T_f} \widetilde{c_v}\, dT \tag{2.22}$$

$$\widetilde{H_f} = c_T \widetilde{H_{f,ref}} + c_T \int_{T_{ref}}^{T_f} \widetilde{c_p}\, dT \tag{2.23}$$

$$\widetilde{U_p} = \varepsilon_p \widetilde{U_{p,f}} + (1-\varepsilon_p)\widetilde{U_{p,s}} \tag{2.24}$$

$$\widetilde{U_{p,f}} = c_T^m \widetilde{U_{p,f,ref}} + c_T^m \int_{T_{ref}}^{T_p} \widetilde{c_v}^m\, dT \tag{2. 25}$$

$$\widetilde{U_{p,s}} = \widetilde{U_{sol}} + \widetilde{U_{ads}} \tag{2.26}$$

$$\widetilde{U_{sol}} = \rho_{cry} \widetilde{U_{sol,ref}} + \rho_{cry} \int_{T_{ref}}^{T_P} \widetilde{c_{P,sol}}\, dT \tag{2.27}$$

$$\widetilde{U_{ads}} = \widetilde{H_{ads}} = q_T \widetilde{H_{ads,ref}} + q_T \int_{T_{ref}}^{T_P} \widetilde{c_{p,ads}}\, dT - (-\Delta \widetilde{H_{ads}})_{T_p} \tag{2.28}$$

$$(-\Delta \widetilde{H_{ads}})_{T_p} = \sum_{i=1}^{N_c} \int_0^{q_i} (-\Delta \widetilde{H_i})_{T_{P,q_{j\neq i}}}\, dq \tag{2.29}$$

$$\widetilde{H_i} = \widetilde{H_{i,ref}} + \int_{T_{ref}}^{T_f} \widetilde{c_{p,i}}\, dT \tag{2.30}$$

$\widetilde{U_{sol}}$, $\widetilde{U_{ads}}$ and $\widetilde{U_{p,f}}$ reffer to the internal energy per unit of volume for the adsorbent, in the adsorbed phase and in the free molecules in the macropores respectively. Here the tilde indicates the molar quantities and the subscript 'ref' indicates the reference value. The total concentrations in the fluid phase and in the macropore are given by c_T and c_T^m, ρ_p is the pellet density, q_T is the total adsorbed concentration in the micropore and $\widehat{c_{P,sol}}$ is the specific heat capacity of the adsorbent at constant pressure. The total heat of adsorption per unit volume $(-\Delta \widetilde{H_{ads}})_{T_p}$is calculated by eq. (2.29).

As it can be observed and as it was previously underlined, the mass and energy balances considering the diffusion model in macropores and micropores would involve undertaking experiments to determine diffusion coefficients as well as solving a complex coupled system of non-linear partial differential equations (PDEs) thus long execution time for the simulation of the system. Two important simplifications in order to reduce the complexity for the modelling of the adsorption dynamics can be found in literature: the LDF model and the assumption of Equilibrium Theory that will be deeply analysed in the next subsections.

2.4.2 Linear Driving Force (LDF) model

The LDF approximation was firstly used by Glueckauf (1949). The LDF model assumes no spatial dependency for the thermodynamic variables in the pores. The variable of interests will change only with time and this change will be proportional (k_{LDF}) to the difference between the values in the pore and the associated values for the closest external gas layer. If the LDF model is assumed for the macropores, the parabolic PDE defined by Eq. (2.14) can be transformed into the ODE (Ordinary differential equation) shown in Eq. (2.31).

$$\varepsilon_p \frac{\partial c_i^m}{\partial t} + \left(1 - \varepsilon_p\right) \frac{\partial \overline{q_\iota}}{\partial t} = k_i^p \frac{A_p}{V_p} (c_i - c_i^m) \tag{2.31}$$

k_i^p refers to the macropore LDF coefficient that can be obtained by using Eq. (2.32) in base of the correlations published by Nakao and Suzuki (Nakao and Suzuki, 1983).

$$k_i^p = \frac{5 D_i^p}{R_p} \tag{2.32}$$

In the case of applying the LDF model to the micropores, it is possible to say that the temporal evolution of the concentration in the adsorbed phase is proportional to the difference between the one predicted using the equilibrium isotherm for the concentration of the adsorbing species in the macropores (q_i^*) and the current value of the concentration of the adsorbed phase as shown in Eq. (2.33)

$$\frac{\partial \overline{q_\iota}}{\partial t} = k_i^{cr} \frac{3}{r_p} (q_i^* - \widetilde{q_\iota}) \tag{2.33}$$

k_i^{cr} is the LDF coefficient in the micropore and can be estimated by using Eq. (2.34)

$$k_i^{cr} = \frac{5 D_i^\mu}{r_p} \tag{2.34}$$

The use of the LDF model also simplifies the energy balance in the pellet as shown in Eq. (2.35)

$$\frac{\partial \widetilde{U_p}}{\partial t} = h_p \frac{A_p}{V_p}\left(T_f - T_p\right) + \sum_{i=1}^{N_c} \frac{\partial \widetilde{Q_i}}{\partial t} \widetilde{H_{i,f}} \tag{2.35}$$

The LDF approximation reduces the complexity of the computational implementation for the problem to be solved; PDEs must be solved just for the gas phase meanwhile ODEs are employed for the modelling of the solid phase. Schemes used for the solution of ODEs are simpler than the ones for bi-dimensional problems requiring a lower number of evaluation of the upgrading expressions. This simplification has been largely employed for the simulation of PSA cycles showing slight or minor differences with the results generated when the full governing equations are implemented in the solvers. However, this approximation may lead to disagreements in the limiting case of rectangular isotherm function or in the initial region of the uptake that it is of little consequence when the column is relatively long but that could be non-negligible in the case of short cycle PSA systems (Ruthven, 1994)

2.4.3 Equilibrium Theory

The assumption of Equilibrium Theory states that the equilibrium between the phases is immediately reached. Based on this premise, the temperature in the adsorbed phase will be the same as the one in the gas phase and the adsorbed phase concentration can be calculated directly from the gas phase concentration by using the equilibrium isotherm function. Neglecting the influence of the axial mass and thermal dispersions is another simplification that is also employed when the Equilibrium Theory simplification is used for modelling adsorption dynamics (Ruthven, 1994). The previous mentioned assumptions convert the mass and the energy balances in a system of hyperbolic-algebraic equations as shown in Eqs. (2.36) to (2.39).

$$\frac{\partial c_i}{\partial t} + \frac{\partial (v c_i)}{\partial z} + \frac{1-\varepsilon}{\varepsilon}\frac{\partial \widetilde{Q_\iota}}{\partial t} = 0 \tag{2.36}$$

$$\frac{\partial \widetilde{Q_\iota}}{\partial t} = \frac{\partial q_i^*(c_i)}{\partial t} \tag{2.37}$$

$$0 = \varepsilon \frac{\partial \widetilde{U_f}}{\partial t} + (1-\varepsilon)\frac{\partial \widetilde{U_p}}{\partial t} + \varepsilon \frac{\partial (v\widetilde{H_f})}{\partial z} + h_w \frac{A_c}{V_c}(T_f - T_w) \tag{2.38}$$

Assuming that the effect of the enthalpy of the adsorbed phase is much lower than the value for the enthalpy of adsorption and that the heat of adsorption is independent of temperature and concentration, $\widetilde{U_p}$ can be written as shown in Eq. (2.39) in which T is same as the gas temperature based upon thermal equilibrium

$$\widetilde{U_p} = \int_{T_{ref}}^{T} \widetilde{C_{p,s}}\, dT + \sum_{i=1}^{Nc} (-\Delta \widetilde{H_\iota}) q_i^* \tag{2.39}$$

The Equilibrium Theory simplification enables the development of PSA cycle solvers that just require the equilibrium isotherm function as input data in order to determine the thermodynamic limit for a given PSA cycle configuration (since kinetic and dispersive effects are considered to be negligible) and to undertake a pre-selection of promising configurations for further study. The high separation performance adsorption units will be simulated by using full governing equation software before being built in order to accurately estimate purity and recovery for the product of interest as well as the associated energy consumption for the separation. These high accuracy simulations need kinetic parameters as input data. The Equilibrium Theory simplification allows a reduction in the number of experiments since diffusivity coefficients will be measured just for the operating conditions for the pre-chosen configurations. This simplification also reduces the number of PDEs for modelling the

adsorption dynamics since the variables in the adsorbed phase are related to their analogous values in the gas phase through the isotherm equilibrium function and the thermal equilibrium condition leading as well to a simpler code implementation (fewer PDEs) for a PSA cycle solver.

Conclusions

The design of pressure swing adsorption cycles requires to understand and model the mass transfer mechanisms between the gas and the solid phase. The use of full governing equation based tools for simulating the adsorption dynamics involves undertaking diffusion determination experiments as well as solving coupled PDEs system of equations. Two simplifications that contribute to reduce the complexity of the problem to be solved have been presented: the LDF model and the assumption of Equilibrium Theory.

The LDF model assumes no spatial dependency of the variables of interest in the pores of the adsorbed phase claiming that their time evolution is proportional to the difference between the variable in the pore and its analogous value in the closest gas layer. This assumption converts the mass and energy balances in the adsorbed phase in a system of ordinary differential equations; reducing the number of PDEs to be solved (just the ones in the gas phase) and enabling a less complex implementation code for the PSA cycle solvers (fewer cycles to reach CSS).

The Equilibrium Theory simplification allows the quantification of the limiting performance than a given PSA cycle may reach by using just the equilibrium isotherm function as input data since kinetic and dispersive effects are neglected. It also enables a pre-selection of promising high performance configurations for further study and optimisation. High separation performance cycles will be then simulated by employing full governing equations that require empirically determined kinetic coefficients. This assumption reduces the number of experiments to be carried out since diffusivity coefficients will be measured just for the operating conditions of the pre-chosen cases. Equilibrium Theory also decreases the number of PDEs to be solved since the variables in the adsorbed phase are related to their analogous in the gas phase through algebraic equations or constrains like the equilibrium isotherm function or the thermal equilibrium condition leading to a less complex code for the PSA cycle simulator

(fewer cycles for CSS reaching).Taking into account the modelling advantages associated with the Equilibrium Theory assumption, it was decided to explore the possibility of developing a generic PSA cycle solver as part of the research undertaken in this thesis. The next two chapters will be devoted to this task.

References

Friedrich D, Ferrari M C , Brandani S. Efficient Simulation and Acceleration of Convergence for a Dual Piston Pressure Swing Adsorption System . Ind. Chem. Eng. Res. 2013; 52: 8897-8905.

Glueckauf E. Theory of Chromatography VII. The general theory of two solutes following non linear isotherms. Discuss. Faraday Soc. 1949; 7: 12-25.

IUPAC Recommendations. Pur. Appl. Chem. 1985;57:603.

Nakao S, Suzuki M. Mass transfer coefficient in cyclic adsorption and desorption. J.Chem. Eng. Jpn. 1983; 16: 114-119.

Ruthven D M, Farooq S, Knaebel K. Pressure swing adsorption. New York; VCH; 1994.

Ruthven D M. Principles of Adsorption and Adsorption Processes. Brunswick : Wiley; 1984.

Webley P.A. Adsorption technology for CO_2 separation and capture: a perspective. Adsorption. 2014

Yang J, Lee C H. Adsorption dynamics of a layered bed PSA for H2 recovery from coke oven gas. AIChE J. 1998 ; 44: 1325-1334.

Chapter 3: The Riemann problem associated to the adsorption dynamics under the assumption of Equilibrium Theory

Introduction

As it was previously pointed out, an Equilibrium Theory PSA cycle solver can be used for identifying a set of promising configurations for the adsorptive units. The pre-chosen high separation cycles will be further studied by employing full governing equation based routines that require experimentally determined kinetic coefficients. As explained in Chapter 2, the assumptions of Equilibrium Theory and negligible axial dispersion convert the mass and energy balances of an adsorption column into a system of algebraic-hyperbolic PDEs that in combination with their initial conditions can be classified as a Riemann-Cauchy problem. This chapter is intended to present a literature review of the exact and approximate Riemann solvers that were used for the simulation of PSA cycles that were modelled based on the Equilibrium Theory simplification. Advantages and disadvantages of these schemes when applied to the development of a software that is able to predict the dynamics of generic multi-transition adsorption system will be deeply discussed.

3.1 The Riemann Cauchy problem

A hyperbolic system (Eq. (3.1)) that exhibits a discontinuity between the boundary and initial conditions is said to be a Riemann-Cauchy problem (Leveque, 2002)

$$\frac{\partial W}{\partial z} + \alpha(W)\frac{\partial W}{\partial t} = 0 \tag{3.1}$$

Eq. (3.1) is a non-conservative generic form of a hyperbolic equation. Further discussion about conservative and non- conservative form will be held along this chapter. If the hyperbolic equation is linear, the difference between the initial and boundary conditions (wave front) will simply evolve in space and time thus for a fixed point of the spatial domain a smooth function of the variable of interest with respect to time will be observed. In the case

of non-linear hyperbolic equations, the wave front may degenerate as far as it travels, causing discontinuities or shocks. Consequently, for a fixed position a discontinuous time evolution of the variable of interest may take place (breakthrough of the variable) (Leveque, 2002).

As it was explained in the previous chapter, the assumptions of Equilibrium Theory and negligible axial dispersion convert the component mass balance, the global mass balance and the energy balance into a hyperbolic system of equations. The hyperbolic system, in combination with its associated initial conditions (piecewise constant function with a jump discontinuity) is a typical case of Riemann-Cauchy problem. Smooth as well as shock or discontinuous solutions are expected and they must be tracked by the PSA cycle solver in order to predict proper adsorption front breakthrough times. Exact and numerical approximate Riemann solvers able to do so will be described in the next sections.

3.2 Exact solution for Riemann problem: Characteristics method

By assuming a constant value of the variable of interest (W), it is possible to rewrite Eq. (3.1) as shown in Eq. (3.2).

$$s = \left(\frac{\frac{\partial W}{\partial x}}{\frac{\partial W}{\partial t}} \right)_W = \alpha(W) \tag{3.2}$$

Eq. (3.2) is said to be the characteristic velocity (Rhee et al., 1970) and it can be defined as the speed at which a determined value of W will travel along the spatial domain. The Riemann problem can be solved analytically by evaluating Eq. (3.2) for different values of W belonging to the interval [$W_{boundary}, W_{initial}$] and obtaining the time at which those values of W will arrive at a chosen spatial point (Rhee et al., 1970).

The level of difficulty in solving Eq. (3.2) will depend on $\alpha(W)$. In the case of a system of equations, the characteristics may be coupled leading to non-linear equations. The solution of the Riemann problem can be understood then as a set of waves that propagate along the

spatial domain by modifying the values of the variable of interest (Leveque, 2002). If $\alpha(W)$ is higher for lower values of the spatial domain, the characteristics will cross as shown in **Figure 3.1**

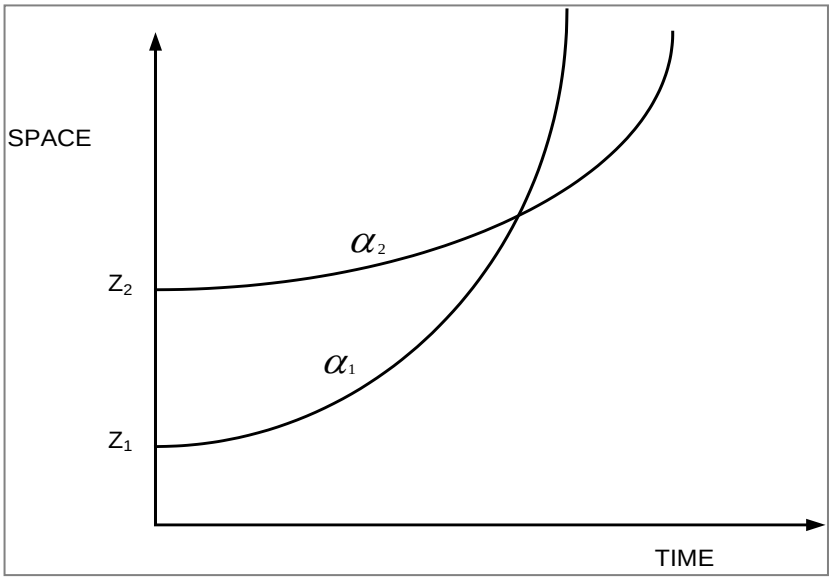

Figure 3.1: Characteristic cross in the plane (z,t)

Due to the characteristic cross it is possible to arrive at the same point (z, t) by two different speeds associated with two different values of the variable of interest thus the solution will present a discontinuity since on the right and on the left of the crossing point the variable will present different values. This phenomenon is known as shock waves, since the faster moving wave catches up to the slower moving front to form a multivalued (multicrest) wave.

The characteristic speed in the case of shocks can be calculated using the Rankine-Hugoniot condition (that will be deduced in the next page). The application of the Rankine-Hugoniot condition for the solution of Eq. (3.1) by its numerical implementation was trialled (Leveque et al. 2002; Castro et al., 2008). They reported the existence of a unique solution for the shock speed when the equation is written under a conservative form underlining as well possible issues regarding shock tracking for non conservative equations. A strict definition for the Rankine-Hugoniot condition can be established if Eq. (3.1) is written in a conservative form. A hyperbolic conservative equation states that the temporal evolution of the variable of interest is consequence of the gradient of a flux that may be a function of the variable of interest, time and space as shown in Eq. (3.3)

$$\frac{\partial W}{\partial t} + \frac{\partial f(w,t,z)}{\partial z} = 0 \tag{3.3}$$

Eq. (3.3) relates with Eq. (3.1) by:

$$\frac{\partial f}{\partial W} = \alpha(W) \tag{3.4}$$

The Rankine-Hugoniot condition represents the speed at which the discontinuity travels. By integrating Eq. (3.3) along the spatial domain between the original position and the shock position, an expression for the shock speed (Eq.(3.8)) can be obtained following the paths described from Eq. (3.5) to Eq. (3.7)

$$\int_{z_1}^{z_2} \frac{\partial W}{\partial t}\, dz + \int_{z_1}^{z_2} \frac{\partial f}{\partial z} dz = 0 \tag{3.5}$$

z_s is the position where a discontinuity takes place. On the left and right of z_s, the variable of interest exhibits constant values (w_1 and w_2)

$$\frac{\partial}{\partial t}\int_{z_1}^{z_s} w_1\, dz + \frac{\partial}{\partial t}\int_{z_s}^{z_2} w_2\, dz + \int_{z_1}^{z_s} \frac{\partial f}{\partial z} dz + \int_{z_s}^{z_2} \frac{\partial f}{\partial z} dz = 0 \tag{3.6}$$

By solving Eq. (3.6) it is possible to arrive to Eq. (3.7)

$$w_1\left(\frac{\partial z_s}{\partial t}\right) - w_2\left(\frac{\partial z_s}{\partial t}\right) + f(w_1) - f(w_2) = 0 \tag{3.7}$$

By rearranging Eq. (3.7), it is possible to arrive for the expression for the wave front speed in the case of discontinuous solution $\left(\frac{\partial z_s}{\partial t}\right)$

$$\left(\frac{\partial z_s}{\partial t}\right) = \frac{f(w_1) - f(w_2)}{w_1 - w_2} \tag{3.8}$$

As it can be appreciated, the velocity of the wave front is different whether a smooth solution or a shock transition is taking place thus it becomes necessary to determine whether a discontinuity will occur (shock formation). Theoretically the solution will present a shock when the characteristics associated with different values of the variable of interests cross in the plane (z, t). Therefore the computational implementation of the exact solvers requires the evaluation of the expression of $\alpha(W)$ for every equation at each time step in each spatial discretisation element. In the case of adsorption dynamics, $\alpha(W)$ will be a function of coupled variables leading to complex system of algebraic-differential equations. The high level of complexity for the computational implementation of the exact solvers has motivated the development of approximate Riemann Cauchy schemes as it will be further explained in this chapter.

3.3 Literature review about exact Riemann solvers applied to adsorption dynamics

A literature review about the solution of the adsorption dynamics under the assumption of Equilibrium Theory and negligible axial dispersion will be presented. The component mass balance will be brought to reader's memory in order to explain how the application of these assumptions simplifies the system of PDEs under study.

$$\frac{\partial(-D\frac{\partial c_i}{\partial z})}{\partial z} + \varepsilon\frac{\partial(c_i v)}{\partial z} + \varepsilon\frac{\partial c_i}{\partial t} + (1-\varepsilon)\frac{\partial \widetilde{q_i}}{\partial t} = 0 \tag{3.9}$$

The assumption of Equilibrium Theory allows replacing $\widetilde{q_i}$ with the concentration in the adsorbed phase calculated directly from the isotherm (q_i^*), avoiding the solution of the PDEs associated to the mass balance for the stationary phase. If the terms related to the axial dispersion are considered to be negligible it is possible to transform the parabolic PDEs for the gas phase into hyperbolic ones as shown in Eq. (3.10).

$$\varepsilon \frac{\partial (c_i v)}{\partial z} + \varepsilon \frac{\partial c_i}{\partial t} + (1-\varepsilon)\frac{\partial {q_i}^*}{\partial t} = 0 \tag{3.10}$$

${q_i}^*$ is a function of the gas phase concentration of each component, by applying the chain rule $\frac{\partial {q_i}^*}{\partial t}$ can be written as shown in Eq.(3.11)

$$\frac{\partial q_i^*}{\partial t} = \sum_{i=1}^{Nc} \frac{\partial {q_i}^*}{\partial c_i}\frac{\partial c_i}{\partial t} = \frac{\partial c_i}{\partial t}\left(\frac{\partial {q_i}^*}{\partial c_i} + \sum\nolimits_{j\neq i}^{Nc} \frac{\partial {q_i}^*}{\partial c_j}\right) \tag{3.11}$$

Consequently Eq. (3.10) can be rewritten as:

$$\frac{\partial c_i}{\partial t}\left\{\varepsilon + \left[(1-\varepsilon)(\frac{\partial {q_i}^*}{\partial c_i} + \sum\nolimits_{j\neq i}^{Nc} \frac{\partial {q_i}^*}{\partial c_j})\right]\right\} + \varepsilon \frac{\partial (c_i v)}{\partial z} = 0 \tag{3.12}$$

Rearranging Eq. (3.12), it is possible to obtain Eq. (3.13)

$$\frac{\partial c_i}{\partial t} + \varepsilon \frac{1}{\left\{\varepsilon + \left[(1-\varepsilon)(\frac{\partial {q_i}^*}{\partial c_i} + \sum_{j\neq i}^{Nc} \frac{\partial qi^*}{\partial c_j})\right]\right\}} \frac{\partial (c_i v)}{\partial z} = 0 \tag{3.13}$$

And in base of Eq. (3.13) the characteristic speed can be defined as shown in Eq. (3.14)

$$s = \frac{\frac{\partial (c_i v)}{\partial c_i}}{\left\{1 + \left[\frac{(1-\varepsilon)}{\varepsilon}(\frac{\partial {q_i}^*}{\partial c_i} + \sum_{j\neq i}^{Nc} \frac{\partial {q_i}^*}{\partial c_j})\right]\right\}} \tag{3.14}$$

In the case of shocks, a similar procedure to the one described from Eq.(3.5) to Eq. (3.8) can be applied to Eq.(3.10).

$$\varepsilon \int_{z_1}^{z_s} \frac{\partial c_i}{\partial t}\, dz + \int_{z_s}^{z_2} \varepsilon \frac{\partial (c_i v)}{\partial z}\, dz + \int_{z_1}^{z_s} (1-\varepsilon) \frac{\partial q_i{}^*}{\partial t}\, dz + \varepsilon \int_{z_1}^{z_s} \frac{\partial c_i}{\partial t}\, dz \int_{z_s}^{z_2} (1-\varepsilon) \frac{\partial q_i{}^*}{\partial t} dz = 0 \tag{3.15}$$

It is possible to arrive at an expression similar to Eq.(3.7) (using the same assumptions)

$$\varepsilon\, c_i^1 \frac{\partial z_s}{\partial t} - \varepsilon\, c_i^2 \frac{\partial z_s}{\partial t} + (1-\varepsilon) q_i^1 \frac{\partial z_s}{\partial t} - (1-\varepsilon) q_i^2 \frac{\partial z_s}{\partial t} + \varepsilon [v c_i]_1^2 = 0 \tag{3.16}$$

By reordering Eq. (3.16), the shock speed can be defined as follow:

$$s = \frac{\partial z_s}{\partial t} = \frac{\frac{[v c_i]_1^2}{[c_i]_1^2}}{1 + \frac{(1-\varepsilon)}{\varepsilon} \frac{[q_i]_1^2}{[c_i]_1^2}} \tag{3.17}$$

The level of difficulty to calculate the wave propagation or shock speed (Eq. (3.14)) or Eq.(3.17)) will vary according to the assumptions (isothermal/ non isothermal, isobaric/non isobaric) as well as the equilibrium model under consideration. In the case of multi-component or non-isothermal systems, it is important to take into account the concept of coherence condition stating that for all the components present in the mixture as well as for the temperature waves the propagation speed must be the same (Ruthven, 1984), An exact or a numerical Riemann solver for adsorption dynamics under Equilibrium Theory cannot violate this condition. As pointed out, the front velocity will be different according to whether a shock or a smooth solution occurs thus the evaluation of the characteristic speeds must be carried out.

The assumption of equilibrium theory has been employed by several authors to solve adsorption dynamics for simplified cases starting from the pioneering work of Glueckauf (1947). In the previous mentioned work and in the one published by Basmadjian and Coroyannakis (1987) thumb rules were presented in order to predict shocks and multi-transitions in trace and isothermal systems in which the adsorbing species obeyed Langmuir monosite isotherm. These rules are based on the characteristic method, the first Basmadjian or the second Glueckauf rule states that there will be a shock or discontinuity if the concentration

of the adsorbing species decreases along the column. By applying the assumption of trace system and Langmuir isotherm to Eq. (3.17), Eq. (3.18) can be obtained.

$$s = \frac{v}{(1 + \left(\frac{1-\varepsilon}{\varepsilon}\right)\frac{q_s b_i}{(1 + b_i c_i + b_j c_j)}} \tag{3.18}$$

If the concentration of the species decreases along the column, the characteristic speed increases thus it is likely that a characteristic cross will take place.

The second Basmadjian (first Glueckauf) rule applies to a mixture of two adsorbing species; it allows the solution of the adsorption dynamics by using a hodograph transformation. By applying the coherence condition, it can be said that characteristic for both species will be the same and it is possible to arrive at a quadratic expression in which the unknown will be $\frac{\partial c_i}{\partial c_j}$. The quadratic equation presents a positive discriminant leading to two real solutions, one negative and one positive. The hodograph transformation is based on the variable change defined in Eq. (3.19) and Eq. (3.20)**.**

$$p_i = \frac{b_i b_j c_i}{(b_j - b_i)} \tag{3.19}$$

$$p_j = \frac{b_i b_j c_j}{(b_j - b_i)} \tag{3.20}$$

The initial condition and the feed composition can be understood as two pairs in the new plane (p_i, p_j). For each pair, the positive and negative roots for $\frac{\partial qi^*}{\partial c_j}$ can be calculated as shown in **Figure 3.2**.

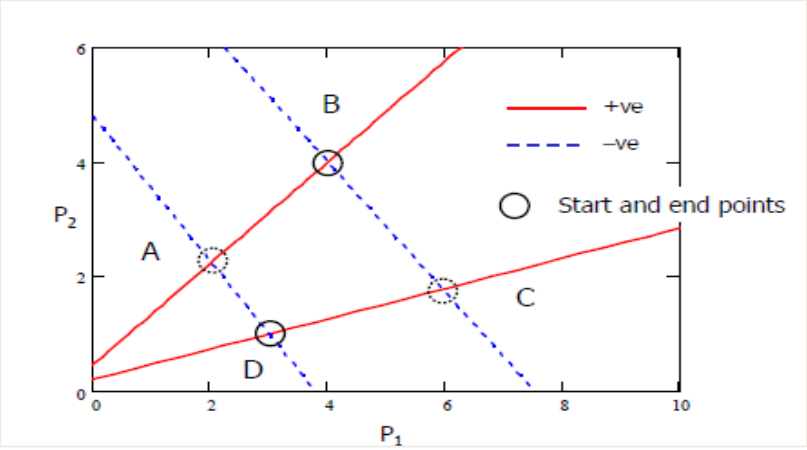

Figure 3.2: Glueckauf hodograph transformation

Each value of $\frac{\partial c_i}{\partial c_j}$ will be a slope in the plane(p_i, p_j). According to the intersection point, single or multiple transitions will be observed. If the intersection point takes place outside the first quadrant, the solution would not have physical meaning and a single transition will take place (as it will be reported for the analysed adsorption systems in chapter 4 and 6). If the intersection point lies in the first quadrant, it will be necessary to determine what path will lead to the correct physical solution using this empirical rule.

The rule states that the initial concentration (B) must travel through the direction of the positive slope till the intersection (A) with the negative slope of the feed composition $({p_i}^{inter}, {p_j}^{inter})$. The pair $({p_i}^{inter}, {p_j}^{inter})$ will be a function of the initial bed and feed compositions and the Langmuir parameters. In the case illustrated in **Figure 3.3,** the coordinates for A for both components (component 2 is the strongest adsorbing species) were higher than the corresponding to D. For component 2, the spatial profile leads to two plateaus that will be connected by a smooth function (following the second Glueckauf rule) as it is displayed in the **Figure 3.3.**

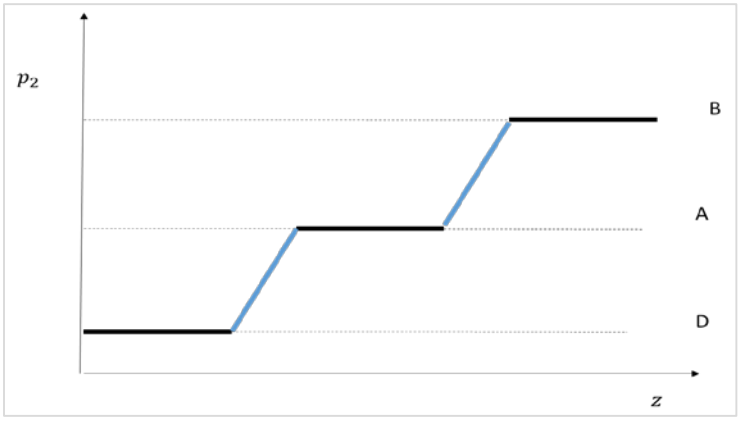

Figure 3.3: Spatial profile for the strongest adsorbing component. Multiple transition, desorption

For the least adsorbing species, the p_1 coordinate associated with the intersection point is lower than the one for D thus a profile like the one in **Figure 3.4** will be observed. This phenomenon can be explained due to the fact that the gas stream that enters to the column displaces further up the gas inside it. The initial gas in the column is richer in component 2 that is the strongest adsorbing species. Molecules of component 2 will tend to be more attracted by the solid thus a lower mole fraction of component 1 will be observed in the middle of the column meanwhile molecules of component 1 will occupy the other end of the column leading to higher mole fraction of this component in the gas mixture (2^{nd} plateau).

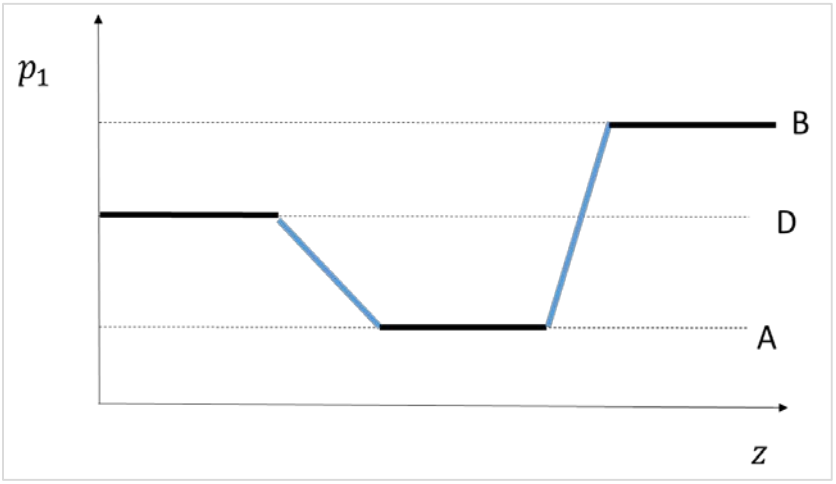

Figure 3.4 Spatial profile for the least adsorbing component. Multiple transition, desorption

In the case of studying the transitions to go from D to B, for the component 2 a decreasing evolution with an intermediate plateau can be observed. Following Glueckauf second rule/ Basmadjian first rule, the plateaus will be connected by shock transition as illustrated in **Figure 3.5**)

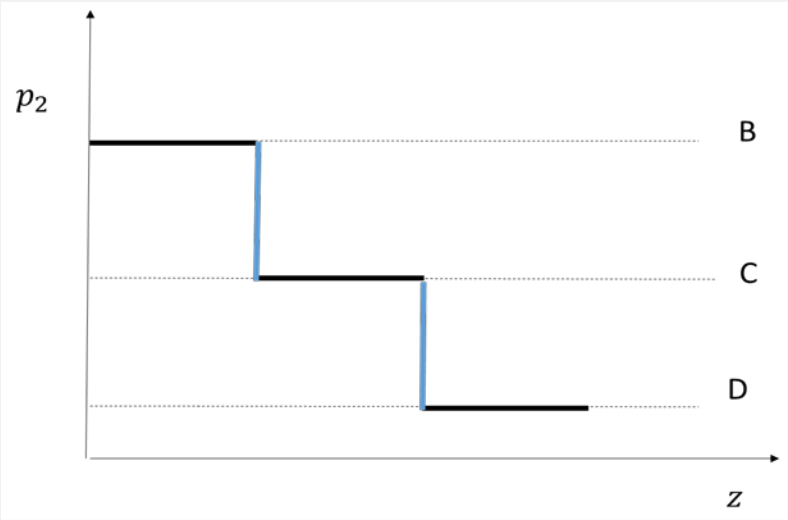

Figure 3.5: Spatial profile for the strongest adsorbing component. Multiple transition adsorption

For the least adsorbing component, an evolution in which the intermediate plateau presents larger values than the feed can be observed **(Figure 3.6**). This situation can be explained due to the fact that the gas that is entering to the column is moving ahead the initial gas in the bed that exhibits a lower mole fraction of both components. The molecules of component 2 will concentrate at the feed end since component 2 is the strongest adsorbing species meanwhile the molecules of component 1 will migrate to the middle of the column (1^{st} plateau). As soon as the front gas displaces, the initial gas in the bed will reach the other end of the column (2^{nd} plateau).

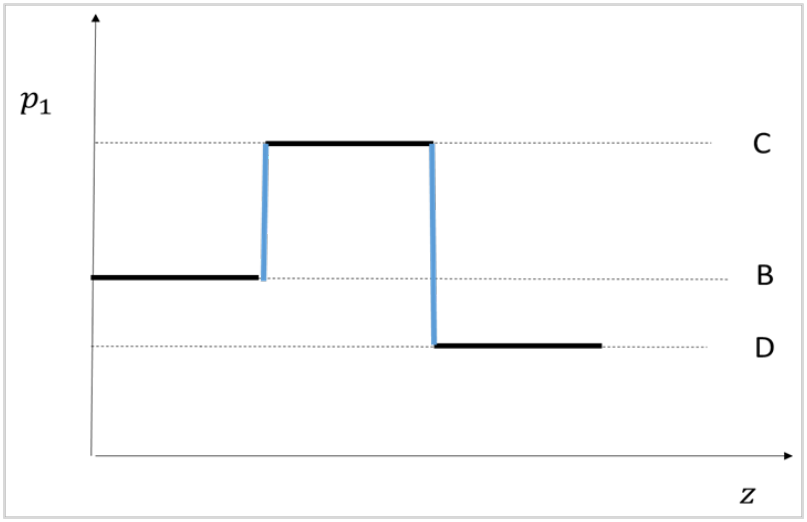

Figure 3.6: Spatial profile for the least adsorbing component. Multiple transition adsorption

As it was previously mentioned, the Glueckauf and Basmadjian rules apply to isothermal trace system but similar approach can be used for analysing non-isothermal systems. The concentration and temperature waves will move through the adsorption bed (Ruthven, 1984) leading to concentration and temperature shocks. The simplification of straight lines in the Glueckauf's hodograph transformation is no longer valid since Langmuir isotherm coefficients are functions of temperature. By applying the coherence condition to the component and energy balances, Rhee. (Rhee et al., 1970) derived an expression for $\frac{\partial c_i}{\partial T}$ and they exhibited the evolution for desorption from the initial conditions to the feed ones (A to B, in **Figure 3.7**) in the hodograph plane (c_i, T) in which $\frac{\partial c_i}{\partial T}$ was a function of the values of the intermediate points between the two states.

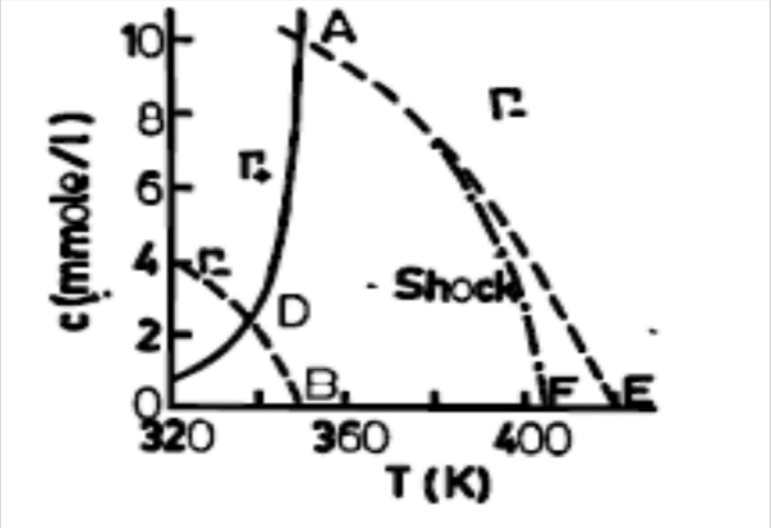

Figure 3.7: Concentration of the adsorbing species versus temperature (Rhee et al., 1970)

For each intermediate point it is possible to obtain the characteristic speed and plot the straight lines in the physical domain(z, t). If, in the physical plane, the evolution through the characteristics from the one corresponding to A to the one associated with B is carried out in a counter clock path, the characteristics will not cross and a smooth solution will be observed before and after the plateau as shown by the spatial profile displayed in **Figure 3.8**

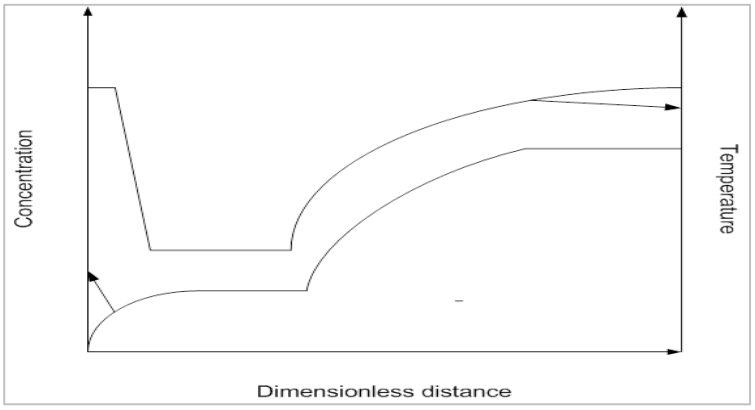

Figure 3.8: Spatial evolution of the concentration and temperature in the column

These authors also analysed a non-isothermal adsorption case and described conditions for which only thermal shocks can be observed (pure thermal wave). These results, despite the

assumption of trace system, are very useful at qualitative level and make it possible to predict what could be expected in more complex systems.

More recently Mazzotti (2006) calculated the exact solution for the Riemann problem associated with a general Langmuir isotherm in which the phase equilibrium for the adsorption species is described by a generalised Langmuir isotherm in which the Langmuir constant may be preceded by a positive or negative sign. By employing the assumption of trace systems they defined criteria to stablish entropy conditions for the different isotherm types under consideration.

All the previously cited works were focused on the dynamics of isobaric systems however in PSA cycles adsorption and desorption may take place during non-isobaric steps like pressurisation and blowdown. One of the first works attempting to solve dynamics in the pressurisation and blowdown steps was carried out by Knaebel and Hill (1987). They simulated air separation PSA cycles for recovering oxygen (less strongly adsorbing component) assuming that the phase equilibrium could be modelled by using linear uncoupled isotherms in order to calculate analytical expression for the column profiles at the cycle steady state. Kayser and Knaebel (1989) extended the work in Knabel and Hill (1987) by using non-linear uncoupled isotherms for the adsorbing species (N_2 and O_2) and they presented a relationship between the blowdown pressure and the mole fraction of the least adsorbing species. Ebner and Ritter (2002) developed an Equilibrium Theory applicable to a PSA system aiming to enrich a trace amount of the most strongly adsorbing component in the feed. They also considered the inclusion of a heavy reflux step in order to increase its purity.

For post combustion capture applications, the CO_2 mole fraction of feed gases to be treated ranges from 10 to 17 % if the stream comes from the burning of pulverised coal in a boiler. This value increases to 20-30 % for pre-combustion carbon capture in coal or biomass gasification plants in which water gas shift reactors are incorporated (NETL, 2007). Thus the assumption of trace system is no longer valid for the modelling of PSA cycles for carbon capture applications. CO_2 is the most strongly adsorbing species in the feed and Langmuir model is the most widely used isotherm to represent the phase equilibrium of CO_2 on the adsorbent. Consequently the application of characteristic methods for the simulation of the adsorption dynamics would lead to a set of non-linear coupled DAEs (differential algebraic equations) in which the concentration, temperature and superficial velocity are related with

each other. Solving the complex DAEs until the cyclic steady state reaching requires substantial computational load and time. The complexity of the problem makes necessary the use of an approximate Riemann solver for the hyperbolic systems under analysis.

3.4 Finite volume methods applied to the solution of hyperbolic problems

This section is dedicated to explain and summarise possible numerical methods based on the finite volume discretisation to be applied for the approximate solution of the Riemann-Cauchy problem. By using the finite volume discretisation method, the spatial domain is divided in cells for which the variable of interest may present a spatial functionality. In the case of the REA (Reconstruct-Evolve-Average), a polynomial function of the variable of interest is defined along the length of the cell (reconstruction); in the simplest cases, a piecewise constant function with the average in the cell can be defined. The Riemann problem is solved by using the values of the boundary of the cells at the current time step ($W^n_{j-\frac{1}{2}}$) (evolution) that allow to obtain the average value at the next time step ($\widetilde{W_j^{n+1}}$). **Figure 3.9** illustrates how the REA algorithm works; in the top part of the figure, the column profile at time t is displayed: a constant function was assumed and consequently $W^n_{j-\frac{1}{2}}$ is equal to$\widetilde{W^n_{j-1}}$. The wave front will evolve (as shown by the lines between the cells in the bottom part of the figure) and a new average for the variable of interest can be obtained at $t + dt$ enabling the redefinition (dotted line) of the cell profile.

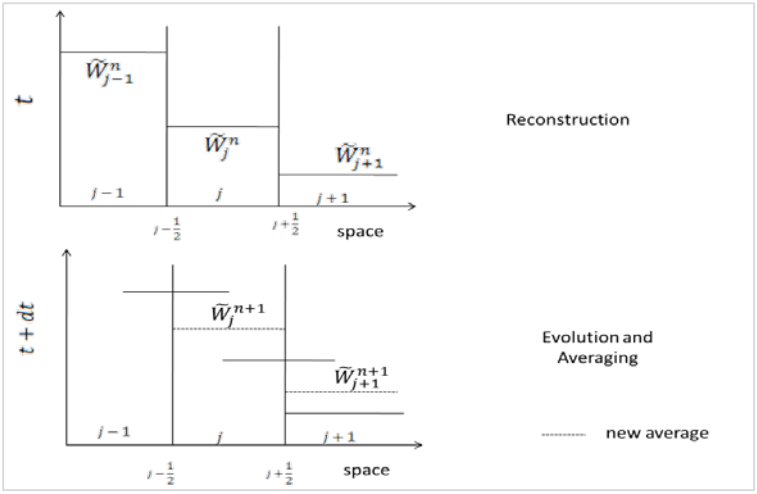

Figure 3.9: Spatial and time discretisation for REA type algorithm

In the case of equations written under a conservative form, the problem can be solved by using wave propagation or flux approach. In the following sub sections both approaches will be summarised; pointing out their advantages and disadvantages when they area applied to the solution of the Riemann problem associated with the adsorption dynamics under the assumption of Equilibrium Theory.

3.4.1 Wave propagation approach

The wave propagation approach is based on the characteristic method. It is possible to say that the temporal evolution of the variable of interest of a hyperbolic equation is caused by a wave that will propagate along the spatial domain. The propagation velocity will be determined by the characteristic function of the equation in the case of smooth solutions or by the velocity predicted by the Rankine-Hugoniot condition for discontinuous solution. The wave will take an amplitude equal to the difference of the variable of interest between the borders. If the propagation velocity is positive, the amplitude will be the difference between the variable of interest at the right border and the left border meanwhile if the velocity is negative, the amplitude will be calculated in the reverse way (Leveque, 2002).

This approach needs the imposition of an “entropy/ shock admissibility condition” to define whether a discontinuity will take place and to determine the way that the propagation velocity will be calculated (characteristics or Rankine Hugoniot). The concept of entropy

condition comes from the conservation laws (mass and energy balances) employed in gas dynamics, where the second law of thermodynamics demands that the entropy of a system must be non decreasing with time. Across a physically admissible shock the entropy of the gas increases but across an expansion shock, the entropy of the gas would decrease, which is not allowed (Sheng and Zhang, 1999). The entropy at each point can be computed as a simple function of the pressure and density. In a generic hyperbolic PDE, the simplest entropy conditions are based on the concept of characteristic crossing. For some problems, this simplified approach is not enough to determine the existence of unique admissible shocks due to the existence of not well understood viscous term path (Castro et al, 2008).

The most basic entropy condition that can be applied to adsorption dynamics is the fact that characteristic speed must decrease along the column in order to avoid a situation of cross like the one shown in **Figure 3.1** thus the evaluation of the characteristic speed is needed in each border of the cell making the simulation slow. Consequently the implementation of the wave propagation approach for the numerical simulation of PSA systems presents similar difficulties than the ones related to the characteristics methods.

Bourdarias et al. (2005; 2010) developed a numerical scheme for the Riemann-Cauchy problem associated with an isothermal, non-pressure drop adsorption step of a non-trace binary mixture using Langmuir isotherm. In the case of smooth solutions, a system of algebraic-differential equations must be solved in order to determine the relationship between the interstitial velocity and the concentration of the adsorbing species.

The assumption of isothermal adsorption as well as constant pressure with respect to time and space leads to say that $\frac{\partial C}{\partial t} = 0$ meanwhile negligible pressure drop yields to $\frac{\partial C}{\partial z} = 0$; consequently the global mass balance can be written as shown in Eq. (3.21)

$$\frac{\partial v}{\partial z} c_T = \sum_{i=1}^{Nc} \frac{\partial q_i^*}{\partial t} \tag{3.21}$$

In the case of one adsorbing species, i, existing, the RHS of Eq (3.21) can be simplified into the RHS of Eq. (3.22) by using the chain rule..

$$\frac{\partial v}{\partial z} c_T = \frac{\partial q_i{}^*}{\partial c_i} \frac{\partial c_i}{\partial t} \tag{3.22}$$

By obtaining $\frac{\partial c_i}{\partial t}$ from the component mass balance and by re-arranging it employing Eq. (3.22), it is possible to arrive at Eq. (3.23)

$$\frac{\partial v}{v} = -\frac{\partial q_i^*}{\partial c_i} \frac{1}{\left(1 + (\frac{1-\varepsilon}{\varepsilon})\frac{\partial q_i}{\partial c_i}\right)\left[C_T + \frac{\partial q_i}{\partial c_i}\frac{1}{(1 + (\frac{1-\varepsilon}{\varepsilon})\frac{\partial q_i}{\partial c_i}} c_i\right]} \tag{3.23}$$

For more than 1 component, the application of chain rule involves the evaluation of $\partial c_i / \partial c_j$ leading to a system of non-linear algebraic equations which complexity depends on the number of components since the solution of the adsorption dynamic problem must obey the coherence condition. The wave propagation approach guarantees stability since, for each cell and time interval, it is possible to obtain the characteristic equations and by using a stability condition (Courant Condition for example) to recalculate the simulation time step in case the numeric solution presents a diverging evolution.

3.4.2. Numerical Flux schemes

For those hyperbolic equations that can be written under a conservative form (Eq. 3.3), it can be said that the temporal evolution of the variable of interest is caused by the gradient of a flux of the same or other variables along the cells thus it is possible to estimate the average value of the variable of interest at the next time step using a numerical flux function. The updating expressions for the numerical approach are capable of tracking shock and smooth transitions; neither the imposition of a numerical entropy condition nor the calculation of the characteristics thus the implementation of the solver becomes independent of the equilibrium isotherm function. However a careful selection of the simulation step and grid size must be carried out to guarantee numerical stability involving choosing smaller simulation step time.

The updating expressions can be obtained by integrating the conservative equation shown in Eq. (3.3) in time and space and by applying the definitions of the average value of interest (Eq. (3.24)) and numerical flux (Eq. (3.27)).

$$\widetilde{W_j^n} = \frac{1}{\Delta z}\int_{z_{j-1/2}}^{z_{j+1/2}} W\,(z,t)\,dz \tag{3.24}$$

The expression for the conservation law defined in Eq. (3.3) can be integrated in the spatial domain as shown in Eq. (3.25).

$$\frac{\partial}{\partial t}\int_{z_{j-1/2}}^{z_{j+1/2}} W\,(z,t)\,dz + f\left(z_{j+\frac{1}{2}},t\right) - f\left(z_{j-\frac{1}{2}},t\right) = 0 \tag{3.25}$$

Integrating Eq. (3.25) in the time domain and applying definition of Eq. (3.22), it is possible to obtain:

$$(\widetilde{W}_j^{n+1} - \widetilde{W}_j^n)\Delta z + \int_{t_n}^{t_{n+1}}\left[f\left(z_{j+\frac{1}{2}},t\right) - f\left(z_{j-\frac{1}{2}},t\right)\right]dt = 0 \tag{3.26}$$

Defining the numerical flux by employing Eq. (3.27), the final expression for the updating formula will be the one presented in Eq. (3.28)

$$F_{j+1/2}^n = \frac{1}{\Delta t}\int_{t_n}^{t_{n+1}} f\left(z_{j+\frac{1}{2}},t\right)\,dt \tag{3.27}$$

$$\widetilde{W}_j^{n+1} = \widetilde{W}_j^n - \left[\frac{\Delta t}{\Delta z}(F_{j+\frac{1}{2}}^n - F_{j-\frac{1}{2}}^n)\right] \tag{3.28}$$

According to the profile of the variable of interest in the spatial and time domains, it was found that the selection of numerical schemes could affect the levels of accuracy (Lax – Wendroff, 1960; Warming-Beam, 1976; Toro, 2009). By using Eq. (3.28), it is possible to convert the coupled PDEs into a system of algebraic non-linear equations that must be solved in each grid at every simulation step time.

3.4.3. Godunov scheme

The Godunov scheme (Godunov, 1962) is a widely used numerical method for the solution of the hyperbolic equations arising from the modelling of several problems in the field of Engineering (Sheng and Zhang, 1999; Guinot 2003; Toro, 2009). It is a first order method (in space) thus the value of the variable of interest in the border of the cell ($W_{j-1/2}^{n}{}^{l}$) is given by the average value of the variable of interest ($\widetilde{W_j^n}$) and the numerical flux is kept constant during the step time. By applying these simplifications in the generic definition of the numerical flux (Eq. (3.29)), it is possible to obtain the updating formulas presented by Eq. (3.30).

$$F_{j-1/2}^{n} = \frac{1}{\Delta t}\int_{t_n}^{t_{n+1}} f\left(x_{j-\frac{1}{2}}, W\left(x_{j-\frac{1}{2}}, t\right).t\right)\, dt = f\left(x_{j-\frac{1}{2}}\widetilde{W}_{j-1}^{n}, t\right) \tag{3.29}$$

$$\widetilde{W}_j^{n+1} = \widetilde{W}_j^{n} - \left[\frac{\Delta t}{\Delta z}(f(\widetilde{W}_j^{n}, t) - (f(\widetilde{W}_{j+1}^{n}, t)\right] \tag{3.30}$$

First order schemes present larger numerical dispersion than higher order numerical methods requiring more grid points for the capture of a sharp shock. However they are stable and they do not generate oscillations. Higher order methods on the contrary present unphysical oscillations in the proximity of shocks in need of the use of flux limiters (Leveque, 2002), resulting in a longer simulation time. Therefore it was decided to use the Godunov scheme in the development of the pressure swing adsorption cycle solver that will be introduced in the next chapter.

Conclusions

The assumptions of negligible axial dispersion in combination with the Equilibrium Theory simplification convert the mathematical problem associated with adsorption dynamics into a system of coupled algebraic (solid phase) hyperbolic PDEs (gas phase). Several authors

have calculated the exact solution for the cases of trace component absorption systems under isothermal or isobaric conditions by using characteristics. For some simplified cases (non- trace and binary Langmuir systems), they managed to obtain thumb rules for shock tracking and predict column spatial profiles for the adsorbing species. These assumptions cannot be employed for modelling PSA cycles in the role of carbon capture technology and consequently the solution of the adsorption dynamics by using exact solvers (characteristic method) leads to complex algebraic-differential equations. An extensive literature review has been carried out in order to identify possible Finite Volume Riemann solvers. The application of wave and flux approach has been critically analysed. As a result of the undertaken literature review, it was decided to employ the Godunov numerical flux scheme in the development of the novel Equilibrium Theory PSA cycle solver that will be introduced in the next chapter.

The Godunov numerical flux scheme allows the solution of a system of hyperbolic equations without the imposition of an entropy condition; enabling the development of a PSA cycle solver that can be employed for simulating adsorption systems that obey any kind of equilibrium isotherm function without modifying its main code. A careful selection of the simulation step time must be carried out since the characteristic speeds are not being calculated thus a stability criteria cannot be used for checking and correcting possible diverging evolution in the solution of the system. Given the fact that the numerical scheme is a first order method, more grid points in comparison with higher order methods are required in order to avoid wave front dispersion. On the other side, numerical non physically realistic oscillations occur in the proximity of shock transitions when higher order schemes are employed for the discretisation of hyperbolic equations. Taking into account that this type of transitions is usually observed for the adsorption systems for carbon capture separation, it was decided that implementing higher order methods would not be suitable in the case of an Equilibrium Theory PSA cycle solver since despite these oscillations could be removed by the use of flux limiter algorithms, the code would be more complex and inefficient.

References

Basmadjian D, Coroyannakis P. Equilibrium Theory Revised. Isothermal Fixed-Bed Sorption of Binary Systems-I. Solutes obeying Binary Langmuir Isotherms. Chem. Eng. Sci. 1986; 42:1723-1735.

Beam R M., Robert F. Warming. An implicit finite-difference algorithm for hyperbolic systems in conservation-law form." Journal of computational physics. 1976; 22: 87-110.

Bourdarias C, Gisclon M, Junca S. Blow up at the hyperbolic boundary for a 2x2 system arising from Chemical Engineering. JHDE. 2010; 07: 297- 317.

Bourdarias C, Gisclon M, Junca S. Some mathematical results on a system of transport equations with an algebraic constraint describing fixed-bed adsorption of gases. J.Math.Anal.Appl. 2005; 313: 551-571.

Castro M J,. LeFloch P G, Muñoz-Ruiz M L, Parés C. Why many theories of shock waves are necessary: Convergence error in formally path-consistent schemes. Journal of Computational Physics.2008;227:8107-8129.

Ebner A, Ritter J. An Equilibrium Theory analysis of a rectifying PSA for heavy component . AIchE J. 2002; 48:1679-1691.

Glueckauf E. Theory of Chromatography VII. The general Theory of two solutes following non-linear isotherm. Discussion of the Faraday Society. 1947; 7.

Godunov SK. The problem of a generalized solution in the theory of quasilinear equations in gas dynamics. 1962 Russ.Math Surv. 17; 5: 145-165.

Kayser J C, Knaebel K S. Pressure Swing Adsorption: Development of an Equilibrium Theory for binary gas mixtures with non- linear isotherm. Chem. Eng. Soc.1989; 44: 1-8.

Knaebel K S, Hill F B. Pressure swing adsorption: development of an equilibrium theory for gas separations. Chem. Eng. Sci. 1987; 40: 2351-2360.

Lax P.D and Wendroff B.Systems of conservation lawsCommun. Pure Appl Math. 1960:13;217–237

Leveque R. Finite Volume Methods for Hyperbolic Problems. Cambridge University Press: Cambridge; 2002.

Mazzotti M. Local Equilibrium Theory for the Binary Chromatography of Species Subject to a Generalized Langmuir Isotherm. Ind. Eng .Chem.Res 2006; 45: 5332-5350.

NETL. Cost and Performance baseline for fossil energy plants , US Department of Energy 2007.

Rhee H, Heerdt E D, Amudson N R. An analysis of an Adiabatic Adsorption Column: Part II. Adsorption of a single solute. Chem. Eng. J. 1970; 1: 279-290.

Ruthven D M. Principles of Adsorption and Adsorption Processes . Brunswick : Wiley; 1984.

Shen W, Zhang T. The Riemann Problem for the Transportation Equations in Gas Dynamics. 1999; 654.

Toro, E. F. Riemann solvers and numerical methods for fluid dynamics: a practical introduction. 2009. Springer Science & Business Media.

Chapter 4: Development of an Equilibrium Theory solver applied to PSA cycles used in CCS.

Introduction

This chapter is scoped to present a new Equilibrium Theory PSA cycle solver (hereinafter called Esim). Numerical implementation for the novel software as well as result validation will be deeply discussed. Esim can be used for determining the thermodynamic limit performance that a given PSA cycle configuration may reach enabling as well a pre-selection of promising configurations for further analysis and optimisation. The novel tool just requires the equilibrium isotherm function as input data enabling the simulation of adsorption dynamics with fewer experimentally determined parameters.

Esim employs a numerical Godunov flux method allowing the simulation of multi-transition adsorption systems (multicomponent, non-trace and non-isothermal) for any kind of isotherm equilibrium functions without modifying the main code implementation neither smoothing the adsorption wave front. Results using the new software for an equilibrium based system for breakthrough curves and CO_2 enriching cycles have been compared against a gPROMS based code in which kinetic and dispersive effects can be accounted in the simulations. The comparison exercises show negligible differences between the outputs generated by both solvers.

4.1 Numerical implementation of Godunov method to solve mass and energy balances in adsorption columns

As it was mentioned in the previous chapter, the Godunov numerical flux scheme requires equations to be in conservative form (Leveque, 2002). The assumptions of the Equilibrium Theory and negligible mass and heat transfer resistances transform the mass and energy balances into non-linear, non-conservative hyperbolic equations as shown in Eq. (4.1), Eq. (4.2) and Eq. (4.3).

$$\varepsilon \frac{\partial (c_i v)}{\partial z} + \varepsilon \frac{\partial c_i}{\partial t} + (1-\varepsilon) \frac{\partial q_i{}^*}{\partial t} = 0 \tag{4.1}$$

$$\varepsilon \frac{\partial c_T}{\partial t} + \varepsilon \frac{\partial (c_T v)}{\partial z} + \sum_{i=1}^{Nc} (1-\varepsilon) \frac{\partial q_i^*}{\partial t} = 0 \tag{4.2}$$

$$\varepsilon \frac{\partial \left(\widetilde{H_f} v\right)}{\partial z} + \varepsilon \frac{\partial \widetilde{U_f}}{\partial t} + (1-\varepsilon) \frac{\partial \widetilde{U_{sol}}}{\partial t} = 0 \tag{4.3}$$

New variables need to be defined as displayed in Eqs. (4.4) to (4.6) in order to transform the mass and energy balances into a system of conservative hyperbolic equations

$$W_i = \varepsilon c_i + (1-\varepsilon) q_i{}^* \tag{4.4}$$

$$W_T = \varepsilon c_T + \sum_{i=1}^{Nc} (1-\varepsilon) q_i{}^* \tag{4.5}$$

$$W_{TE} = \varepsilon \widetilde{U_f} + (1-\varepsilon) \widetilde{U_{sol}} \tag{4.6}$$

The conservative numerical fluxes can be written as follow:

$$F_i = \varepsilon v c_i \tag{4.7}$$

$$F_T = \varepsilon v c_T \tag{4.8}$$

$$F_{TE} = \varepsilon \widetilde{H_f} v \tag{4.9}$$

The resulting conservative equations are presented in Eq. (4.10), Eq.(4.11) and Eq.(4.12)

$$\frac{\partial W_i}{\partial t} + \frac{\partial F_i}{\partial z} = 0 \tag{4.10}$$

$$\frac{\partial W_T}{\partial t} + \frac{\partial F_T}{\partial z} = 0 \tag{4.11}$$

$$\frac{\partial W_{TE}}{\partial t} + \frac{\partial F_{TE}}{\partial z} = 0 \tag{4.12}$$

The suggested variable change allows the use of the Godunov numerical flux scheme (Godunov, 1962) for the solution of the system. As explained in **Chapter 3,** the application of the Godunov numerical flux scheme (Eq. (3.30)) convert the system of PDEs into an algebraic system of equations as shown in Eq. (4.10), Eq. (4.11) and Eq. (4.12) respectively.

$$\widetilde{W_{i_j}^{n+1}} = \widetilde{W_{i_j}^{n}} - \left[\left(\frac{\Delta t}{\Delta z}\right)\left(F_{i_j} - F_{i_{j-1}}\right)\right] \tag{4.13}$$

$$\widetilde{W_{T_j}^{n+1}} = \widetilde{W_{T_j}^{n}} - \left[\left(\frac{\Delta t}{\Delta z}\right)\left(F_{T_j} - F_{T_{j-1}}\right)\right] \tag{4.14}$$

$$\widetilde{W_{TE_j}^{n+1}} = \widetilde{W_{TE_j}^{n}} - \left[\left(\frac{\Delta t}{\Delta z}\right)\left(F_{TE_j} - F_{TE_j-1}\right)\right] \tag{4.15}$$

In each cell of the column, the non-linear system of equations defined by Eqs. (4.4) to Eq. (4.9) and Eqs. (4.13) to Eq. (4.15) must be solved. According to the adsorption system under study (isotherm/non-isotherm or isobaric/non-isobaric) backward or forward schemes will be used for undertaking the discretisation of the spatial domain as it will be further discussed in the next section.

4.2 Numerical scheme for isobaric steps

In this work, the pressure drop along the column is considered to be negligible. The boundary conditions are assigned to the first cell of the column that is considered to be a ghost cell. As it was previously explained, neglecting axial dispersion transforms parabolic equations into hyperbolic equations and consequently just single sided boundary conditions for each variable are required (**Table 4.1).**

Table 4.1: Boundary conditions for-isobaric steps

Variable	Value
$c_i\ (z = 0)$	c_i^{feed}
$v\ (z = 0)$	v^{feed}
$T\ (z = 0)$	T^{feed}

In each cell, the non linear system of equations defined by Eq. (4.13) to Eq. (4.15) must be solved. In the case of non-isothermal simulations: $c_{i_j}^{n+1}, T_j^{n+1}, v_j^n$ and C_j^{n+1} must be calculated. Since no pressure drop and ideal gas law are assumed, the C_j^{n+1} can be obtained knowing T_j^{n+1} and P^{feed}.

4.3 Numerical scheme for non isobaric steps

For the non-isobaric steps (pressurisation and blowdown), there is a pressure evolution with time during the step. This evolution is quantified in Esim by using a linear relationship with the difference between the current pressure in the column and the sink/source pressure (Eq. (4.16) and Eq. (4.17)).

For pressurisation step:

$$\frac{\partial P}{\partial t} = \alpha \, (P_{source} - P) \tag{4.16}$$

For blowdown step:

$$\frac{\partial P}{\partial t} = \alpha \, (P - P_{sink}) \tag{4.17}$$

During the pressurisation and blowdown steps, the gas velocity at either ends of the column must be zero. This restriction acts as a boundary condition for the velocity, consequently the equations must be solved backwardly or forwardly starting from the cell where the gas velocity is zero. The unknowns in each cell will be v_{j-1}, $c_{i_j}^{n+1}$, C_j^{n+1} and T_j^{n+1}. Since both negligible pressure drop and ideal gas law have also been assumed, C_j^{n+1} can be calculated by using the column pressure estimated by either Eq. (4.16) or Eq. (4.17) and the temperature in each grid.

4.4 Validation of the results

Validation of the results is a crucial activity for the development of novel simulators. In general, this task is performed by using simple cases for which exact solutions are available. However, for the adsorption units under study, analytical expression for non-isothermal and non-trace systems cannot be found in literature. Since it is essential to prove that the novel software enables the simulation of multi-transition adsorption dynamics, the validation of the new tool must be undertaken by employing other available PSA cycle solvers.

The validation of the outputs of the novel software was carried out by employing an in house developed gPROMS based PSA cycle solver (Luberti et al., 2015) that enables to consider the influence of kinetic and dispersive effects. This application allows the simulation of the mass and energy balances in the adsorption column by using parabolic PDEs (Eq. (2.14) and (2.20) for the gas phase and macropore LDF model (Eq. (2.35) and Eq. (2.31)) for the adsorbed phase assuming micropore equilibrium as well. Isothermal and non-isothermal adsorption systems with or without pressure drop can be simulated; the user can choose different discretisation methods from the gPROMS library to solve the PDEs. Adsorption breakthrough curve and PSA cycle simulations have been undertaken and the results of the comparison/validation exercise are further described in the next sub-sessions.

4.4.1. Breakthrough simulations

Isothermal and non-isothermal CO_2 adsorption breakthrough curves have been modelled in order to show that Esim manages to track shocks at proper time and it is also capable of identifying multi transition systems (non-isothermal cases). Orthogonal Collocation Finite Elemental Method (OCFEM) with an order of 3 is the discretisation method in the gPROMS based code. To emulate the limiting assumption of the Equilibrium theory in the above mentioned application, the gPROMS simulations have been effectuated by using very small axial dispersion coefficients (1000 times smaller than the real ones) and very large k_{LDF}values (approx. 10 times larger than the real ones since oscillations were observed in those simulations in which more than 10 times larger k_{LDF}values)

The feed gas is a binary mixture of CO_2 and N_2 of which the CO_2 mole fraction is 0.15 as in the exhaust gas of a coal fired boiler power plant. Since these runs are intended to validate the software, possible impurities and their effect in the performance of the adsorptive units have not been considered. The presence of impurities would cause a decrease of CO_2 purity and recovery or else it would involve larger energy consumption to reach the same carbon capture targets when a CO_2 enriching cycle is being studied. In terms of solver implementation, each component that is included involves adding 2 equations (one PDE for the gas phase and 1 algebraic for the isotherm function in Esim or 1 ODE in the gPROMS code). Multicomponent systems will lead to multiple transitions even though for isothermal cases.

The parameters for activated carbon have been taken from Kikkinides et al. (1993), and the isotherms of CO_2 and N_2 on this adsorbent were fitted using Origin software under the Langmuir monosite extended model (Rao et al., 1999). The values for the gas specific heat at constant pressure used in the simulations are based on Reid (1987)**. Table 4.2** illustrates the values for the parameters used in the simulations.

Table 4.2: Parameters used in test simulation cases

Variable	Value	Variable	Value
L (m)[1]	0.5	q_s (mol/m^3)	2233
D_c(m)	0.025	$b^o_{CO_2}$(bar^{-1})	8.41e-6
ε	0.4	$b^o_{N_2}$(bar^{-1})	2.79e-4
Feed Flow (mol/s)	0.0051	ΔH_{CO_2} (J/mol)	30558
$y^{feed}_{CO_2}$	0.15	ΔH_{N_2}(J/mol)	15907
$y^{feed}_{N_2}$	0.85	Cpa_{CO_2}(J/mol K)	19.80
T^{feed}(K)	298	Cpb_{CO_2}(J/mol K^2)	0.0734
ρ_s(kg/m^3)[2]	708	Cpa_{N_2}(J/mol K)[3]	31.50
cp_s(J/kg k)	1046	Cpb_{N_2}(J/mol K	-0.01375e-2
$t_{ads} = t_{purge}$	50	$t_{press} = t_{blow}$	50

Figures 4.1 to 4.4 exhibit the temporal evolution of CO_2 concentration and temperature at the top end of the column for the isothermal and non-isothermal cases. The difference in CO_2 front breakthrough time between the two cases is consequence of the non-isothermal effect (**Figure 4.3)**. For the non-isothermal adsorption step time, two transitions can be observed. The

[1] Column dimension and flow to be processed based on the UoE VPSA Rig

[2] Solid properties and equilibrium data from Kikkinides et al., 1993

[3] Gas specific heat at constant pressure coefficients from Reid 1987.$C_{p_i} = C_{p_{a_i}} T + C_{p_{b_i}} T^2$

first one corresponds to thermal and concentration shocks at approx. 77 seconds at which the CO_2 mole fraction reaches the value of 0.146 (8.3614 mol/m^3) and then at around 1000 seconds a smooth transition takes place due to the incoming feed gas cooling the column gradually. The state of adsorption column reaches the feed temperature and concentration during the second transition ($y^f_{CO_2}$=0.15, $C^f_{CO_2}$=9.08 mol/m^3). For both the isothermal and non- isothermal cases it was confirmed that Esim managed to track the shocks properly since the two breakthrough curves around the sharp transitions have the same first order moment. It was observed that Esim could capture the shock properly with less smoothing effect for an equal number of grid points (150 volumes corresponds to 75 orthogonal collocation elements) thus it could be also said that Esim would manage to capture the shock with equal sharpness by using less number of grids.

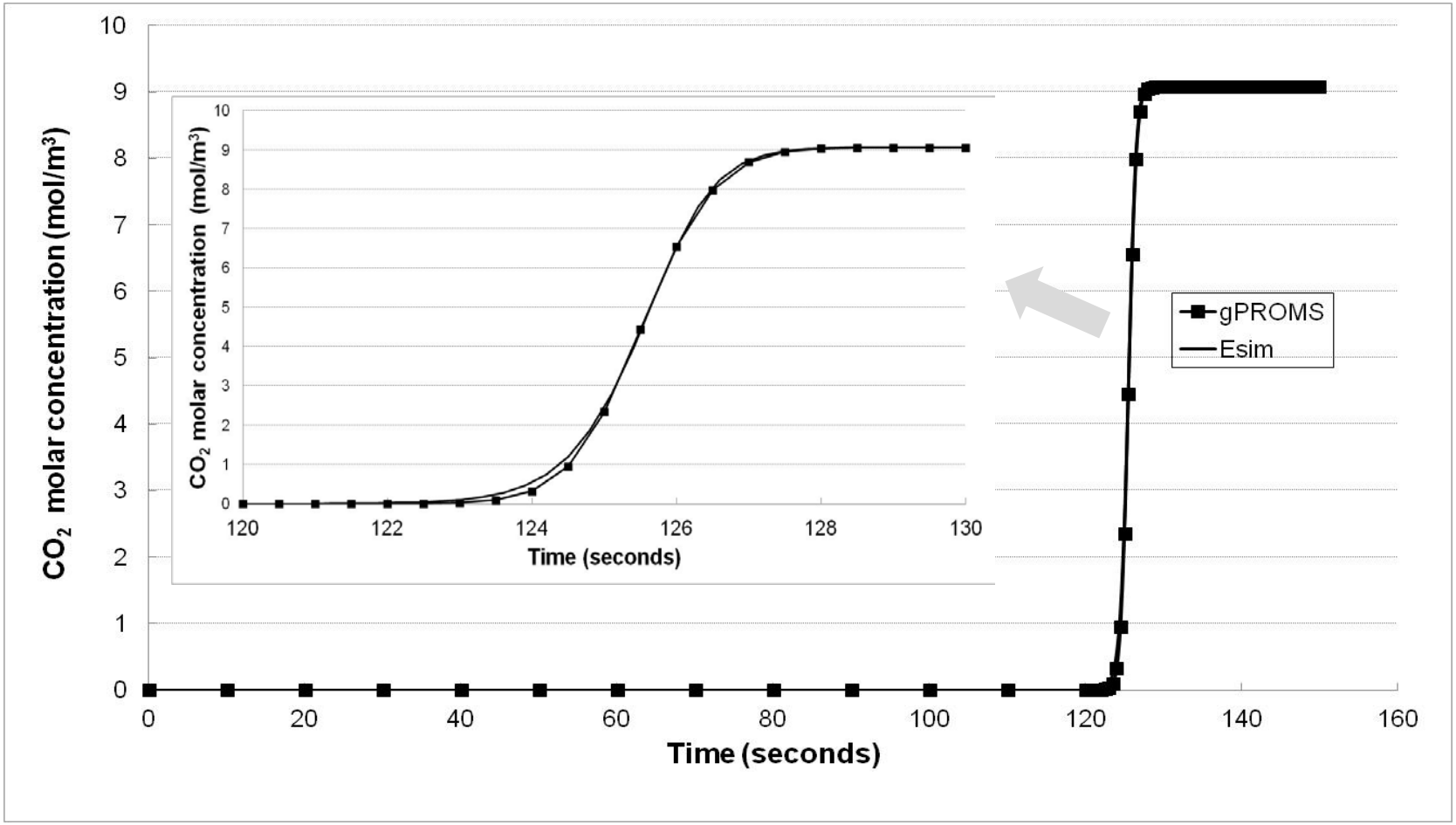

Figure 4.1: Isothermal concentration breakthrough curve

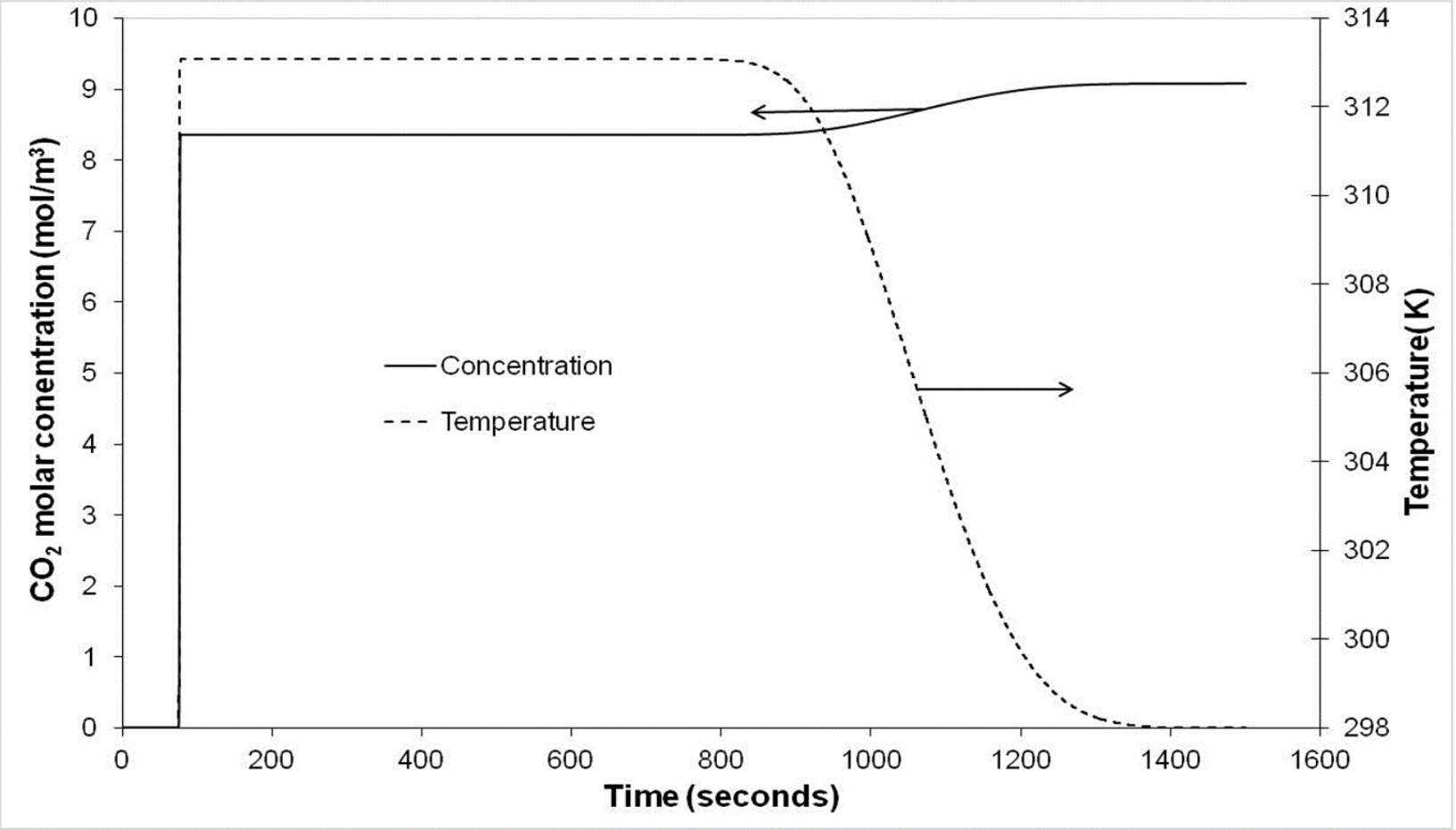

Figure 4.2: Transitions in the non –isothermal breakthrough simulation

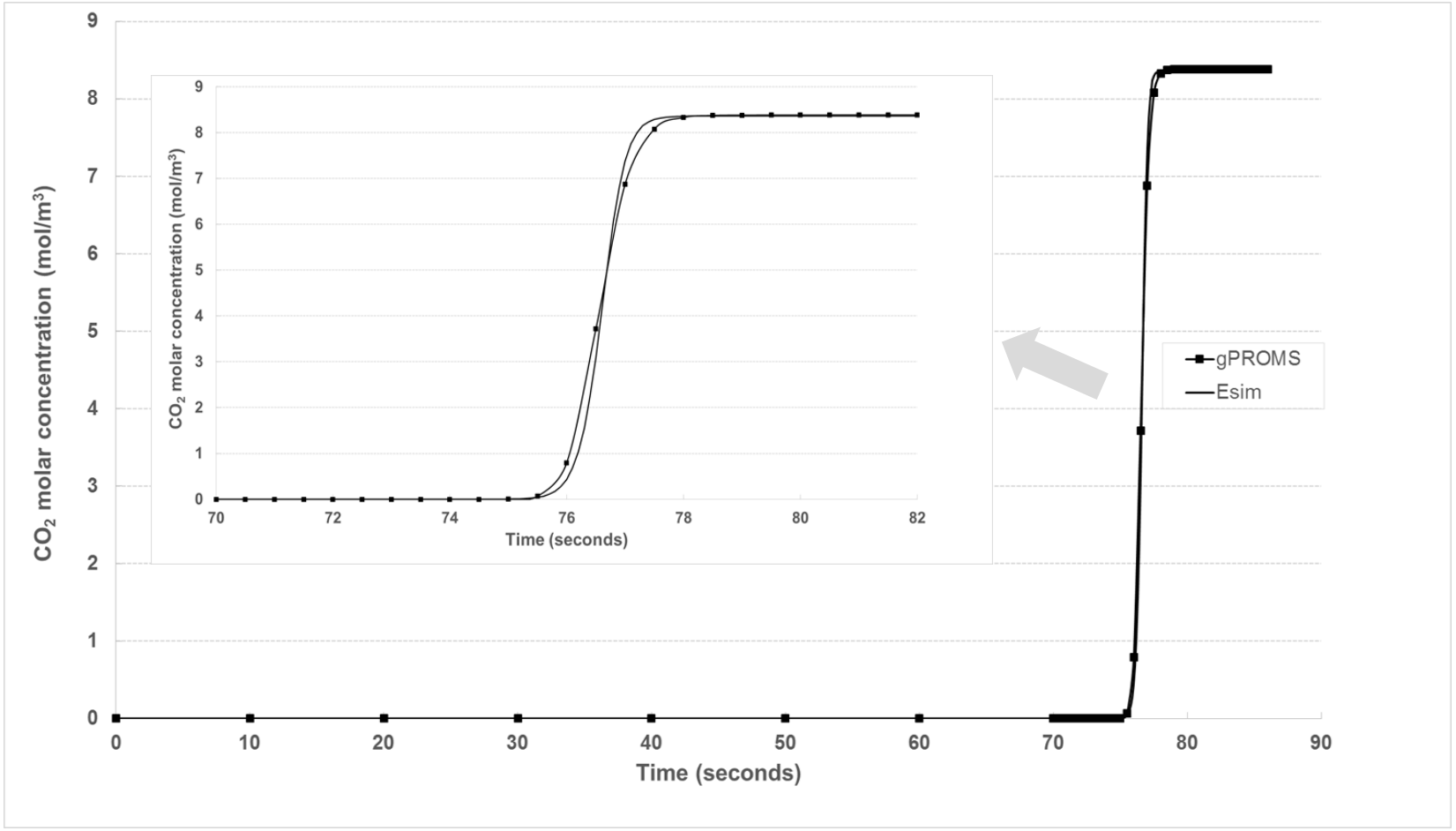

Figure 4.3: Non isothermal concentration breakthrough curve (1st transition)

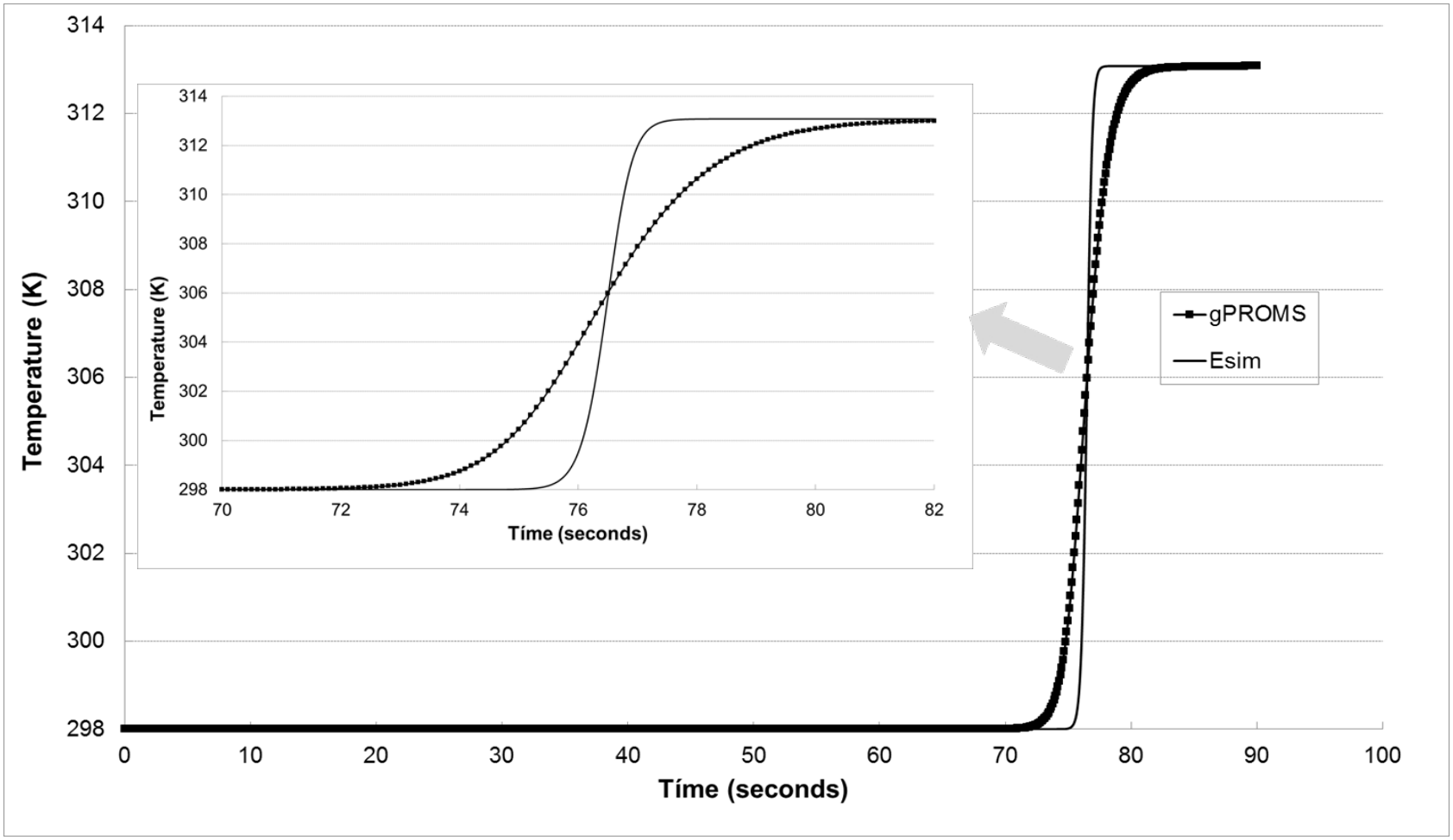

Figure 4.4: Temperature breakthrough curve

4.4.2. Numerical dispersion in Esim

The limiting case simulation imposed by the assumptions of the Equilibrium Theory and negligible axial and thermal dispersions may be useful to quantify intrinsic numerical dispersion associated with the schemes employed to solve the system of PDEs. It is possible to study the relationship between the number of grid points and the numerical dispersion by calculating the second order moment for an exponential decay (Eq. (4.18)). This approximation is valid when the concentration of the adsorbing species is very low (trace system) thus breakthrough curve simulations in which the CO_2 molar fraction was 0.01 and the balance N_2 was inert were carried out. **Figure 4.5** and **Figure 4.6** show the results for isothermal and non-isothermal breakthrough simulations using Esim, the corresponding gPROMS simulations with kinetic and axial dispersions coefficients that emulate the assumption of Equilibrium Theory and breakthrough curves for which the actual values for the these coefficients were employed.

Table 4.3 shows the values for the second order moment for each curve. The breakthrough simulations using Esim exhibit the lowest values for the second moment and the Equilibrium Theory emulation using gPROMS can be employed as a way of studying the intrinsic dispersion of the implemented scheme in the software since as it was previously explained limiting values for dispersion and kinetic coefficients were used.

$$\sigma^2 = 2\int_0^t (1 - \frac{c_i(t)}{c_{feed}})\, t\, dt - \gamma^2 \tag{4.18}$$

μ refers to the first order moment that can be obtained by using Eq. (4.19)

$$\gamma = \int_0^t \left(1 - \frac{c_i(t)}{c_{feed}}\right) dt \tag{4.19}$$

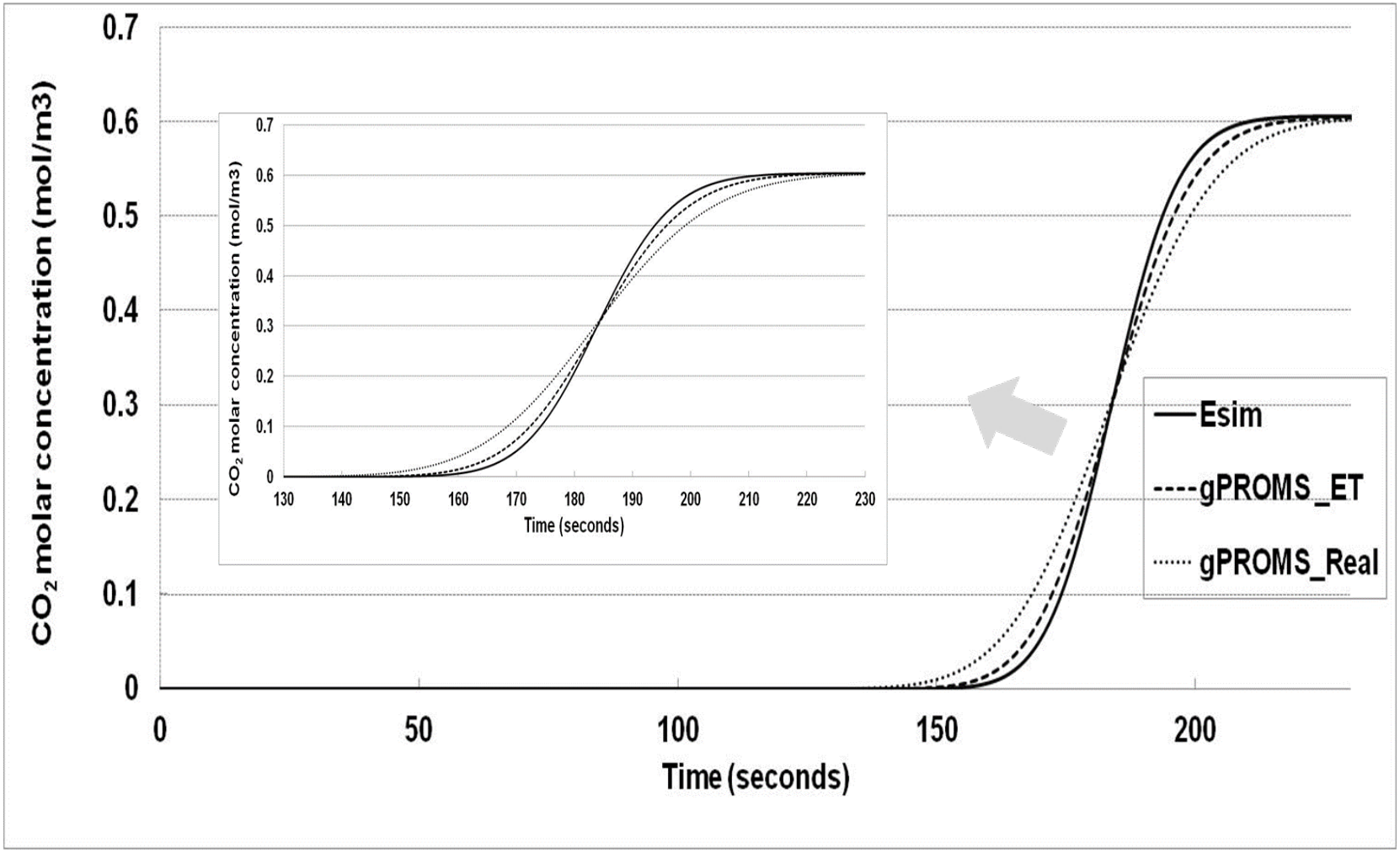

Figure 4. 5: Isothermal concentration breakthrough curve for trace systems

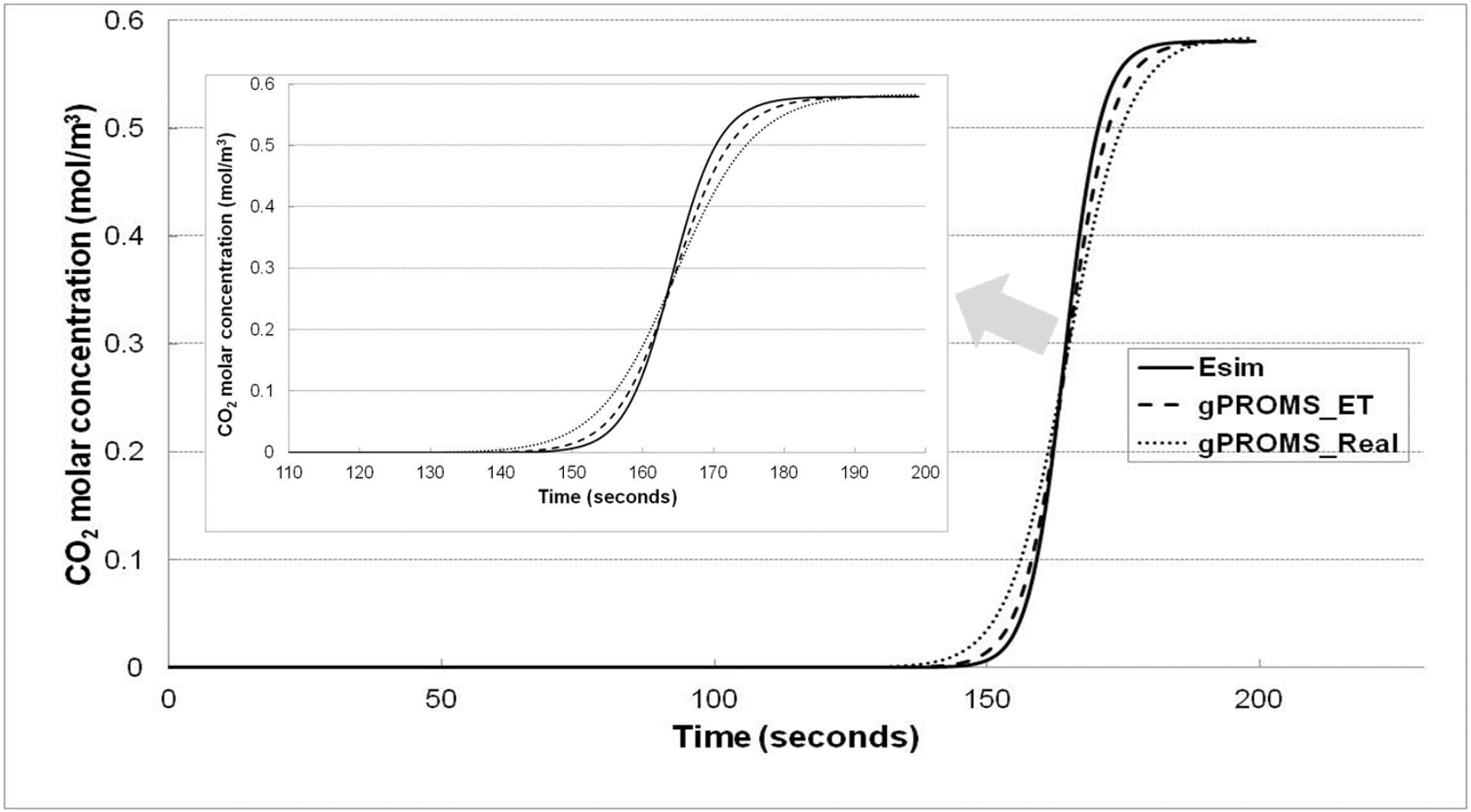

Figure 4. 6: Non Isothermal concentration breakthrough curve for trace system

Table 4.3: Second order moments for the isothermal and non-isothermal breakthrough

Breakthrough curve	Isothermal (σ^2)	Non Isothermal (σ^2)
Esim	80	35
gPROMS_Eq. Theory	92	53
gPROMS_Real	262	91

Isothermal breakthrough curve simulations with 100, 150, 200 and 400 grid points were carried out using Esim (**Figure 4.7**). The values for the second order moments for each curve are presented in **Table 4.4** and plotted against the associated number of grid points in **Figure 4.8.** A nearly quadratic inverse relationship between the number of grid points and the second order moment was found as can be seen from the regression shown in the plot.

Table 4.4: Second order moments

Grids	Second order moments
50	570
100	180
150	80
200	45
400	15

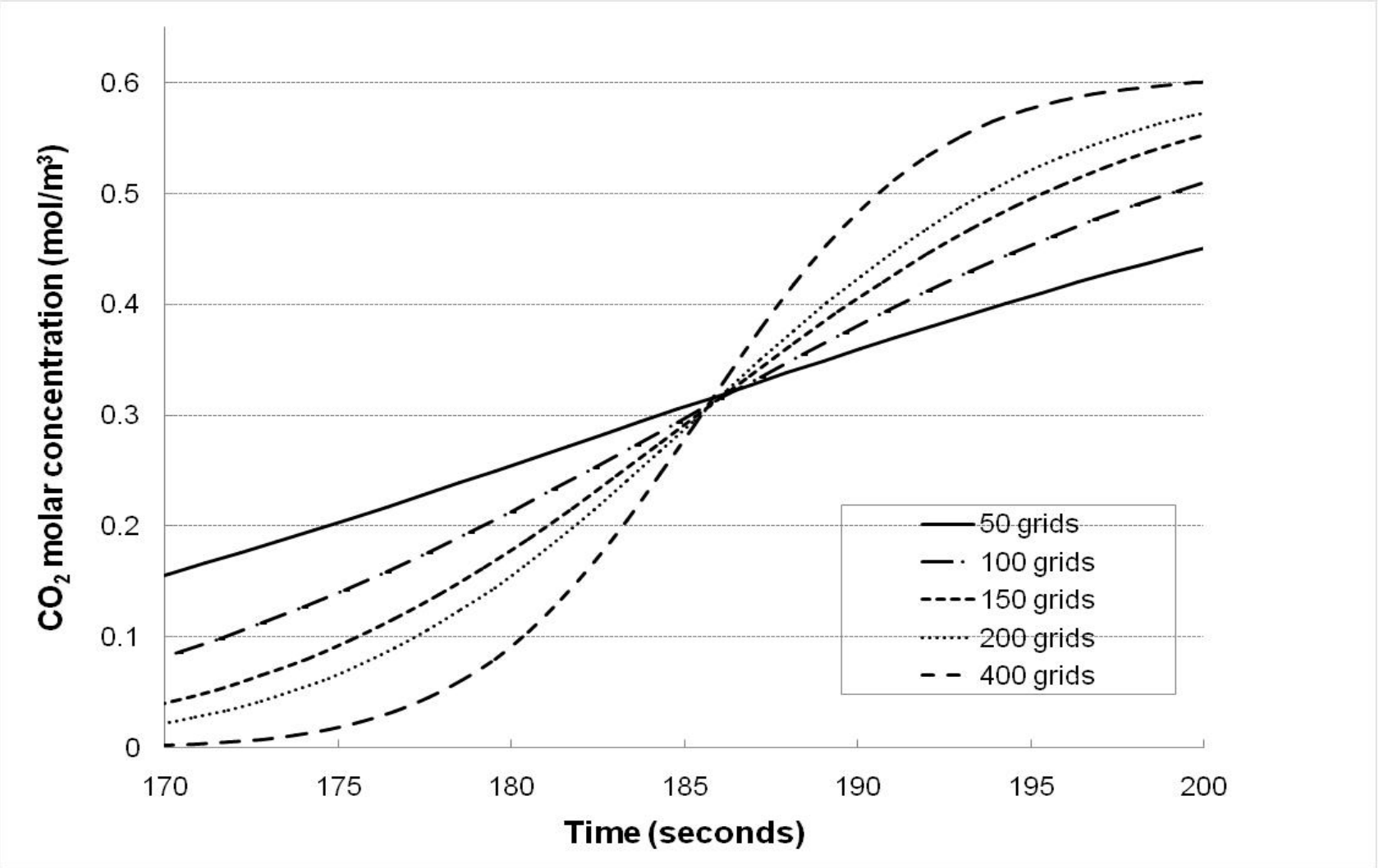

Figure 4.7: Isothermal breakthrough curves generated by Esim employing 100,150,200 and 400 grids for the simulation

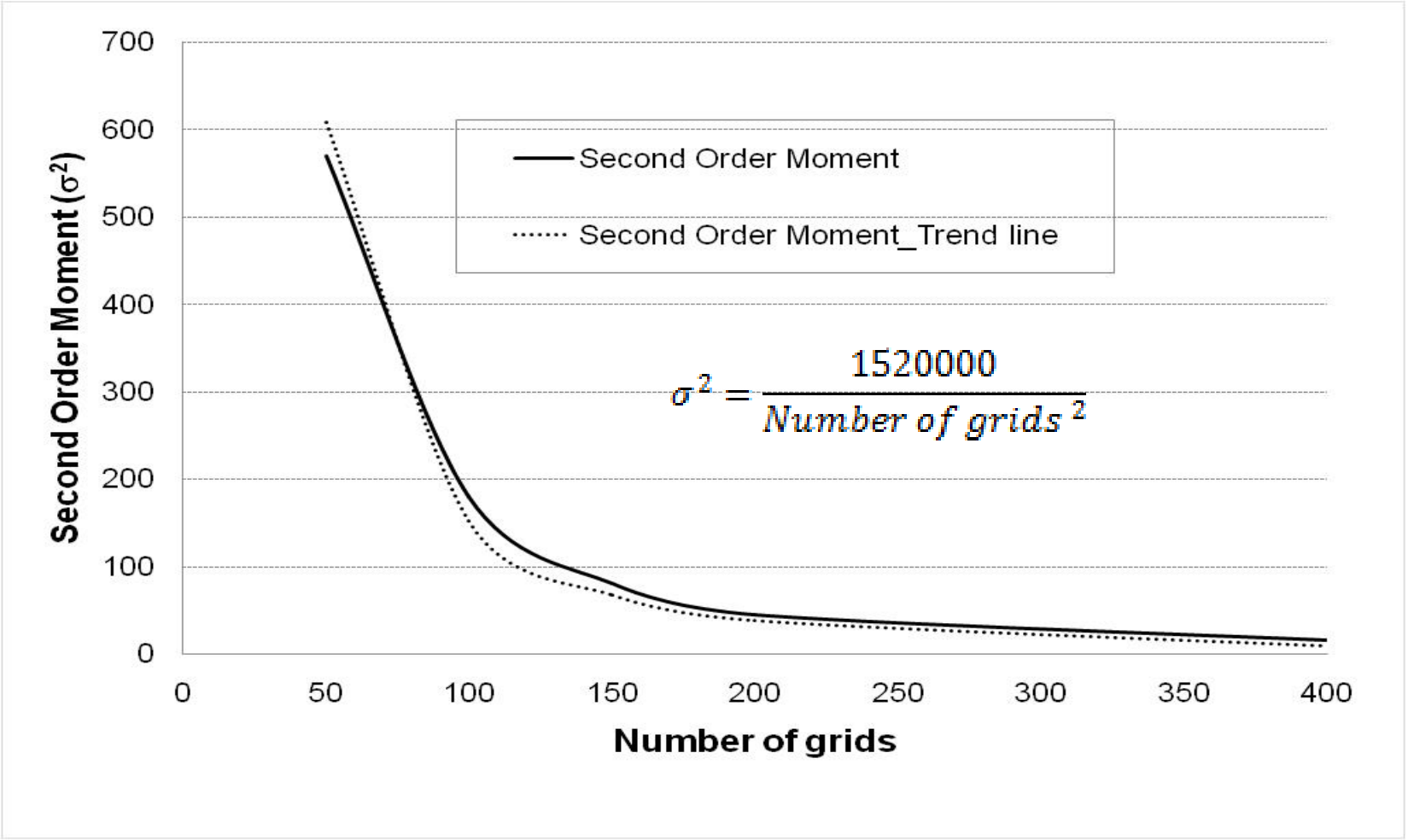

Figure 4.8: Relationship between the number of grids and the second order moment for the breakthrough curve

4.4.3. CO_2 enriching PSA cycle simulations

The generated results employing Esim for a CO_2 enriching PSA unit at its cyclic steady state have been validated against the simulations for the same system produced by using the gPROMS based code in which the full governing equations are implemented and the actual mass and heat resistances parameters were used as input. As a test/validation/application case, a non-isothermal, non-trace system was considered. It was decided to simulate the first stage of a post combustion adsorptive unit. The changes in pressure, CO_2 mole fraction and temperature at the bottom end of the column in a cycle at CSS are presented in **Figure 4.8, 4.9 and 4.10** respectively. It can be observed a close agreement (at cycle steady state) between the results produced by the two simulation tools since the CO_2 enriching PSA system under study is dominated by adsorption equilibrium rather than by adsorption kinetics. It was also noted that the Esim simulation managed to reach CSS with a lower number of cycle (16 cycles) than the gPROMS simulation (30 cycles) as shown in **Figure 4.12 and 4.13**.

During the first cycles in which kinetic and dispersive effect are more relevant, larger differences between the performance parameters predicted by Esim and gPROMS can be observed. Esim results for the first cycles are more optimistic than the values predicted by the gPROMS based code thus it shows that the novel software could be useful for undertaking a pre-selection of promising configurations, discarding those ones with poor performance and focusing optimisation studies for high separation efficiency cycles by employing full governing equations with empirically determined diffusion coefficients. It must be underlined that in the case of kinetically driven separation (crystalline sorbents, low temperature and high pressure), non-negligible differences could be found between the CSS performance parameters predicted by Esim and the real ones thus simulations using full governing equations should be effectuated in order to design these PSA cycles.

.

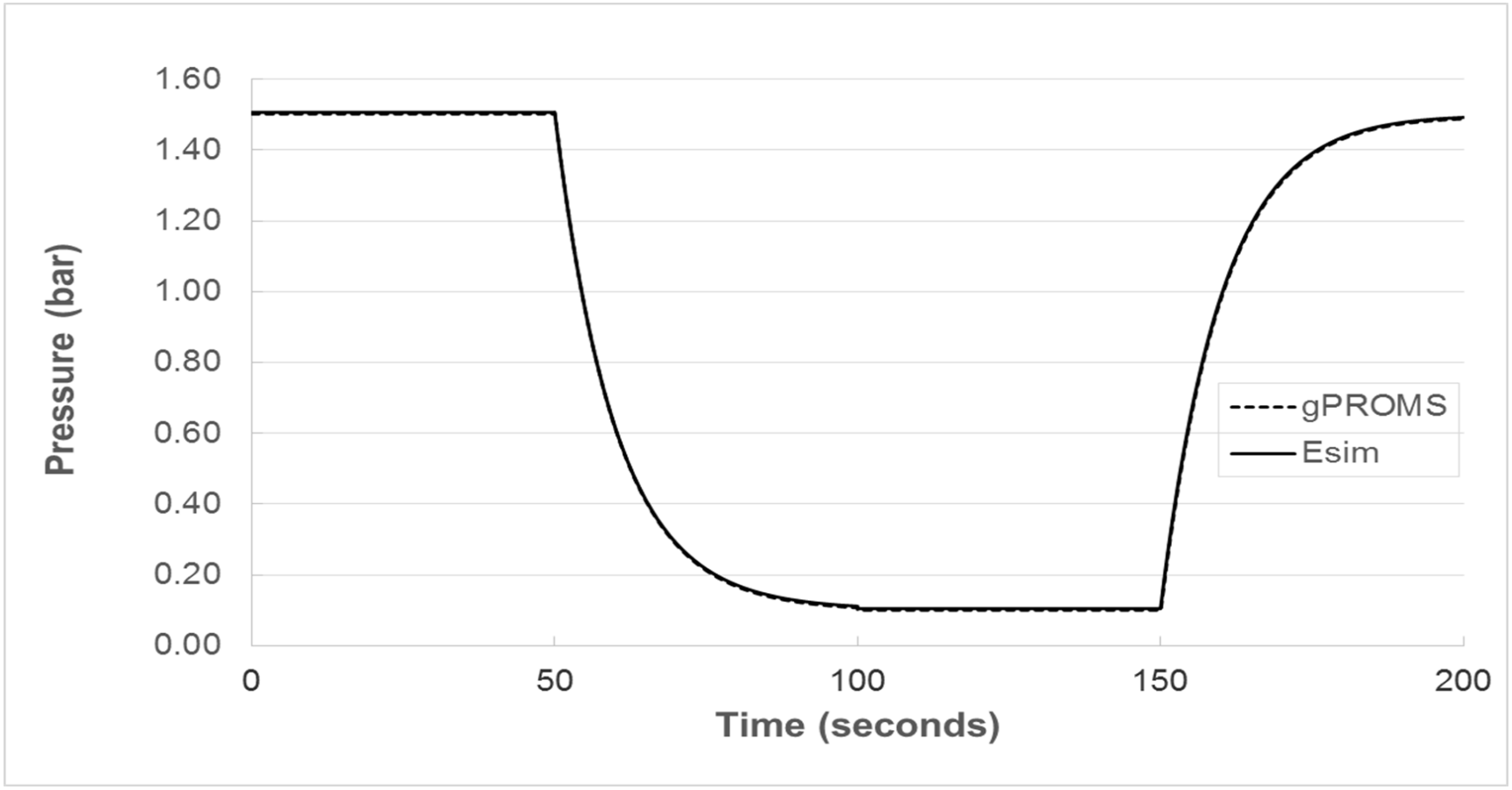

Figure 4.9: Comparison of pressure cyclic evolution at CSS

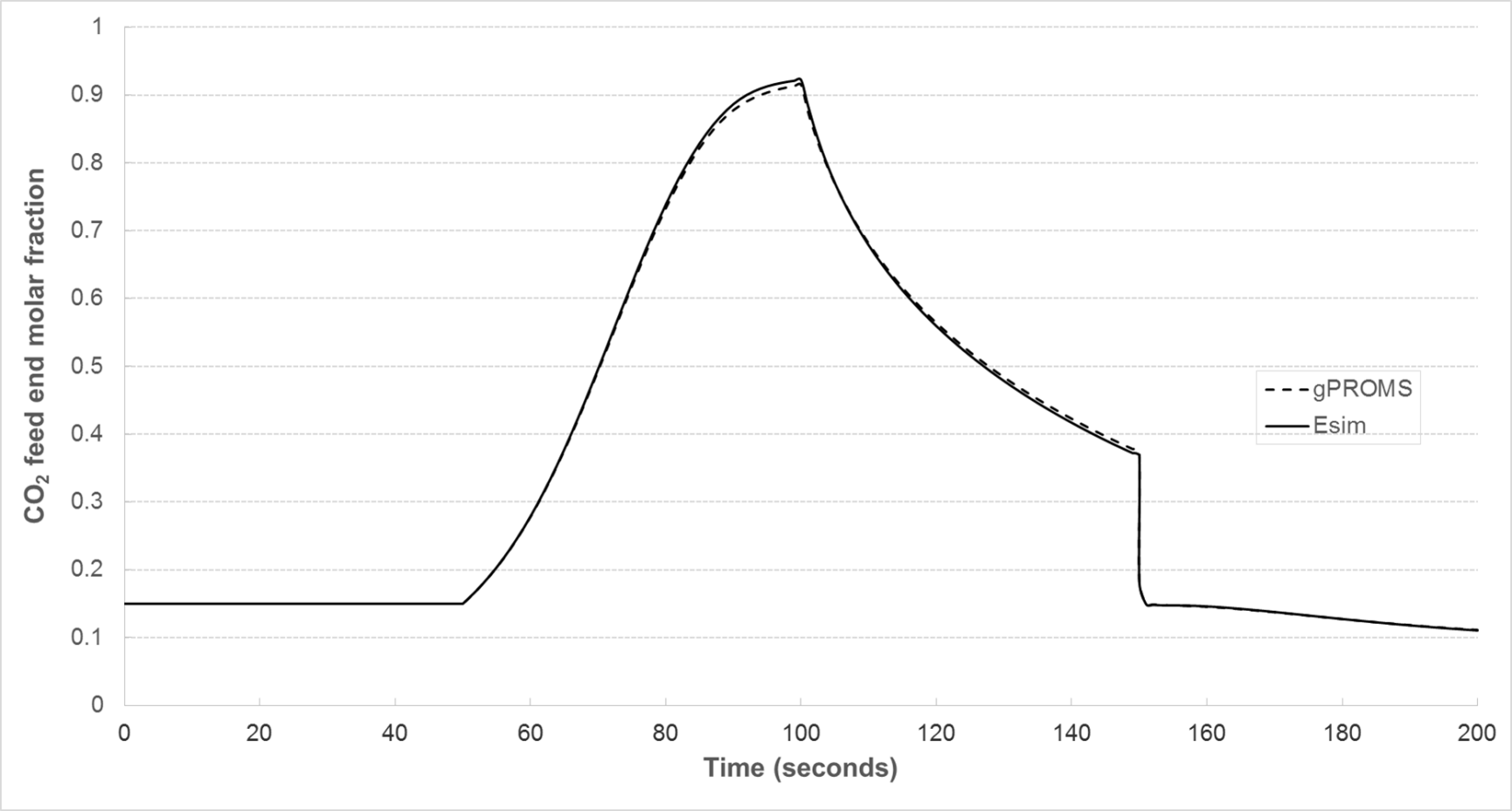

Figure 4.10: Comparison of CO_2 molar fraction cyclic evolution at CSS

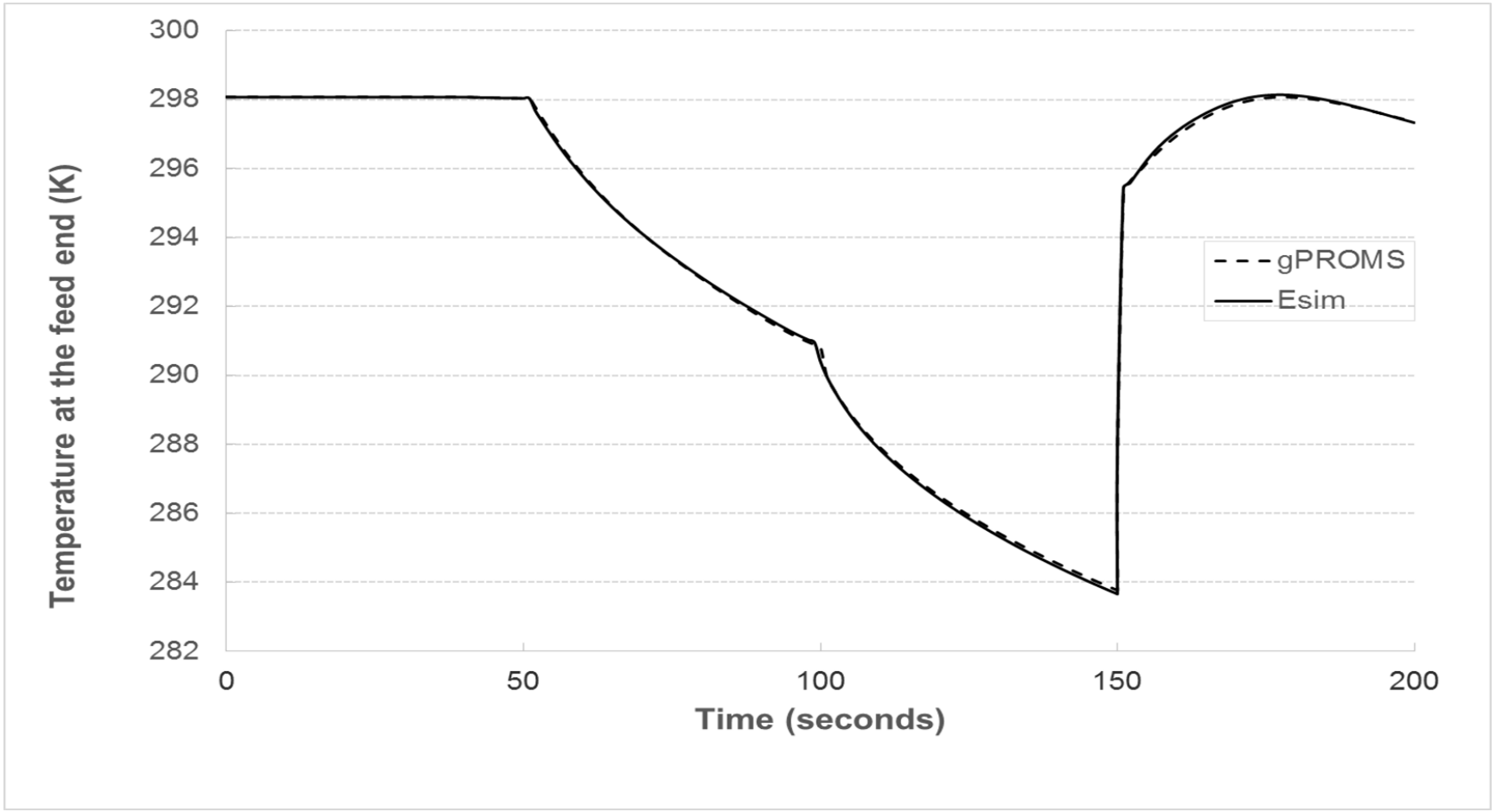

Figure 4.11: Comparison of temperature cyclic evolution at CCS

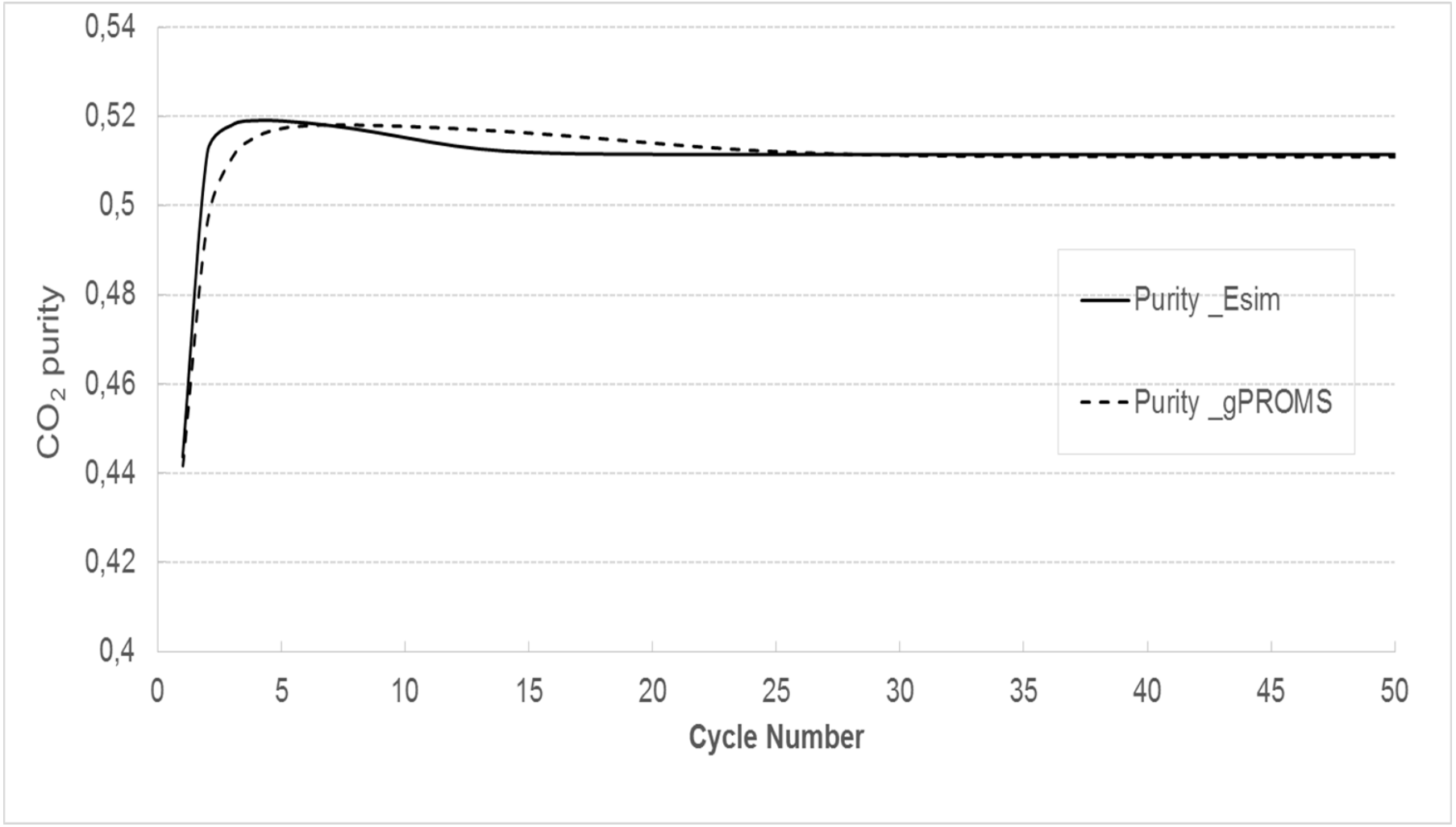

Figure 4.12: Evolution of CO_2 cyclic purity

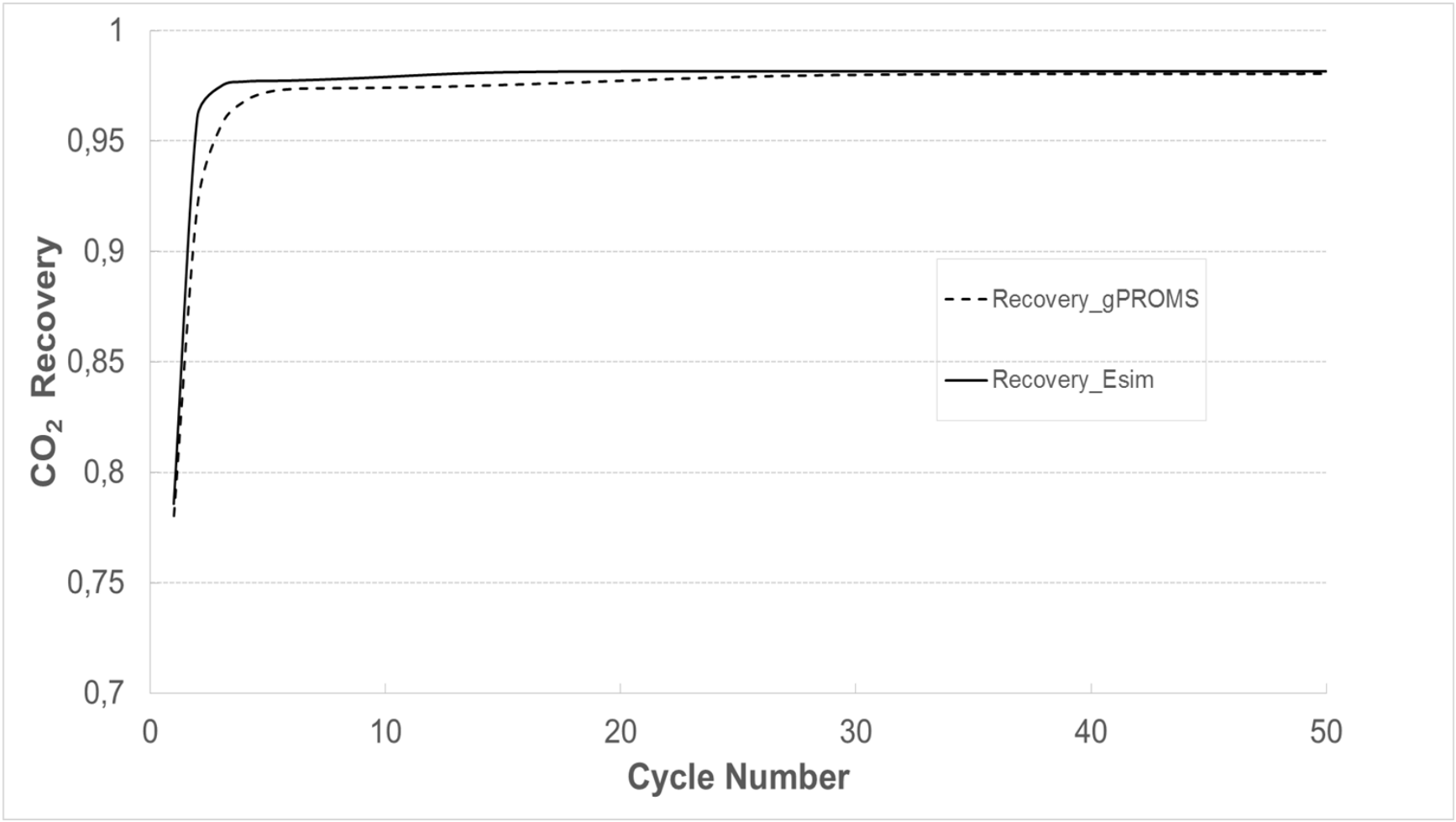

Figure 4.13: Evolution of CO_2 cyclic recovery

Conclusions

In this chapter, a new Equilibrium Theory PSA cycle solver was introduced. The novel tool allows the estimation of the equilibrium limiting performance for a given adsorption process and the identification of a set of high separation efficiency configurations by just using the isotherm equilibrium function as input data. The pre-selected PSA cycles will be modelled by employing full governing equation solvers before being installed in the role of an adsorption separation unit. These accurate simulations require experimentally determined kinetic coefficients. The undertaken pre-selection of operating conditions by using the Eq. Theory solver enables to focus the experiments for a narrower range of operating conditions thus reducing the number of empirical determinations for the diffusion coefficients. Results generated by Esim present negligible differences than the ones produced by full governing equation software when equilibrium based systems are modelled. However larger differences could be observed in the case of kinetically driven separations (crystalline sorbents, low temperature and relatively high pressure) consequently, for those cases, Esim can be used as a first approximation tool for discarding poor performance cycles before carrying out full governing equation simulations that, as it was previously explained, need empirically determined diffusion coefficients as input data

The simplifications associated with the Equilibrium Theory and the fact of considering axial dispersion to be negligible convert the mass and the energy balances in an adsorption column into a system of hyperbolic equations. A conservative variable change has been defined allowing the use of the Godunov numerical flux scheme. Esim is capable of solving the dynamics associated with multicomponent non-isothermal non trace multi transition adsorption systems without the need of imposing a numerical entropy condition; enabling the use of the solver for modelling systems that obey any kind of isotherm equilibrium function without the need of modifying the main code of the software.

Esim results were validated by comparing them against the outputs of a gPROMS based application in which simulations were undertaken by using micropore

equilibrium and macropore LDF model. The limiting case assumption of the Equilibrium Theory was emulated by employing very large k_{LDF} and very small axial dispersion coefficients. It could be observed as well that Esim manages to properly track shocks and smooth transitions since the first order moment for the breakthrough curves generated by Esim are equal to the ones corresponding to the curves produced by the gPROMS based solver; showing the correct implementation of the novel tool.

Esim convergence to CSS has also been studied by simulating a non-isothermal non trace binary adsorption equilibrium based system in the role of CO_2 post combustion capture technology. Cyclic pressure, CO_2 mole fraction and temperature evolution were compared against the ones produced by the gPROMS based code and negligible differences were reported. Esim managed as well to converge at CSS by using fewer cycles (approx.. 16 cycles are required not to observe significant changes in CO_2 recovery and purity meanwhile 30 cycles are needed in the case of the gPROMS based application).

It can be concluded that the new software introduced in this chapter reduces the complexity of the modelling of adsorption dynamics by requiring less empirical data and a simpler code in order to undertake a quick scan of operating conditions and cycle configurations for the design of PSA cycles. Its implementation enables the simulation of generic adsorption systems without modifying the code structure allowing as well CSS reaching with fewer cycles, being pioneer in its kind due to these features.

References

Friedrich D, Ferrari M C , Brandani S. Efficient Simulation and Acceleration of Convergence for a Dual Piston Pressure Swing Adsorption System . Ind. Chem. Eng. Res. 2013; 52: 8897-8905

Leveque R. Finite Volume Methods for Hyperbolic Problems. Cambridge University Press: Cambridge; 2002.

Godunov SK. The problem of a generalized solution in the theory of quasilinear equations in gas dynamics. Russ.Math Surv. 1962; 17; 5: 145-165.

Hindmarsh A C, Brown P N, Grant K E, Lee S L, Serban R, Shumaker D E, Woodward C S. SUNDIALS: Suite of non-linear and differential/ algebraic equations solvers. Journal ACM Transition on Mathematical Software (TOMS)- Special issue on the Advanced Computational Software (ACTS) Collection. 2005; 31; 3: 363-396.

Kikkinides E S, Yang R T, Cho S H. Concentration and Recovery of CO_2 from Flue Gas by Pressure Swing Adsorption. Ind. Eng. Chem. Res. 1993; 32: 2714-2720.

Luberti M, Kim Y H, Lee C. H, Ferrari, M. C, Ahn, H. New momentum and energy balance equations considering kinetic energy effect for mathematical modelling of a fixed bed adsorption column. 2015 Adsorption, 1-11.

Rao M B ,Sircar S. Thermodynamic Consistency for Binary Gas Adsorption Equilibria. Langmuir. 1999; 15: 7258-7267

Reid R,Prausnitz,Bruce E. The Properties of Gases and Liquids. McGraw-Hill, New York;1987.

Chapter 5: Biomass gasification combined heat and power plant (CHP)

(Base case without carbon capture)

Introduction

One of the key goal of this thesis is to study the feasibility of adsorptive processes in the role of CCS technologies in energy generation plants. Given the fact that the University of Edinburgh is planning to build a biomass gasification CHP in one of its campus, it was decided to study the feasibility of the incorporation of PSA cycles to reduce the carbon intensity of this kind of power plants. It is also relevant to underline that BioCCS plants are expected to play a key role in the future energy matrix since they allow electricity generation with negative CO_2 emissions thus they are considered to be an economically viable tool for mitigating climate change impacts for energy industries (Azar et al., 2013 and IPCC, 2014).

A biomass gasification CHP with a gas engine was designed following the flow sheet of the currently operating Gussing plant (Simader, 2004); excluding the Fisher Tropsch process in which part of the syngas is converted into liquid fuels. This plant is considered to be “a best practice case” in Europe due to its high overall efficiency (Coach Bioenergy, 2015) and it has been in operation for more than 13 years. In the above mentioned plant, the biomass feed is converted into syngas in a steam, atmospheric Fast Internally Circulating Fluidized Bed (FICFB) reactor and the produced syngas is burned in a GE Jenbacher Type 6 gas engine for power and heat generation.

This chapter is intended to present the flow-sheet of the plant under study, to explain the advantages of the FCIFB configuration against other currently available gasification technologies and to describe the gasifier and gas engine modelling effectuated using Unisim Honeywell Process Design. The outputs of the simulations

were validated against peer reviewed journal papers for the reference plant and against the information provided by the gas engine vendor.

5.1 CHP plants and their role in the energy matrix

CHP plants enable the cogeneration of heat and power, they are used for satisfying the demand of the residential sector and small to medium companies (DEEC, 2010). A large proportion of the low temperature (between 60 to 90°C) heat production takes place in this kind of plants in Northern European countries as displayed in **Figure 5.1**

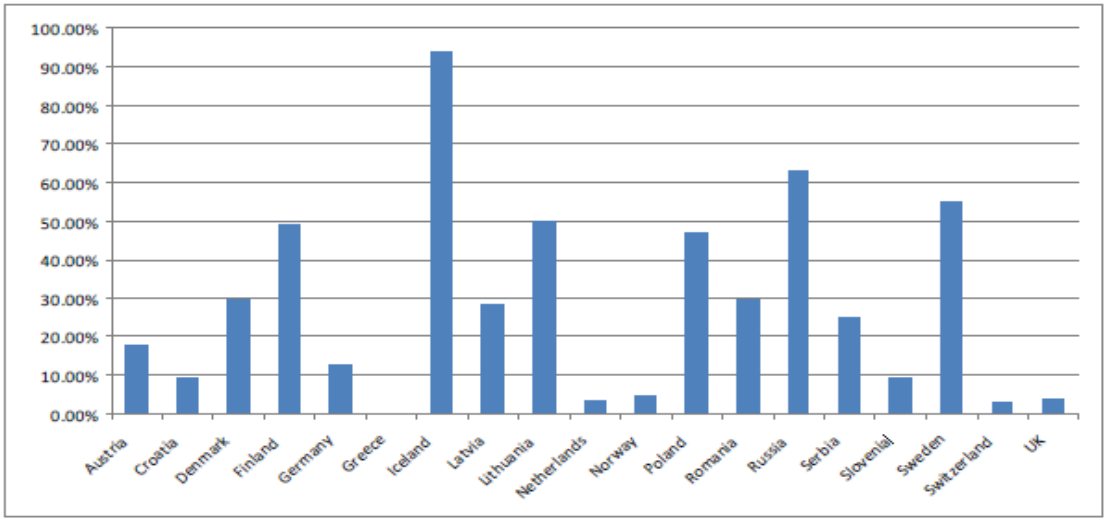

Figure 5.1: CHP share in heat demand in the European Union (JRC, 2012)

Data regaring the CHP share in electricity generation in several European countries can be observed in **Figure 5.2**. Analogously to the heat market, the role of CHPs in the electricity market is more relevant in Scandinavian and Northern European

countries. In the case of Denmark, 55 % of electricity generation takes place in this type of plants.

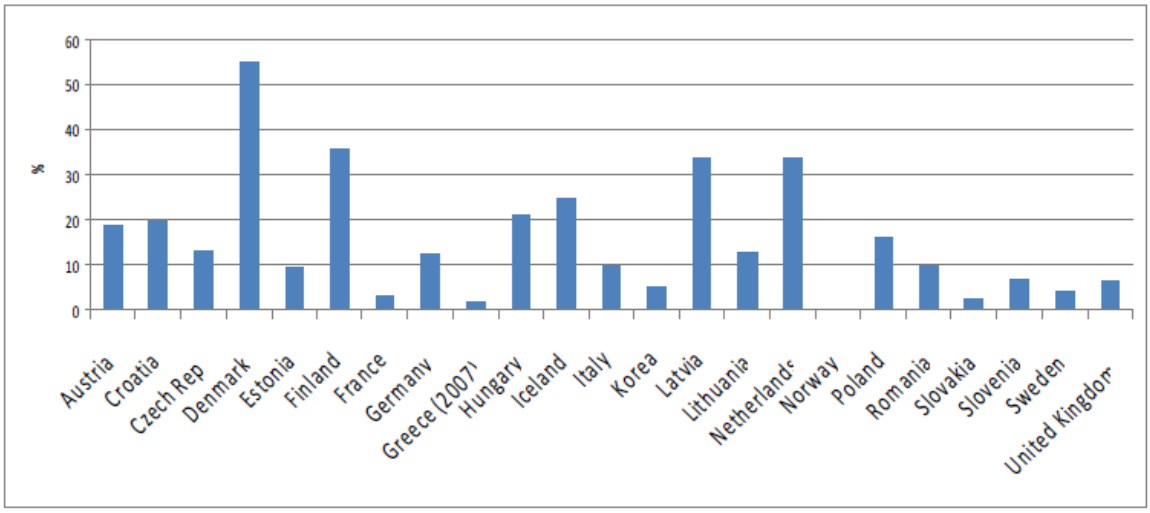

Figure 5.2: CHP share in electricity generation in the European Union (JRC, 2012

Natural gas dominates the CHP fuel market with about 40% share, followed by coal at 27%. Renewable sources, mainly biomass, but also combustible waste are becoming increasingly important having contributed to 10% of the electricity generation in this kind of energy production plant (COGEN, 2011). Biomass fuelled CHPs allow energy generation with lower carbon and environmental footprint than fossil based generation plants enabling energy production with CO_2 negative emissions when CCS processes are incorporated (Spath and Mann, 2004, Carpentieri et al.,2003 and Schakel et al., 2015). However, biomass fuelled plants have got a higher capital investment and lower electrical efficiency than fossil based ones (IEA, 2007). It must also be noted that feedstock availability could be a barrier for the development of this technology in some regions where woody biomass cultivation would occupy land employed for agriculture production (IEA, 2007). Biomass gasification CHPs exhibit higher electrical efficiency than combustion plants however their capital cost are higher, driven in large proportion by the cost of the gasifier (IRENA, 2012 and IEA, 2007).

The biomass share as fuel for CHP plants for electricity generation in EU countries is displayed in **Figure 5.3.** Using the data in the previous 2 figures and the information from **Figure 5.3**, it can be concluded that biomass fuelled CHPs play an important role in the energy system of Northern European countries (Sweden and Finland) and in some central European countries as well (Austria and Poland)where a significant percentage of the electricity demand is supplied by this kind of plants. In the case of Austria, vast research about bio CHP design has been carried out. The University of Vienna has designed and scaled up several bio-fuelled CHP plants, their gained experience at pilot scale was very useful for the design and operation of the Gussing plant that will be subject of discussion in the next sessions of this chapter (Hobfauer, 2002)

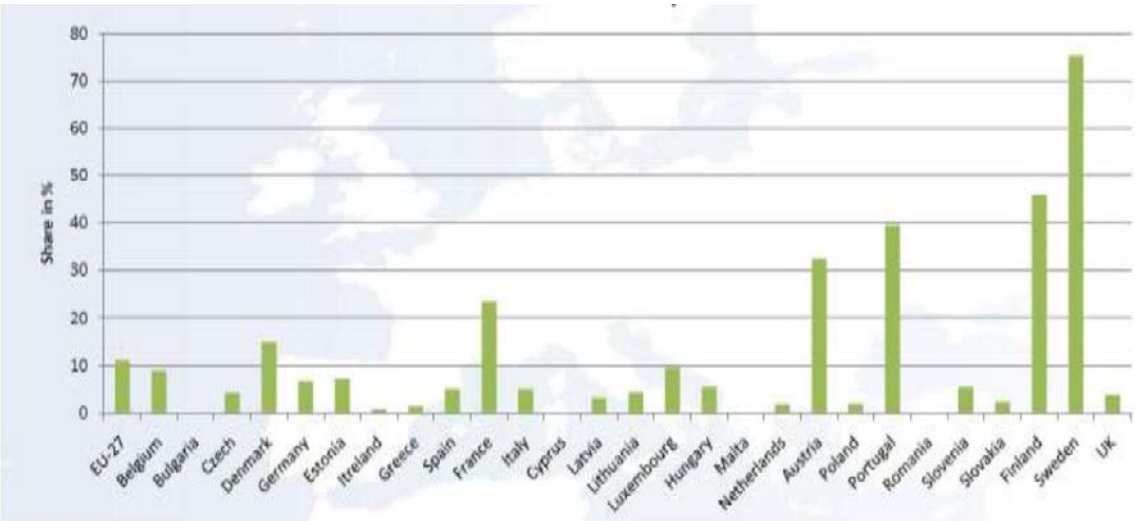

Figure 5.3: Biomass fuel share for CHP plants in Europe during 2010 (COGEN, 2011)

5.2 Biomass gasification technologies

Biomass gasification is an industrial process converting an organically derived carbonaceous feedstock into a gaseous product: synthesis gas or "syngas," which consists primarily of hydrogen (H_2) and carbon monoxide (CO), with lesser amounts of carbon dioxide (CO_2), water (H_2O), methane (CH_4), higher hydrocarbons (C_2^+), and

nitrogen (N_2). The reactions are carried out at elevated temperatures (between 500-1400°C; NETL, 2002) and at atmospheric or higher pressures (up to 33 bar; NETL, 2002). The reaction oxidants can be air, pure oxygen, steam or a mixture of both. Air-based gasifiers typically produce syngas containing a relatively large concentration of nitrogen and LHV values that range from 4 to 6 MJ/Nm^3. Oxygen and steam-based gasifiers produce syngas with a relatively high concentration of H_2 and CO with LHV values between 7 and 20 MJ/ Nm^3.(NETL,2002 and US Patent 3729298)

Biomass gasification involves two steps: the pyrolysis reactions and the gasification ones. During the pyrolysis reactions, the biomass is transformed in liquids, gases and char, a non-volatile solid with high carbon content. These products are then gasified. A few of the major reactions involved in this step are:

Exothermic Reactions:

(1) Combustion: {*biomass volatiles/char*} + $O_2 \longrightarrow CO_2$

(2) Partial Oxidation: {*biomass volatiles/char*} + $O_2 \longrightarrow CO$

(3) Methanation: {*biomass volatiles/char*} + $H_2 \longrightarrow CH_4$

(4) Water-Gas Shift: $CO + H_2O \longrightarrow CO_2 + H_2$

(5) $CO + 3H_2 \longrightarrow CH_4 + H_2O$

Endothermic Reactions:

(6) Steam-Carbon reaction: {*biomass volatiles/char*} + $H_2O \longrightarrow CO + H_2$

(7) Boudouard reaction: {*biomass volatiles/char*} + $CO_2 \longrightarrow 2CO$

The gasification processes can be classified according to the way the heat that enables the endothermic reactions to take place is delivered. In the case of the direct gasifiers, the pyrolysis and the gasification reactions occur in the same vessel. Indirect gasifiers separate the combustion reaction from the syngas-producing reactions. The syngas stream from these gasifiers is practically free of nitrogen and is therefore more

energy dense allowing energy generation by employing lower size electricity generation device and associated piping. Indirect gasification enables the production of this high energy dense syngas without the need of high purity O_2 that would require a costly and energy intense air separation unit. An example of this kind of gasifier is the FCIFB reactor (Hofbauer, 1997), in which the gasification takes place at atmospheric pressure using steam as oxidising agent. Two reactor configurations are used in operating plants: fixed and fluidised bed reactors (IRENA, 2012) that will be deeply discussed in the next sub-sessions.

5.2.1 Fixed bed gasifiers

Fixed bed gasifiers have simpler design and lower costs than fluidised bed reactors (NETL, 2002). The main disadvantages of this kind of gasifiers lie in the difficulties related to scaling up, particularly gas distribution and streak (Held, 2012) and that they must be operated using pure O_2 in order to obtain a nitrogen-free syngas, (with high volumetric energy density).. Since they are direct gasifiers, between 5 and 15% of the thermal input is employed to provide heat for the endothermic gasification reactions (NETL, 2002). Two types of fixed bed reactors of can be found in operation: updraft and downdraft gasifiers.

a) Updraft gasifiers

These are the oldest and simplest form of gasifier and are still used for coal gasification. Biomass is introduced at the top of the reactor and a grate at the bottom supports the reacting bed. The gasification agent (air, oxygen or steam) is introduced below the grate and it diffuses up through the bed of biomass and char. The complete combustion of the char takes place at the bottom of the bed, liberating CO_2 and H_2O. These hot gases (~1000°C) pass through the bed where they are reduced to H_2 and CO and cooled to 750°C. Continuing up the reactor, the reducing gases (H_2 and CO) pyrolyse the descending dry biomass, dry the incoming wet biomass and finally leave

the reactor at a low temperature (~500°C). Different examples of the application of this gasifier type can be found in literature, such as the PUROX (Pure oxygen process), in which municipal waste is converted into useful heating gas and inert cider. The production of the required ultra-pure oxygen in the PUROX process takes place in a liquid air fractional distillation column with high energy consumption. The resulting syngas has H_2 mole fraction in the range of 18-31%, CO mole fraction from 32 to 54% and CO_2 mole fraction from 9 to 25%. The lower heating value varies from 7.45 to 13.05 MJ/Nm^3 (US Patent 3729298).

Advantages:

- Simple, low cost process.
- Able to handle biomass with a high moisture and high inorganic content (e.g., municipal solid waste).
- Proven technology.

Disadvantages:

- Syngas contains 10-20% tar by weight, requiring extensive syngas clean up system.

Operating plants using this gasification technology present thermal inputs up to 10 MW (IRENA, 2012)

b) Downdraft gasifiers

The mechanical configuration of the downdraft gasifier is an analogue of the updraft gasifier except that the oxidant and product gases flow down the reactor in the same direction as the biomass. A major difference is that these processes can combust up to 99.9% of the formed tars. Low moisture biomass (<20%) and the gasification agent (air or oxygen) are ignited in the reaction zone at the top of the vessel. The flame generates pyrolysis gas/vapour, which burns intensely, producing between 5 to 15% char and hot combustion gases. These gases flow downward and react with the char (800°C -1200°C), generating more CO and H_2. The combustion gases are cooled to

below 800°C (NETL, 2002) and the unconverted char and ash pass through the bottom of the grate to be sent for disposal.

Advantages:

- Up to 99.9% of the tar formed is consumed, requiring minimal or no tar clean up.
- Minerals remain with the char/ash, reducing the need for a cyclone.
- Proven, simple and low cost process.

Disadvantages:

- Requires feed drying to a low moisture content (<20 %).
- 4-7% of the carbon remains unconverted (NETL, 2002).

This type of gasifier is currently operated in plants which thermal inputs are in the range from 10 kW to 1 MW (IRENA, 2012)

5.2.2 Fluidised bed gasifiers

Contrary to fixed bed reactors, fluidised bed reactors are suitable for scaling up. This configuration enables indirect gasification processes with the associated advantages that were previously described in page 114.

a) Bubbling fluidised bed

A bubbling fluidised bed consists of fine, inert particles of sand or alumina, which have been selected for size, density, and thermal characteristics. As the gasification agent is forced through the inert particles, a point is reached in which the frictional force between the bed particles and the gas counteracts the weight of the bed particles. At this gas velocity (known as minimum fluidisation), bubbling and channeling of gas through the media occurs so that the particles remain in the reactor and appear to be in a “boiling state”. The fluidised particles tend to break up the biomass feed, ensuring good heat transfer throughout the reactor. (NETL, 2002).

Advantages:

- Yields an uniform product gas and it exhibits a nearly uniform temperature. distribution throughout the reactor.
- Able to accept a wide range of fuel particle sizes.
- Provides high rates of heat transfer between inert material, fuel and gas.
- High conversion with low tar and unconverted carbon.

Disadvantages:

- Large bubble size may result in gas bypass through the bed.

This type of gasifier has proven to be reliable with a variety of feedstocks at pilot scale and commercial applications in the small to medium scale up to 25 MW_{th}. The range of capacity is limited as they have not yet been significantly scaled up; the gasifier diameter is much larger for bubbling fluidised beds than for circulating fluidised bed for a given feedstock (Bridgewater, 2001).

b) Circulating fluidised bed

Circulating fluidised bed gasifiers operate with gas velocities higher than the minimum fluidisation point. This results in the entrainment of the particles in the gas stream. The entrained particles exit from the top of the reactor, are separated in a cyclone and returned to the reactor.

Advantages:

- Suitable for rapid reactions.
- High heat transport rates possible due to high heat capacity of bed material.
- High conversion rates.

Disadvantages:

- Temperature gradients occur in direction of solid flow.

This kind of gasifier has been operated in a wide range of operating conditions since its design allows easy scaling up (Bridgewater, 2001); it appears to be the preferred system for large scale applications and it is employed by most industrial companies such as Foster Wheeler (Nieminen, 1999), Battelle (Paisley et al., 2001) and Lurgi (Vierrath and Greil., 2001).

Hobfauer (Hobfauer et al, 1997) developed an indirect steam atmospheric FICFB reactor. The basic concept behind this gasifier type is to divide the fluidised bed vessel into two zones, a gasification zone and a combustion zone. Between these two zones, a circulation loop of bed material is created but the gases remain separated. The circulating bed material acts as a heat carrier from the combustion to the gasification zone. The resulting syngas is therefore nearly free of nitrogen and has a higher energy density. Consequently, lower volumetric flow rates are required to meet the plant power output, allowing for smaller, less costly piping systems and energy generation devices. The bed material, together with some char, circulates to the combustion zone. This zone is fluidised with air and the char is partly burned. The exothermic reaction in the combustion zone provides the energy for the endothermic gasification with steam. Therefore the bed material at the exit of the combustion zone has a higher temperature than at the entrance. The flue gas is removed without coming into contact with the product gas (Hofbauer, 1997). With this design, it is possible to obtain a high-grade product gas without using pure oxygen neither high pressures. This kind of gasifier is considered to be a best practice technology in Europe (Coach Bioenergy, 2015).

5.3 Biomass gasification plant under study

This section provides further details regarding the biomass gasification plant that will be employed as base case in this thesis. As mentioned in the introduction, operating conditions for the steam atmospheric gasifier are based on the paper published by Schuster et al. (Schuster et al., 2001) while the downstream processes for heat and power generation replicate the configuration employed in the Gussing biomass CHP plant (Simader et al., 2004). The resulting syngas is cooled to provide thermal energy for district heating, cleaned up and a part of it is burned in a Jenbacher gas engine as displayed in **Figure 5.4.**

The CHP plant was designed on a basis of 10 MW_{th} biomass input. This capacity corresponds to that of Schuster et al. (Schuster et al., 2001) in his paper for the preliminary design for the gasifier in the Gussing plant. Existing plants using FCIFB as gasification technologies exhibit thermal inputs in the range of 5 to 10 MW_{th} (IRENA, 2012).

In this thesis, biomass elemental compositions (**Table 5.1)** are based on the information presented by the above cited bibliography. Cl and F compositions are not reported in this source, however, other studies such as the one undertaken by ECN (ECN, 2014) states that the value for Cl and F content in woody biomass is quite low (0-0.02% maf). These components were therefore not considered in the simulation since their influence in the syngas energy properties is negligible.

Table 5.1: Biomass feedstock properties reported in Schuster et al. 2001

Proximate analysis		Ultimate analysis (maf)	
LHV (kJ/kg)	12430	C	48.26 wt.%
HHV (kJ/kg)	13994	H	5.82 wt.%
Volatiles (mf)	80 wt.%	O	45.67 wt.%
Water content	25 wt.%	N	0.22 wt.%
Ash content (mf)	0.61 wt.%	S	0.03 wt.%

Beech chips are the fuel in the Gussing CHP plant due to the agreements that this plant has signed with the local producers. The decision regarding the type of woody biomass fuel (chips, pellets and dried biomass) depends on costs, local supply, available storage site and energy generation efficiency (Biomass Energy Centre, 2014). In this work, it was also decided to use biomass chips as fuel for the designed plant. This choice is based on the following arguments:

a) Biomass chips (with 25% moisture) exhibit lower (3.1 p/kWh) prices than pellets (4.4 p/kWh) (Biomass Energy Centre, 2014)
b) There are wood chip producers in the region that can provide the required fuel for the operation of the plant (Forestry Commission Scotland, 2007) not requiring extensive transport distance.
c) Although biomass chips may require a larger storage site since they exhibit lower energy density, the share of this cost driver in the total investment cost of the plant is quite low, less than 2 % (Orbernberger and Thek, 2008).
d) In the case of a FICFB reactor, the cold gas efficiency presents small differences (from 72% to 66% Schuster et al., 2001) when the water content of the fuel increases from 10% (pellets) to 25% (chips). This difference leads to a lower power output when chips (0.78 kWh_e/kWh_{bi}) are used instead of pellets (0.84kWhe/kWh_{bi}). However, the reduced profits resulting from lower electrical output corresponds to 25% of the fuel cost savings described in a) (EUROSTAT, 2014 and Bio Ennergy Centre, 2014).

Considering that torrefied biomass commands an even higher price than pellets, biomass wood chips seem to be most cost effective solution for the plant to be designed (Ehrig, 2013).

As previously mentioned, the biomass is gasified using steam. The steam is generated due to the recirculation of the effluent from the combustion zone that downstream cools down allowing as well the heating of part of the water that enters to

the CHP plant (DH2). The effluent from the gasification zone is also employed as heat source (DH1), and a fraction of it is recirculated to the combustion zone while the rest is burned in the gas engine. Both the fraction of the syngas used to generate electricity and the fraction that is employed as fuel in the combustion zone are cleaned in order to remove tar, ash, acid components and NH_3. The gas stream in the combustion zone and the char generated in the gasification zone are burned in order to provide energy for the endothermic gasification reactions by heating the sand that circulates between the two reactor zones.

The product gas cleaning train consists of a fibre filter and a scrubber. The fabric filter is intended to separate particles and a fraction of tar. The spent material and the separated particles are returned to the combustion chamber to burn the trapped carbon and hydrocarbons. Most of the tar and some ammonia is removed by the scrubber. This scrubber uses a biodiesel-based solvent (Hobfauer et al., 2004 and SES6-CT-2003-502705,). The spent solvent with the captured tar components are fed into the combustion zone and burned, the flue gas from the combustion zone is filtered upstream the stack. The temperature of the syngas is further reduced to about 40–50°C in the scrubber which is necessary for the gas engine. The final impurity content in the product gas downstream of the cleaning system is displayed in **Table 5.2** based on data from reports of the Gussing CHP plant.

Table 5.2: Composition of "impurities or trace components" in the syngas stream downstream of the gas cleaning train (Hobfauer, 2002 and SES6-CT-2003-502705)

Component	Composition (unit)	value
H_2S	v-ppm (dry)	20-40
Organic S	v-ppm (dry)	30
HCl	v-ppm (dry)	5
NH_3	v-ppm (dry)	400
Benzene	g/ N m³ (dry)	5...8
Naphthalene	g/ N m³ (dry)	1..2
Tar (PAH larger than Napthalene)	g/ N m³ (dry)	0.02…0.05
Particulates	g/Nm^3 (dry)	0.02

The electricity is generated in a GE Jenbacher 620 (Payhurber and Trapp, 2011). The Jenbacher Type 6 gas engine is currently one of the most advanced gas engines in the market. It can generate power in the range of 1.5 to 4.4 MW with electrical efficiency ranging from 41 to 45% (GE Energy, 2009). As the syngas must be at 45°C to be processed in this gas engine, this configuration also allows a large heat production upstream of the device from the cooling of the effluents leaving the gasifer. Among several Jenbacher Type 6 models, J620 was chosen for this study since the electricity capacity (3.1 MWe) is close to those designed in this study (GE Energy, 2010a). **Table 5.3** displays the main process conditions associated to the gasifier and the gas engine in the CHP plant under study.

Table 5.3: Main operating conditions for the gasifier and for the gas engine

Gasifier/Gas engine	Variable	Value	Source of information
Gasifier	Steam flow rate (kg of steam/kg of biomass)	0.17	Schuster et al., 2001
	Air to flow ratio (CZ)	1.1	Schuster et al., 2001
	Gasification zone (°C)	800	Schuster et al., 2001 Simader et al., 2004
	Combustion zone (°C)	870	Schuster et al., 2001
	Air inlet temperature (°C)	300	Schuster et al., 2001
	Syngas recycle inlet temperature (°C)	400	Schuster et al., 2001
Gas engine	Compression ratio	11	GE, 2009
	Pressure ratio. Comb. Chamber	2.26	Estimated
	Air Excess	1.96	GE,2009

	Intercooler temperature (°C)	50	GE, 2009

The plant configuration with the gas engine allows higher electricity generation than alternative technologies like organic Rankine cycle (ORC). Most advanced ORC configurations on the market such as those commercialised by Mitsubishi (TURBODEN, 2014) exhibit electrical efficiencies close to 20% (measured as the ratio of electricity produced and the thermal energy released by the latent heat, syngas cooling down) when they are operated with a hot source that decreases its temperature from 800 to 100°C and cooling water is used in the condenser. The total generated electricity would be around 240 kW since the sensible heat associated with the syngas cooling is approximately 1200 kW. By comparison, the plant with the gas engine has a power output of approximately 2700 kW.

5.4 Plant modelling and results validation

In this work, it was decided to use UniSim to simulate the CHP plant. The FICFB gasifier was modelled as two Gibbs reactors (one for the combustion zone and one for the gasification zone) as illustrated in **Figure 5.5.** One of the main problems by using this tool for the simulation of the gasification plant is the fact that the biomass feed must be converted into conventional process compounds (H_2, N_2, H_2O and C). As consequence of this transformation, the enthalpy of the biomass stream entering to the gasifier in UniSim will be different to the real one. The difference in the biomass inlet enthalpy would lead to different syngas properties that would affect plant outputs such as electricity and heat generation.

The real biomass enthalpy of formation can be estimated by using Eq. (5.1.)

$$h^f_{biomass} = bh^f_{CO_2} + ch^f_{H_2O} - LHV - ah^f_{O_2} \quad (5.1)$$

Eq. (5.1.) is obtained by assuming complete combustion of the biomass. By writing the biomass as an imaginary compound in base of the ultimate analysis and carrying out the stoichiometric reaction balances for a complete combustion, it is possible to obtain the coefficients a, b and c .

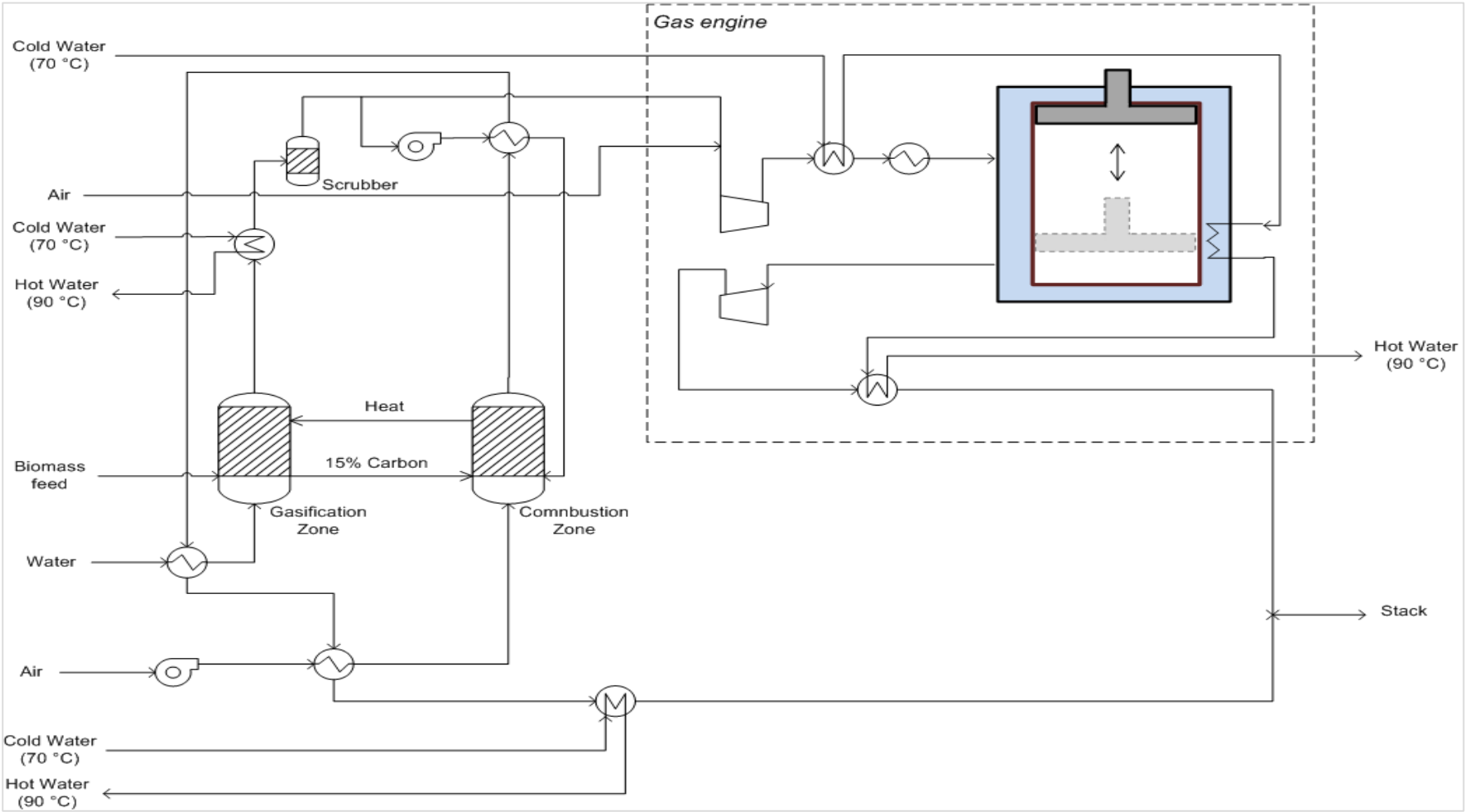

Figure 5.4: Flow sheet for the biomass CHP plant

The values for $h^f_{CO_2}$, $h^f_{H_2O}$ and $h^f_{O_2}$ are estimated at 25°C and 1 atm by UniSim. The difference between the estimated value using Eq. (5.1) and the corresponding value for the emulated biomass stream must be subtracted from the simulated heat generation in the combustion zone of the gasifier (Q correction in **Figure 5.5**).

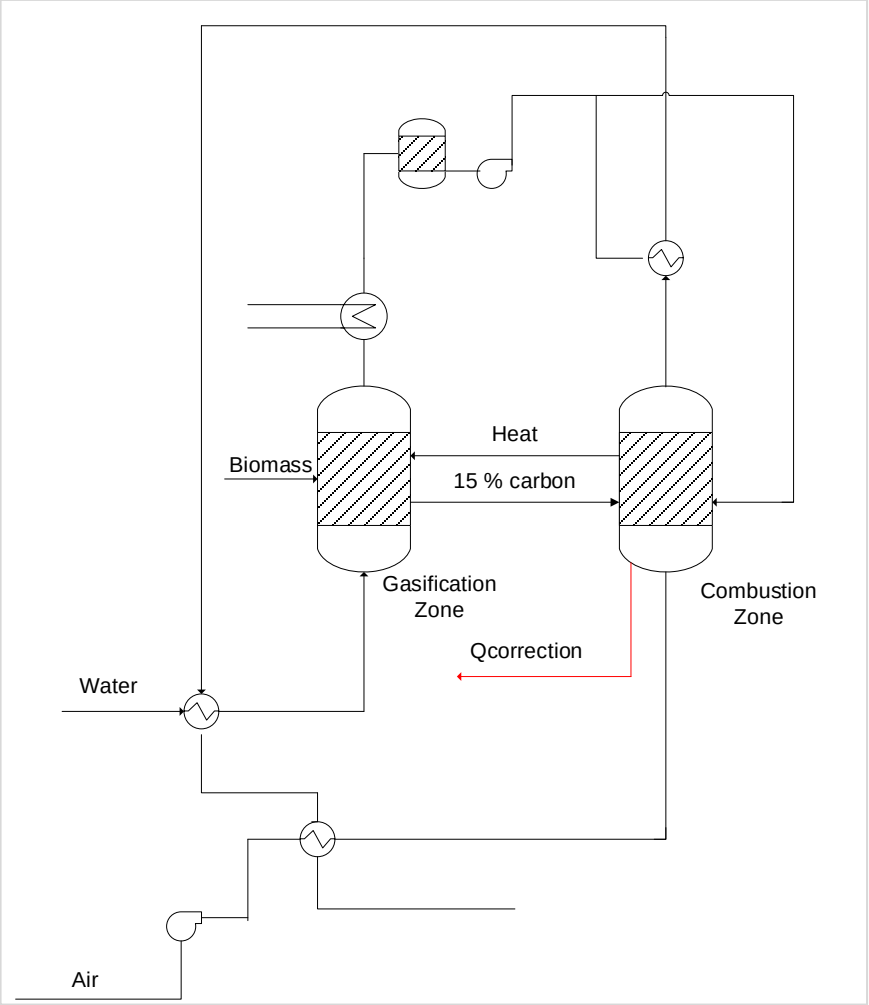

Figure 5.5: FCIFB gasifier modelling

The results for the modelling of the gasifier in this work has been compared against the composition and the LHV for the syngas that was reported by Schuster (Schuster et al.,2001) in which a detailed modelling of the equilibrium constants of the gasification reactions have been considered. As shown in **Table 5.4**, a total agreement between the values of the two research works can be observed

Table 5.4: Comparison of syngas properties

Syngas properties	(Schuster et al., 2001)	This work (UniSim simulation)
CH_4	0.09 %	0.08%
CO	25.84 %	26.44%
CO_2	10.30 %	9.80%
H_2	46.57 %	46.23%
H_2O	17.11 %	16.59%
Others	0.09 %	0.09%
LHV	11781 kJ/kg	11790 kJ/kg

With the intention of showing the robustness of the developed model for the gasifier, it was decided to undertake a sensitivity analysis studying how changes in the gasification temperature and the biomass moisture composition (water content) affect the performance of the gasification process.

Figure 5.6 displays the influence of the gasification temperature in the process performance. The increase of temperature favours endothermic reactions (ie: the steam carbon and Boudouard reaction) causing higher CO mole fraction in the product gas when the temperature goes up from 800 to 1000°C however a slight decrease in the H_2 mole fraction is observed. This trend can be explained due to the fact that a higher gasification temperature and larger CO compositions reduces the equilibrium conversion of the water gas shift reaction leading as well to a decrease of the CO_2 dry mole fraction and an increase of the water content of the raw syngas. Negligible differences in the value for the LHV of the raw product gas were reported when changing the reaction temperature however an increase of the LHV of the dry syngas can be observed since as it was previously explained, the syngas exhibits higher water content when the gasification temperature goes up. It must be noted however that operating the gasifier at a higher temperature involves recirculating more syngas to be burned in the combustion zone of the gasifier thus a possible increase in chemical efficiency associated to a larger value for syngas dry LHV is compensated by a lower amount of product gas available as fuel for the gas engine.

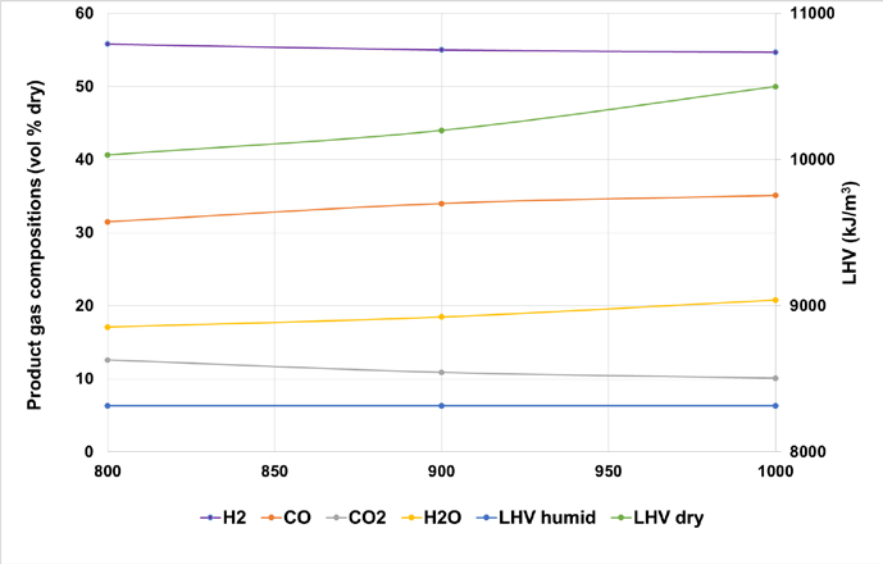

Figure 5.6 : Product gas composition and LHV in function of gasification temperature

As it can be appreciated in **Figure 5.7**, higher water content in the biomass moisture shifts the equilibrium of product gas towards H_2 and CO_2, decreasing CO and CH_4 concentrations. It can also be observed that the employment of higher water content fuel would lead as well to a decrease in the value of the humid LHV associated with the larger water content in the syngas. Chemical efficiency also goes down as consequence of the reduction in the values for LHV as well as due to the fact that biomass moisture has to be evaporated in the gasifier resulting in a higher energy demand thus a larger fraction of the syngas must be employed as a fuel in the combustion zone of the gasifier.

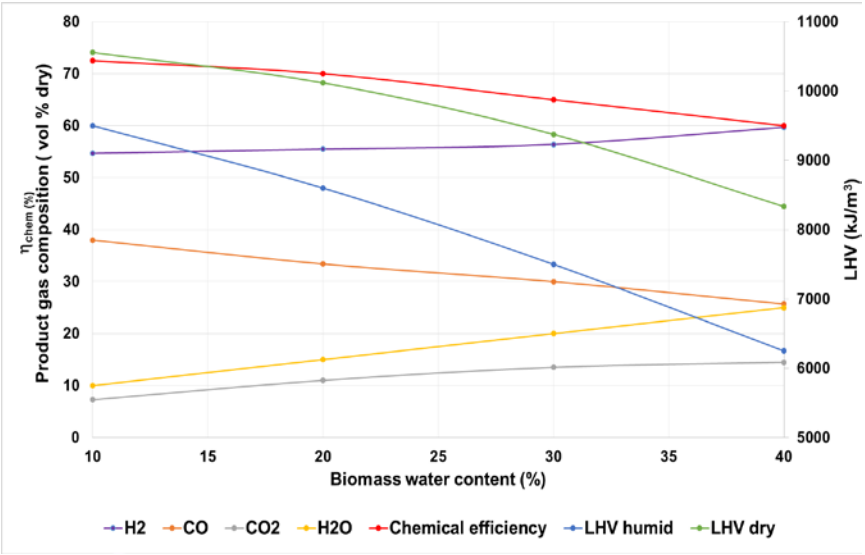

Figure 5.7: Product gas composition, chemical efficiency and LHV as function of biomass water content

Analogously to the sensitivity analysis that was previously presented, Schuster (Schuster et al., 2001) studied variation in syngas compositions and LHV as a function of gasification temperature and biomass water content, negligible differences were observed with the results displayed in **Figure 5.6** and **5.7**.

The gas engine was also simulated using UniSim to find out operating conditions of its various units and stream. Constructing a reliable simulator for this gas engine is essential for estimating the power and thermal outputs of a gas engine running with different feed gases. The single-stage turbocharged Otto cycle of the J620 gas engine was configured in reference to GE Energy (GE, 2010b), all the operating conditions of the four steps of the Otto cycle, a compressor and a turbine as well as heat exchangers and coolers were determined such that they could reproduce the electrical and thermal efficiencies reported by the vendor in case ofa natural gas feed having a methane number of 70 (GE Energy, 2009). The gas engine simulation must meet the following design parameters presented by the technical datasheet (GE Energy, 2009):

- The mean efficiency pressure is around 20 bar for a feed having a methane number of 70.
- The compression ratio is 11, implying that the pressure of a gas at the end of the compression step can vary with the gas composition to achieve the same compression ratio.
- The exhaust gas outlet temperature = 120◦C for natural gas and 180◦C for biogas.
- Hot water temperatures at inlet and outlet = 70/90◦C

When simulating the gas engine with the natural gas feed (methane number = 70), it was tried to set up the gas engine simulation so that the electrical and thermal outputs could be as close to those in the reference (GE Energy, 2009) as possible with the above-mentioned design parameters were met at the same time. The resulting electrical and thermal efficiency of 45.3% and 43.6% were very similar to 45.2% and 43.4% reported in the GE technical datasheet respectively (GE Energy, 2009). It is well known that a gas engine would operate with less electrical efficiency if fed by a fuel gas having a lower heating value. As the syngas stream in this study has a LHV (lower heating value) of 187.4 kJ/mol (or 11.8 kJ/g) which is

lower than 951.3 kJ/mol (or 49.0 kJ/g) of the natural gas, the estimated electrical efficiency was reduced to 41.9% while there was a slight increase of the thermal efficiency from 43.6%. to 43.8% when the gas engine is operated using the top end stream of the stages of the PSA unit (further details about the absorptive unit can be found in chapter 6).

In this study, it was assumed that the heat loss and the heat recovery at the gas engine with the syngas feed would be the same as those at the gas engine with natural gas feed since the gas flowrates in the two cases were effectively the same. However, in a case where the gas mass flowrate is notably lower than those in the reference study and the base case, i.e. pre-combustion capture unit integration case, both heat loss and recovery were reduced in proportion to the ratio of the two gas mass flowrates. GE Energy (2010) also reported the electrical and thermal efficiencies of 42.3% and 42.7%, respectively, in running the Jenbacher 620 gas engine with a wood gas originating from the FICFB biomass gasifier that this study is based on. The gas engine simulation with syngas feed was implemented making use of the UniSim simulation constructed for natural gas feed with the same adiabatic efficiencies of the devices that presurise or depressurise fluid and with the same compression ratio of 11. The electrical and thermal efficiencies (41.9% and 43.8%) with syngas feed were close to those in the reference. The reduction in the power efficiency can be explained by the mean efficiency pressure of the gas engine decreasing with lower fuel gas LHV. For the gas engine with the syngas feed, the mean efficiency pressure was reduced to 17.8 bar while it was close to 20 bar for natural gas feed. These comparisons indicate that the gas engine model is good enough to be capable of estimating reasonably the change of electrical and thermal efficiencies with varying fuel gas LHV. This gas engine model will be used later for estimating the electrical and thermal efficiencies of the Jenbacher 620 gas engine running with a new fuel gas generated by treating the raw syngas with shift reaction followed by decarbonisation in case of a pre-combustion adsorptive carbon capture.

5.5 Plant performance parameters

A CHP plant performance is measured by taking into account the chemical/ cold gas efficiency (Eq. (5.2)), the electrical (Eq. (5.3)), the thermal (Eq. (5.4)) and the overall efficiency (Eq. (5.5))).

The chemical or cold gas efficiency relates the heat content of the syngas entering to the gas turbine with thermal biomass input of the plant. This parameter can be used as a tool for measuring the efficiency of the gasification process

The electrical efficiency relates the net electricity generation (difference between the power generated ($P_{el,GT}$) by the gas turbine and the consumed power by the compressors ($\sum P_{el,C}$)) with the thermal input of the plant.

$$\eta_{el}= \frac{P_{el,GT}-\sum P_{el,C}}{\dot{m_F}\, LHV_F} \tag{5.3}$$

The thermal efficiency can be defined as the ratio between the amount of the generated thermal energy in the plant (to provide district heating) with the heat that the biomass would produce if it were combusted.

$$\eta_{th}= \frac{DH1+DH2+Heat\ recovered\ in\ the\ GE}{\dot{m_F}\, LHV_F} \tag{5.4}$$

The overall efficiency relates the energy output of the plant with the plant thermal input. The output of the CHP plant consists on the generated power as well as the thermal duties (DH1, DH2 and the heat recovered in the gas engine that also can be used to produce district heating).

$$\eta_{ov}= \frac{P_{el,GT}-\sum P_{el,C}+DH1+DH2+Heat\ recovered\ in\ GE}{\dot{m_F}\, LHV_F} \tag{5.5}$$

Table 5.4 reports the value for the previous mentioned four parameters obtained in the simulations carried out in this work

Table 5.4: CHP plant parameters

	Efficiency (%)
η_{chem}	66.9

η_{el}	29.8
η_{th}	50.0
η_{ov}	79.8

The obtained electrical and thermal efficiency were compared against the values reported by the studies undertaken by IRENA (IRENA, 2012) and IEA (IEA, 2007). In the case of a biomass gasification plant with thermal inputs in the range from 7 to 13 MW, these surveys inform electrical efficiency in the interval that goes from 29 to 33% meanwhile the overall efficiency is in the range from 70 and 82%. It can be said that the developed methodology and the selection of the operating conditions for the simulated units lead to a plant design in agreement with the CHP plants that are currently in operation.

Conclusions

Biomass combined heat and power plants (CHP) are a promising heat and electricity generation technology due to its consideration as a renewable source and their lower carbon and environmental footprints in comparison with fossil fuel plants. However, biomass exhibits higher prices (coal:0.01 pounds/kWh< natural gas: 0.047 pounds/kWh < crude oil: 0.035 US$/kwh[4] < biomass chips: 0.05 US$/kWh) and higher capital investment costs may be expected in comparison with analogous plants that are projected to be operated with fossil fuels (IEA, 2007 and IRENA, 2012). In this work a 10 MW_{th} input gasification plant was designed by following partially the process configurations for the currently operating Gussing CHP plant (Schuster et al., 2001 and Simader, 2004). Biomass is processed in a FIFCB and the produced syngas is burned in a Jenbacher gas engine. The designed plant exhibits an electrical efficiency of 29%, a thermal efficiency of 50%, an overall efficiency of 79 % and a chemical/ cold gas

[4] Fossil fuel prices are based on monthly statistics for Dec. 2014 pubblished by The Financial Times (FT,2014). Natural gas price reported in this thesis corresponds to the European values meanwhile crude oil price corresponds to the Brent crude index.

efficiency of 66.9%. These values are in agreement with published literature for the most advanced biomass gasification plants (IRENA, 2012).

Special methodology was developed in Unisim in order to model the FCIFB reactor and to build a reliable simulator for the gas engine. The results of the simulations for the gasifier were compared against the data reported by Schuster (Schuster et al., 2001) for the syngas composition and thermal properties as well as for a special sensitivity analysis that was carried out for testing the robustness of the model. Although the gasifier was simulated as a generic Gibbs free energy reactor, very small differences were observed with the published results in the previous cited work in which experimentally determined equilibrium constant for the reactions were taken into account for the modelling of gasification process.

The relationship between the feed composition (LHV) and the electrical and thermal efficiency for the gas engine was validated by comparing the results of the simulations with data regarding device performance provided by the vendor when the gas engine is operated by using natural gas and the syngas produced in the Gussing CHP plant as fuel. Slight differences between the predicted efficiency by the simulations undertaken in this work and the data for the real operation of the device were reported. Thus it can be concluded that the model that was developed for both devices provide accurate and robust results.

References

Azar C, Johansson D JA, Mattson N. Meeting global temperature targets- the role of bioenergy with carbon capture and storage. Environmental Research Letter.2013;8..

Bridgwater AV. Progress in Thermal Biomass Conversion. Blackwell Sciences Ltd. 2001.

Biomass Energy Centre. Fuel cost per kwh (input).2014.http://www.biomassenergycentre.org.uk

Carpentieri M, Corti A, Lombardi L. Life cycle assessment (LCA) of an integrated biomass gasification combined cycle (IBGCC) with CO2 removal. Energy Conversion and Management. 2005; 46:1790-1808

COACH Bio energy. Biomass power plant in Gussing. 2015. www.coach-bioenergy.eu/en/cbe-offers-services/best-practice-network/185-biomass-power-plant-in-guessing.htm

COGEN Europe (2011) Cogeneration as the foundation of Europe's 2050 low carbon energy policy, COGEN Europe, Brussels

ECN. Phyllis database; 2014. www.ecn.nl/phyllis

Ehrig R, Gugler H, Kristofel C, Pointner C, Schumutzer-Rossender I, Feldmeier S, Kolck M, Rauch P, Strasser C, Schipfer F, Kranzl L, Worgetter M. Economic comparison of torrefaction based and conventional production to end chains. 2013. 21st European Biomass Conference and Exhibition.

EUROSTAT. Electricity prices by type of user. http://ec.europa.eu/eurostat/tgm/table.do?tab=table&init=1&language=en&pcode=ten00117&plugin=1

FT. Financial Times Commodities. 2014. www.markets.ft.com/research/Markets/Tearsheets/Summary?s=IB.1:IEU

Forestry Commission Scotland. Biomass action plan for Scotland. 2007. www.gov.scot/Resource/Doc/1086/0047855.pdf

IPCC. Fifth Assessment Report. IPCC. 2014Cambridge University Press, Geneva,Switzerland

GE Energy, 2009. Cogeneration Application Considerations. GE Energy. http://site.geenergy.com/prod serv/products/tech docs/en/downloads/GER3430G.pdf_ as of 12/01/15

GE Energy, 2010a. Jenbacher Type 6. GE Energy. http://site.ge-energy.com/prodserv/products/recip engines/en/downloads/ETS E T6 10 screen August2010.pdf as of 12/01/15

GE Energy, 2010b Jenbacher Gas Engines a Variety of Efficient Applications. GE Energy. http://teb.com. ro/teb/upl/pdf/ev-prez2.pdf as of 12/01/15

Held. Gasification: Status and technology.2012

Hobfauer H, Veronik G, Fleck T, Rauch R. The FICFB-Gasification process. Developments in Thermochemical Biomass Conversion. 1997: 1016-1025.

Hofbauer H, Rauch T, Bosch K, Aicherning C. Biomass CHP Plant Gussing: A success story. Expert meeting on pyrolysis and gasification of biomass and waste.2002

IEA. Energy Technology Essentials: Biomass for power generation and CHP. 2007

IRENA. Biomass for power generation. Vol 1. 2012

Jacobs J A and Schneider M. Cogeneration Application Considerations.GE Energy. 2009

JRC Scientific and Policy Reports. Background Report on EU-27 District Heating and Cooling Potentials, Barriers, Best Practice and Measure of Promotion. 2012.

Knoef H A M. Inventory of Biomass Gasifier Manufacturers & Installations, Final Report to European Commission. 2000. Contract DIS/1734/98-NL, Biomass Technology Group B. V., University of Twente, Enschede, (see http://btgsl.ct.utwente.nl/).

NETL. Benchmarking Biomass Gasification Technologies for Fuels, Chemicals and Hydrogen Production. 2002.

Nieminen, J. Biomass CFB gasifier connected to a 350 MWth steam boiler fired with coal and natural gas — THERMIE demonstration project in Lahti, Finland. 1999. Power Production from Biomass III, Gasification & Pyrolysis R&D&D for Industry, (Ed. by K.Sipila & M.Korhonen), VTT Symposium 192, VTT Espoo.

Obernberger I, Thek G. Cost assessment of selected decentralised CHP applications based on biomass combustion and biomass gasification. Proceedings of the 16th European Biomass Conference and Exhibition. June 208, Valencia.

Paisley M A, Overend R P, Farris M. C. Preliminary operating results from Battelle/FERCO gasification demonstration plant in Burlington, Vermont, USA. (2001).1st World Biomass Conference In Proceedings 1st World Conference & Exhibition on Biomass for Energy & Industry, (Ed. by S. Kyritsis, A. A. C. M. Beenackers, P. Helm, A. Grassi & D. Chiaramonti), James & James.

Payrhurber K and Trapp C. GE's new Jenbacher Gas Engines with 2-stages Turbocharging. IEWT 2001.

Rauch, R. "Steam gasification of biomass at CHP plant Guessing-Status of the demonstration plant." 2nd world conference and technology exhibition on biomass for energy, industry and climate protection, Rome, Italy. 2004.

Schakel W, Meerman H, Talei A, Ramirez A, Faaij A. Comparative life cycle assessment of biomass co-firing plants with carbon capture and storage. Applied Energy. 2014; 131: 441-467

Schuster G, Loffler G, Weigl K, Hofbauer H. Biomass steam gasification –an extensive parametric modelling study. Bioresource Techno.2001; 77: 71-79.

SES6-CT_2003502705.RENEW. Renewable fuels for advanced powertrains. Optimum processing route for FT synthesis. 2007

Simader, G.R.,. Case study: 2MWel biomass gasification plant in Gussing(Austria). 2004 In: European Commission (Directorate-General for Energy and Trans-port).

Spath P, Mann M. Biomass power and conventional fossil systems with and without CO2 sequestration – comparing the energy balance. National Renewable Energy Laboratory: Greenhouse Gas Emissions and Economics;2004.

TURBODEN. Organic Rankine cycle power calculator.2015. www.turboden.eu/en/rankine/rankine-calculator.php

US Patent 3729298. Improved Prylosis Process for converting refused to fuel gas.

Vierrath H, Greil C. Energy and electricity from biomass, forestry and agricultural waste. In Proceedings 1st World Biomass Conference. 2001. 1st World Conference & Exhibition on Biomass for Energy & Industry, (Ed. by S. Kyritsis, A. A. C. M. Beenackers, P. Helm, A. Grassi & D. Chiaramonti), James & James.

Chapter 6: Biomass gasification combined heat and power plant (CHP) with carbon capture

Introduction

One of the main objectives of this thesis is to study the feasibility of the incorporation of pressure swing adsorption cycles in the role of carbon capture technology in energy generation plants. This chapter is aimed to present the design of an adsorptive unit to be applied as a pre-combustion process in the biomass gasification CHP plant introduced in Chapter 5. A two-bed, two-stage pressure vacuum swing adsorption (PVSA) system was designed and the role of several operating parameters (such as vacuum pressure, purge and feed ratio, adsorption step time and the inclusions of pressure equalisations) in cycle performance (CO_2 purity, CO_2 recovery and energy consumption) was studied. The goal of this investigation is to reduce the energy penalty required to meet the carbon capture targets. Through process simulation, the performance of the CHP plant with the adsorptive carbon capture unit was compared to the same CHP plant but with an installed amine-based post-combustion carbon capture process. The undertaken estimations show that the pre-combustion PSA cycles exhibit lower energy consumption per unit of captured CO_2 than MEA based process thus promoting the deployment of this carbon capture technology for small to medium capacity power plants.

6.1 Pre-combustion adsorptive unit and modifications to the plant

As previously mentioned, an adsorptive CCS unit was designed to process the effluents of the 10 MW_{th} biomass CHP plant described in Chapter 5. The relatively low gas flowrates at a plant of this scale make an adsorption process a viable alternative to conventional absorption-based separation processes (Yang, 1997; Ruthven, 1984). The PSA unit could be incorporated upstream of the gas engine or downstream, at the mixing point between the flue gas from the combustion zone and the Jenbacher gas engine. The pre-combustion location is the preferred option due to the resulting lower energy consumption associated to a lower volumetric flowrate

to be processed and a higher CO_2 mole fraction for the inlet stream of the PVSA cycles (as consequence of the water gas shift reaction, WGSR) .The study undertaken in this chapter is focussed on optimising the cycle configurations in order to minimise the energy penalty while meeting the carbon capture targets (90% CO_2 feed recovery and CO_2 purity greater than or equal to 95%).

The plant installed with a pre-combustion adsorptive unit will be compared against a conventional MEA post-combustion configuration. Overall carbon capture rate, specific energy consumptions, and thermal and electrical efficiency are considered. Both units have been designed to achieve 90% CO_2 recovery from the feed inlet recovery and CO_2 purity over 95%. Note that the CO_2 feed inlet recovery is not equal to the carbon capture rate of the whole plant; this is further discussed in section 6.3. In the case of the CHP plant with pre-combustion PSA, the carbon capture rate is approximately 48%, while for the absorptive process is approximately 59%. Although the MEA based configuration is intended to capture 90% of the CO_2 emitted in the biomass gasification plant, the overall recovery is lower. The reduced overall recovery is attributed to CO_2 emissions from the boiler of the CHP combustion module that are not being captured yielding to a quite similar percentage of avoided CO_2 emissions for both plants with CCS (PSA: 41.11 % vs MEA: 43.80%)

The installation of pre-combustion PVSA cycles involves several modifications in the plant flow sheet (**Figure 6.1**). As previously mentioned, two water-gas shift reactors (WGSR) in series are incorporated downstream of the gasifier. The product stream from the WGSR is cooled and passes through a silica gel column to adsorb the water in the stream before entering to the PVSA system. The captured CO_2 is then compressed (compression train) to approximately 75 bar, the critical pressure of the stream leaving the capture unit and estimated by using the Peng-Robinson model in UniSim. The liquid CO_2 stream is then pumped to a pressure of nearly 110 bar.

The water enters the plant at 1 bar, is heated to 100°C, vaporised and the resulting steam is superheated to 300°C. The heat required to increase the water temperature and to produce steam at 100°C is provided by the cooled down effluent from the gasification zone of the gasifier. The thermal duty required to superheat the stream is obtained by the recirculation of the products of the first WGSR, which are cooled down to 200°C before entering the second reactor. Part of the heat for the WGSR is recovered; the effluent of the second reactor is cooled

to 100°C when used for increasing the temperature of the water entering the CHP plant at 70°C. This water then leaves the plant at 90°C. The cooled down effluent exchanges heat with cooling tower water in order to reduce its temperature to 25°C. The water contained in the effluent is partially condensed and the remaining water fraction is removed via adsorption in a silica gel column. The silica gel column is designed to treat effluents for a minimum of 3 months without bed saturation when the plant is running at 75% capacity. The water mole fraction of the feed to the column is approximately 3% and the column is approximately 4 m tall with a diameter close to 2 m. The composition of the gas entering to the adsorptive two-stage unit is displayed in **Table 6.1**

Table 6.1: VPSA feed molar fraction

	Molar Fraction (%)
H_2	65.9
CO_2	32.6
CO	0.6
N_2	0.7
CH_4	0.1

The top end streams of the two stages are mixed and enter the gas engine where they are burned with air. The gas engine effluent is mixed with the cooled effluent from the combustion zone of the gasifier. The resulting mixture is released to the atmosphere. The bottom end stream from the second stage has a CO_2 mole fraction higher than 95%. This stream is processed in an oxy combustor to combust the impurities (H_2 and CO) such that the compression inlet stream is made up by 96% CO_2 and 4% water after being cooled down till 28°C. Given the relatively low O_2 requirements in the oxy-combustor, it was decided that the incorporation of an air separation unit would not be economically convenient opting for external supply of commercial high purity O_2.

6.1.1 Water-gas shift reactors (WGSR)

As previously mentioned, two water-gas shift reactors are installed in series with the intention to increase the mole fractions of CO_2 and H_2 in the PSA inlet stream. The water-gas shift reaction allows the conversion of CO into H_2 and CO_2 as shown below:

$$CO + H_2O \rightarrow CO_2 + H_2$$

The reaction is exothermic; a lower temperature would favour the equilibrium to the product side, however, the reaction rate is low, thereby requiring a catalyst for practical purposes (NETL, 2007). Such catalysts may be Fe, Cu or Pt (NETL, 2007; Koryabkina et al., 2003 and Mendes et al., 2009). The effluent of the gasification zone and the stream leaving the first WGSR provide the heat to produce the superheated steam. Part of the heat employed in the WGSR can be recovered by the cooling down of the effluents of the second reactor that allows to produce hot water for district heating.

The mole ratio of steam to CO is a key parameter in the design of WGSR systems. Higher steam to CO ratios increase CO conversion, thus requiring larger amounts of thermal energy to produce the steam. In this work, the steam to CO mole ratio is 2, which is the value used in the simulations in the 2007 DOE report (NETL, 2007). A larger steam to CO ratio cannot be used in the example plant in this thesis since an additional heat source would be necessary to produce the steam due to temperature crosses in the designed heat exchanger network.

The use of two reactors in series with an intercooler is suggested in previous works (NETL, 2007 and Mendes et al., 2009). Since the water-gas shift reaction is an exothermic reaction, the temperature increases as the reaction proceeds and shifts the equilibrium towards reactant side, thus reducing the CO conversion rates; the use of intercoolers prevent this occurrence and saves energy as more steam would be necessary if the reaction occurred in a single vessel. **Table 6.2** shows the main parameters associated with the designed water-gas shift reactor system.

Table 6.2: Main variables for the WGSR system

Inlet temperature 1st reactor (°C)	300
Steam/CO ratio	2
Conversion 1st reactor (%)	87.05
Outlet temperature 1st reactor (°C)	349.70
Inlet temperature 2nd reactor (°C)	200.00
Overall conversion (%)	97.63
Net heat balance (kW)	-270.60

The achieved CO conversions rates are greater than 97%. Lower CO conversion rates would reduce the H_2 and CO_2 content of the effluent that enters the capture unit. A lower CO_2 mole fraction would either increase the energy duty required to reach the 95% CO_2 purity in the VPSA unit or result in a reduced CO_2 recovery and purity.

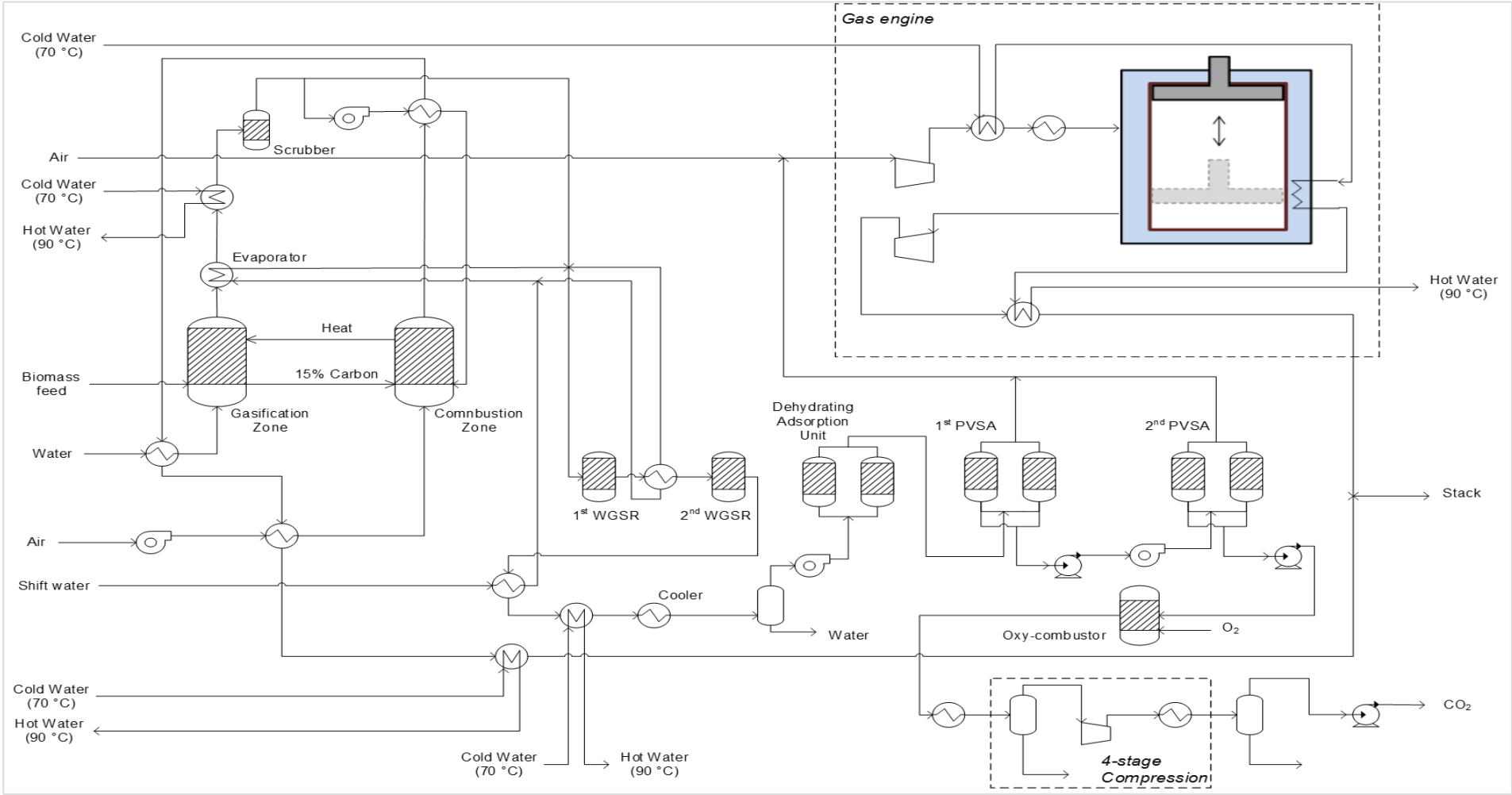

Figure 6.1: Flow sheet for the CHP with adsorptive carbon capture unit

6.1.2 Compression train

The CO_2-rich stream must be pressurised to 150 bar according to the DOE report (long distance transport; NETL, 2007) or 110 bar if the European guidelines for carbon capture are used (CAESAR Project, FP7—ENERGY, 2011). For the outlet stream of the PVSA system under study, the critical pressure is nearly 70 bar (Peng-Robinson model). The CO_2 stream is compressed from approximately 1.0 bar (adsorptive unit) or 1.35 bar (absorptive unit) to approximately 75 bar by employing a compression train. The compression train consists of three units and it was designed by using the pressure ratios and compression efficiency reported by the European Guidelines for Best Practice (CAESAR Project, FP7—ENERGY). Intercoolers downstream of each compressor cools the gas to 28°C (CAESAR Project, FP7—ENERGY). The configuration, presented in the above mentioned bibliography, was adopted in this study since the operating and design variables for the compression train were decided based on a cost assessment study using data from devices currently in operation in power plants. The most relevant compression train parameters are shown in **Table 6.3.**

Table 6.3: Main variables for the compression train (Adsorptive unit)

Value	Variable	Source of information
Total compression train (using 150 bar as final pressure) (kW)	184.95	Estimated
Total power compression train (using 110 bar as final pressure) (kW)	189,98	Estimated
Outlet pressure 1st stage (bar)	4.35	CAESAR project
Efficiency compression 1st stage	80	CAESAR project
Outlet pressure 2nd stage (bar)	18.65	CAESAR project
Efficiency compression 2nd stage	80	CAESAR project
Outlet pressure 3rd stage (bar)	75	CAESAR project

Intercooling temperature (°C)	28	CAESAR project
Power 1st compression stage (kW)	60.96	Estimated
Power 2nd compression stage (kW)	62.25	Estimated
Power 3rd compression stage (kW)	57.62	Estimated
Pump power till 150 bar (kW)	9.14	Estimated
Pump power till 110 bar (kW)	4.12	Estimated

6.2 PSA system

6.2.1 Sorbents, selectivity and working capacity

A two-stage, two-bed PVSA cycle configuration has been applied to recover 90% of the CO_2 content from the effluent of the gasification zone upstream the gas engine. As a post-combustion carbon capture technology, the series configuration of the two stages has successfully achieved high CO_2 recovery, equalling or exceeding 90% and CO_2 purity higher than 95% (Wang et al., 2012; Wang et al., 2013 and Shen et al., 2012).

Zeolite 13X has been chosen as adsorbent for the PVSA in this work. Several authors (Xiao et al., 2008 and Wang et al., 2012) have designed PVSA cycles using this adsorbent to treat the effluent from coal-fired boilers. Other works (Liu et al., 2011 and 2012), however, have employed zeolite 5A instead, claiming that it exhibited higher working capacities than 13X based on their own measured equilibrium data for 5A (Liu et al., 2010 and Wang et al., 2009 (5A and 13X)). A maximum CO_2 working capacity is reported at an operating temperature approaching 60°C (Park et al., 2002 and Xiao et al., 2008). The use of zeolite 13X or 5A for carbon capture applications has also been discussed in other works such as Merel (Merel et al., 2008) and Dircar and Loughlin (Dircar and Loughlin., 2013). These authors reviewed equilibrium data for both sorbents and concluded that the measurements reported in literature varied widely. It thus becomes necessary to use data measured under the same conditions and using the same methodology for the two sorbents. In this thesis, a comparison of the working capacities for CO_2 in zeolite 13X and 5A was carried out using the equilibrium

data measured at the Adsorption Lab of The University of Edinburgh. It was found that zeolite 13X exhibited the largest value for CO_2 working capacity.

Table 6.4 lists the physical properties of the zeolite 13X sample, the parameters for the equilibrium isotherm functions and the values for other variables considered in the simulations carried out in this work. The extended mono-layer Langmuir model was used to fit the experimental CO_2 equilibrium data since the value for the correlation coefficient was close to 0.99; the parameters were estimated by Origin 8.5 software (OriginLab, 2010) and applying the thermodynamic consistency criteria reported by Rao et al., 1999. Due to the low H_2 partial pressure (nearly 1 bar), it was assumed that H_2 behaves as an inert species. Since no measurements for CO equilibrium data were carried out at the UoE lab and the low CO partial pressure, it was assumed that the adsorption equilibrium isotherm of CO on zeolite 13X would be reasonably the same as that of N_2 on zeolite 13X. The measured N_2 isotherms on 13X were very close to those reported (Saha and Deng, 2009) for CO within the range of the PVSA process operation. The isotherms for the species of interest at 298 K, 330 K and 350 K are plotted in **Figure 6.2, Figure 6.3** and **Figure 6.4.**

Table 6.4: Physical properties of zeolite 13X pellet and parameters for PVSA simulation in this study.

Physical properties	
Pellet density, ρ_p	1200 kg/m^3
Pellet void fraction, ε_p	0.25
Pellet average diameter, d_p	4 mm
Pellet specific heat capacity, C_p	920 J/kg K
Equilibrium and kinetic parameters	
Saturated adsorption capacity, q_s	5.219 mol/kg
Mono-site Langmuir isotherm parameter, $b^o_{CO_2}$	$3.95 \cdot 10^{-5}$ bar^{-1}
Mono-site Langmuir isotherm parameter, b^o_{CO}	$2.08 \cdot 10^{-5}$ bar^{-1}
Heat of adsorption, ΔH_{CO_2}	32.6 kJ/mol
Heat of adsorption, ΔH_{CO}	20.3 kJ/mol
Linear Driving Force coefficient, $k^{LDF,macro}_{CO_2}$	75.1 s^{-1}
Linear Driving Force coefficient, $k^{LDF,macro}_{CO}$	37.5 s^{-1}
Bed parameters	
External bed void fraction, ε_b	0.4
Axial mass dispersion coefficient, D^L	$1.80 \cdot 10^{-4}$ m^2/s
Axial thermal dispersion coefficient, λ^L	1.50 W/m^2 K
Wall heat transfer coefficient, h_w	80 W/m^2 K

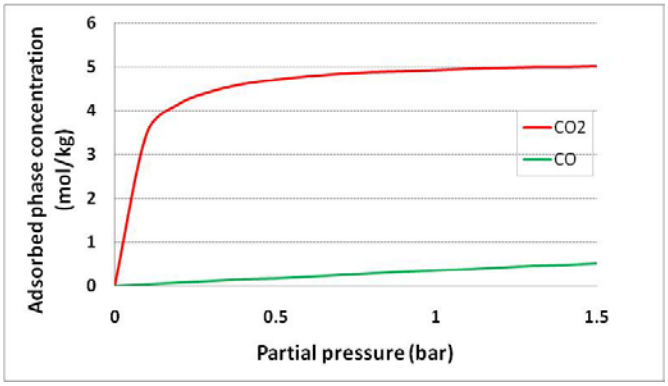

Figure 6.2: Isotherms for adsorbing species at 298K

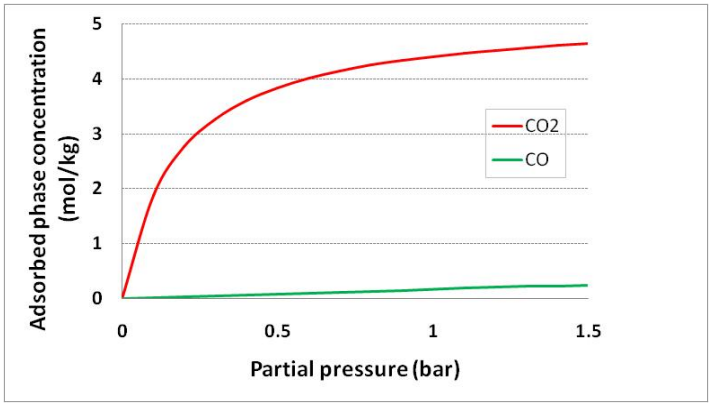

Figure 6. 3: Isotherms for adsorbing species at 330 K

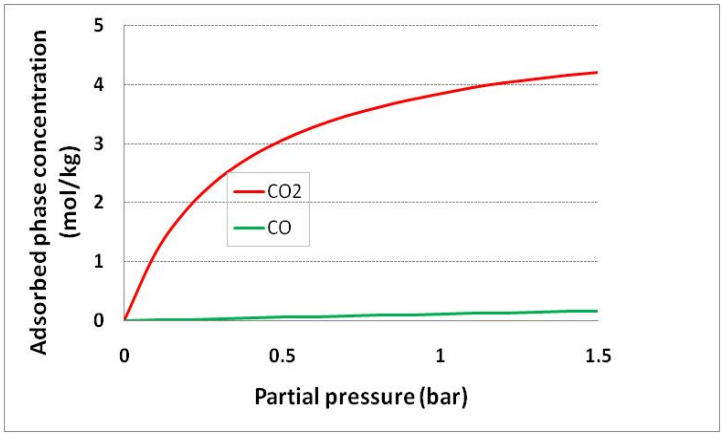

Figure 6. 4:Isotherms for adsorbing species at 350K

The feed temperature is a key parameter in optimisation of PVSA cycle performance. A preliminary choice can be done without requiring simulations by evaluating the equilibrium working capacity and the selectivity of the species of interest. In this work, the feed temperature has been based on the CO_2 working capacity; the effect of the selectivity has not been studied as CO composition is very low and H_2 is considered inert. The working capacity in a PSA separation process has been estimated as the difference of adsorbed concentration between the

feed conditions and the target purity at purge conditions. **Table 6.5** shows the preliminary values used for the calculation of the CO_2 working capacity for the first and the second stages.

Table 6.5: Parameters used to estimate working capacity

Variables	Feed conditions	Purge feed end conditions (1st stage)	Purge feed end conditions (2nd stage)
P (bar)	1.5	0.1	0.1
y_{CO_2}	0.319	0.70	0.95
y_{H_2}	0.665	0.288	0.038
y_{CO}	0.01	0.012	0.012

Figure 6.5 shows the CO_2 working capacity for both stages for temperatures ranging from 298 to 363 K.

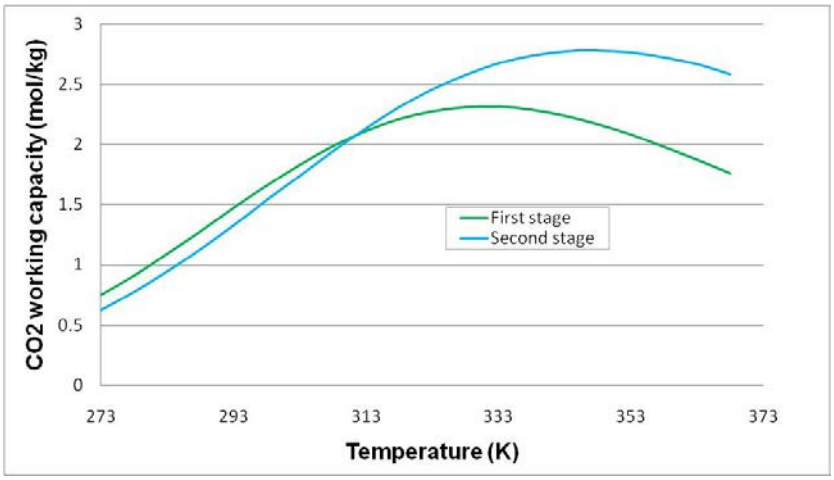

Figure 6.5: CO2 working capacity for a range of temperature from 298K till 363K

It can be observed that the maximum CO_2 working capacity occurs close to 330K. This maximum is a consequence of the non-linearity of the isotherm **(Figure 6.2, Figure 6.3** and **Figure 6.4**), which decreases the adsorbed concentration due to the increased effects of rising temperatures at lower partial pressures. Increased working capacity can be obtained at temperatures between 298 and 333 K. Beyond this range, the working capacity decreases if the

temperature is raised since lower adsorbed concentrations are observed at higher partial pressure.

6.2.2 PVSA cycle simulation strategy and choice of column size

For the simulation of the PVSA cycles in the biomass gasification plant, an University of Edinburgh-owned PSA cycle solver, CySim, was used. CySim (Fiedrich et al., 2013) aims to be a generic adsorption solver. For the gas phase, the mass and the energy balances include parabolic dispersion terms while the user can select different mass transfer mechanisms for the adsorbed phase (micropore and macropore diffusion, LDF or equilibrium).

CySim allows the simulation of isothermal and non-isothermal PSA cycles and it quantifies as well the pressure drop in the columns. The unibed approach is implemented in the software, enabling the simulation of polybed systems by solving the mass and the energy balances of a single bed that goes through the different steps of the cycle configuration. The information of the streams that leave the column is stored in buffer tanks to be used in the next cycle step. Multi-layer columns as well as symmetric and asymmetric configurations can be also be simulated by using this tool. **Figure 6.6** shows a scheme for a two-layer polybed system in CySim.

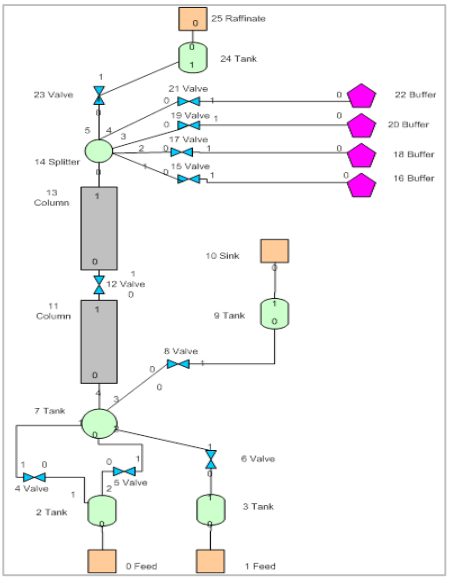

Figure 6.6: Schematics for the modeling of unibed configuration in CySim (Friedrich et al., 2013)

Esim was not employed to effectuate these simulations since the Equilibrium Theory solver was still under development when this research began. It is also important to underline that Esim should be used for estimating the limiting separation performance (since kinetic and dispersive effects are being neglected) that a given PSA cycle configuration may reach. The Eq. Theory based software enables as well a pre-selection of promising configurations for being further studied by employing full governing equation solvers that require experimentally determined diffusion coefficients as input data. The simplifications associated with the assumption of Equilibrium Theory allow the modelling of the adsorption dynamics with less empirical input data (experiments must be run just for the operating conditions for the high separation performance processes) and with fewer PDEs, enabling as well cycle steady state reaching with a lower number of cycles. However, it must be noted that for those separations in which kinetic effects are not negligible (crystalline sorbents at low temperature and / or relatively high pressure), large differences between the cycle performance parameters predicted by Esim and the ones estimated by a full governing equation software could be observed thus the results generated by Esim should be used as a first approximation and the simulator as a tool to carry out a preliminary choice for design and operating variables for high separation efficiency PSA cycles that will be optimised by employing more detailed models

For the PVSA cycles analysed in this chapter, accurate results for cycle performance indicators are required since the configurations are designed with an optimisation purpose and a strict CO_2 purity restriction must be obeyed (the rich CO_2 stream must leave the adsorption unit with CO_2 purity higher than 95%). Zeolite 13X was chosen as an adsorbent and it had been proved that macropore diffusion is the prevailing mass transfer mechanism (Hu et al., 2014) for CO_2 separation thus tools that account for kinetic and dispersive effects like CySim (Friedrich et al., 2013) should be employed since Esim would produce results that would over quantify CO_2 purity and CO_2 recovery predicting as well a lower energy consumption for the adsorption unit. The separation under study was modelled by using the assumptions of micropore equilibrium (based on previous diffusion experiments undertaken in our research group) and the macropore LDF simplification. The macropore LDF constant was estimated by considering the contribution of the molecular and Knudsen diffusivity meanwhile superficial diffusivity was considered to be negligible

The simulations were conducted on a mole basis, i.e., the feed flow to the PSA system was assumed to be 1 mol/s. The results for the required mass of the adsorbent and the consumed

power were modified based on the real feed flow. The idea of the downscaling is to make the PSA simulations be independent of the feed flows as well as to favour the convergence of the software since larger values for the flows produce oscillations or crashing specially in the equations related to the dynamics of the valves that connect the different units.

The optimisation of the PVSA cycles is a multi-objective, multi-variable problem due to the fact that at least three parameters must be optimised: CO_2 purity, CO_2 recovery and energy consumption. In addition, the effects of the operating conditions and the design variables in the optimisation targets may counter each other (Fiandaca, 2009). The number of design and process operating variables to be studied can be reduced by using data from already optimised configurations or by using constraints for that variable in other fields of the chemical engineering discipline.

In this thesis, the adsorption step times are in the same order of magnitude as those reported in several previous works: (Liu et al., 2011; Shen et al. 2012, Wang et al., 2013 Khrisnamurty et al., 2014. In these articles, however, the flow to be treated differs significantly from the case investigated here. As a result, column dimensions (diameter and height) must be chosen such that the residence time considered in this work is similar to the one reported in the previous papers. Column diameters were selected so that the superficial velocity for the gas in the column was in the range of 0.1 to 0.4m/s (Liu et al. 2011, Xiao et al. 2009, Wang et al, 2012). A column length in the range of 3m satisfies the residence time condition while column diameters for the first stage is around 2.4 m and 2 m for the second stage satisfy the velocity specification.

6.2.3 Cycle performance parameters

As it was previously mentioned in this chapter, the role of different operating conditions have been studied with the purpose of optimising the PSA performance parameters. Of particular interest is the specific energy consumption required to meet CO_2 capture targets.

The specific energy consumption for a PSA cycle that satisfy the required values for the CO_2 recovery defined by Eq. 6.1 and for CO_2 purity in Eq. 6.2 can be estimated by using Eq. 6.3. As explained in Chapter 2, a CO_2-rich stream (i.e., of high purity) leaves the column

through the feed end during blowdown and purge while the CO_2-containing feed is used to pressurise the column.

$$CO_{2_{recovery}} = \frac{\int_0^{t_{blow}} c_{CO_2} v(z=0)dt + \int_0^{t_{purge}} c_{CO_2} v(z=0)dt}{\int_0^{t_{feed+press}} c_{CO_2} v(z=0)dt} \tag{6.1}$$

$$CO_{2_{purity}} = \frac{\int_0^{t_{blow}} c_{CO_2} v(z=0)dt + \int_0^{t_{purge}} c_{CO_2} v(z=0)dt}{\int_0^{t_{blow}} C\, v(z=0)dt + \int_0^{t_{purge}} C\, v(z=0)dt} \tag{6.2}$$

$$PSA\ Specfic\ work\ = \frac{\int_0^{t_{feed+press}} power_{blower}\, dt + \int_0^{t_{blow+purge}} power_{vacuum} dt}{\int_0^{t_{blow}} c_{CO_2} v(z=0)dt + \int_0^{t_{purge}} c_{CO_2} v(z=0)dt} \tag{6.3}$$

In the case of the PSA cycles applied to CCS, the purge must be operated at pressures lower than 1 bar; most of the configurations reported in literature operate at pressures that are below 0.4 bar. During the blowdown step, the column pressure decreases from the adsorption step (between 1 and 1.5 bar) to the purge pressure below 1 bar. The power consumed in the blower and in the vacuum pump can be calculated by using Eq. (6.4) and Eq. (6.5).

$$power_{blower} = \frac{\frac{\gamma}{\gamma-1} RT_{feed} \left[\left(\frac{P_{feed}}{P_{atm}}\right)^{\frac{\gamma-1}{\gamma}} - 1 \right] mole\ flow\ _{fed\ to\ the\ column}}{\eta_{Blower}} \tag{6.4}$$

$$power_{vacuum} = \frac{\frac{\gamma}{\gamma-1} RT_{blow} \left[\left(\frac{P_{atm}}{P_{blow}}\right)^{\frac{\gamma-1}{\gamma}} - 1 \right] mole\ flow\ _{leaving\ the\ column}}{\eta_{Vacuum\ pump}} \tag{6.5}$$

Thus, the overall mechanical/electrical separation energy can be defined as:

$$Specific\ EC = \frac{Power\ PSA\ 1st\ unit + Power\ PSA\ 2nd\ unit}{CO_2 Overall\ Recovery\ \times CO_2\ Feed\ Flow} \quad (6.6)$$

The value for the overall CO_2 overall recovery for the PSA cycle can be calculated by using Eq. 6.7:

$$CO_2 PSA\ overall\ recovery = Recovery\ CO_{2_{first}} \times Recovery\ CO_{2_{second}} \quad (6.7)$$

6.2.4 Selection of the operating conditions for the VPSA cycles

The purpose of the two-stage two-bed system is to achieve 95% CO_2 purity in the stream to be stored and an overall CO_2 recovery close to 90% (+/-2%). Several examples of this kind of configuration applied as post combustion units can be found in literature (Park et al., 2002; Wang et al. 2012; Shen et al 2012 and Liu et al. 2011). In these works, the first stage is used for achieving the CO_2 recovery target (more than 90.9%) such that the target for overall CO_2 recovery (Eq. 6.7) can be accomplished. The range of purity for the first stage is between 50 and 60%. It must be underlined the fact that these configurations were designed for post-combustion adsorptive units in which the CO_2 feed inlet mole fraction is around 15%. This value is lower than the CO_2 content of the gasifier effluent downstream the WGSR and the silica gel column at approximately 31%. A higher CO_2 purity in the first stage of approximately 70-72% therefore minimise the separation work for the overall two-stage PSA system for a total CO_2 recovery of 90%.

Different operating conditions have been analysed to choose 4 configurations for the first stage. The choice of these four configurations attempt to study the influence of the operating conditions in the performance of the overall capture unit in order to find out possible solutions that meet the carbon capture targets with the lowest energy consumption. In all of the runs, a conventional Skarstrom cycle (Skarstrom, 1960) has been used. For each given first stage configuration, the operating conditions for the second stage are chosen such that the carbon capture targets are met. Overall energy consumption are estimated and compared for the different runs.

The sensitivity analysis studies the role of the next variables:

- Purge/final blowdown pressure/ vacuum pressure
- Purge and feed ratio (P/F), expressed as a percentage
- Adsorption step time (t_{ads})

By reducing the purge pressure, higher CO_2 recovery is possible as more molecules leave the column at greater vacuum. However, energy penalty also increases at greater vacuum, as shown in Eq. (6.5). The power consumed during the blowdown step is proportional to the ratio between the atmospheric pressure and the final blowdown pressure. **Figure 6.7** shows the evolution of recovery when the vacuum pressure is varied and all the other variables are kept constant, i.e., adsorption time of 240 s and P/F equal to 10.

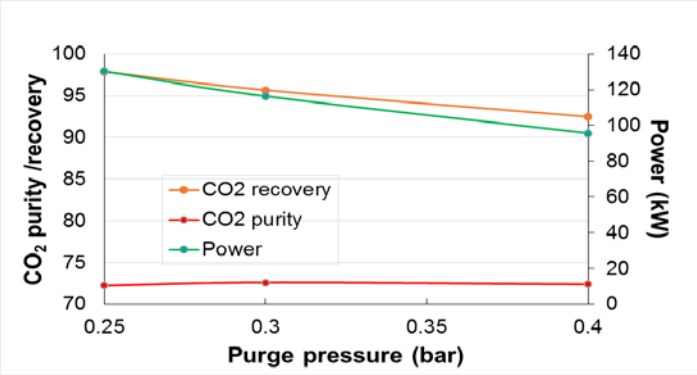

Figure 6.7: Evolution of cycle performance parameter in function of the purge/ vacuum Pressure

Larger P/F ratios increase CO_2 recovery since it is possible to remove more CO_2 from the column for a given purge step time. However, since the purge is undertaken by using the effluent leaving the adsorption product end, CO_2 purity decreases when P/F ratio increases as shown in **Figure 6.8** (adsorption time =220 s and purge pressure =0.3 bar).

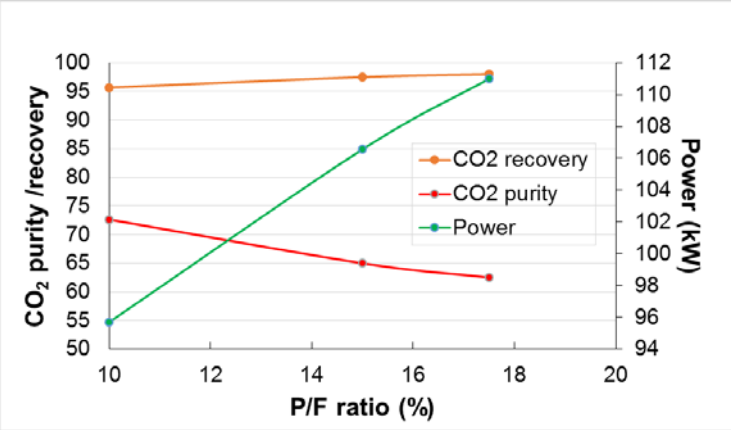

Figure 6. 8: Evolution of cycle performance parameter in function of P/F ratio

An increase of the adsorption step time decreases CO_2 recovery and increases CO_2 purity. The longer adsorption step time causes the saturation of a larger fraction of the column and prevents CO_2 from being adsorbed. This reduced recovery means that the effluent that leaves the product end enters the second column with a higher CO_2 mole fraction. Consequently, the gases at the bottom end of the column being purged will have a larger CO_2 mole fraction, i.e., higher purity**. Figure 6.9** shows the influence of the adsorption step time in cycle performance with P/F=17.5 % and purge pressure of 0.4 bar. As the starting point for the selection of the adsorption step time, it was decided to simulate the breakthrough curves for CO_2 clean beds for the feed and operating conditions being studied. The time in which complete saturation of the bed takes place was estimated, and adsorption step times were set to 50% of these values. This conservative criterion is based on the fact that over a number of cycles, the column will become more and more saturated, and less CO_2 can be adsorbed due to the incomplete purge. Consequently, the breakthrough time will be less than that for the initial clean bed.

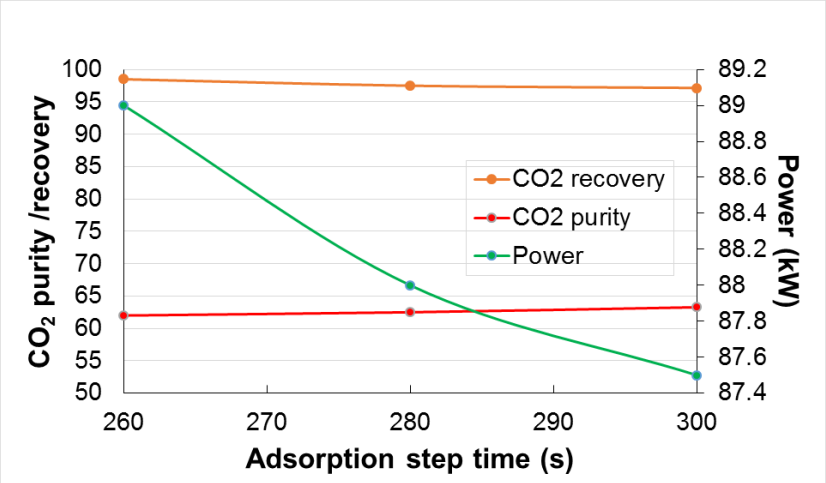

Figure 6.9: Evolution of cycle performance parameter in function of the adsorption step time

The literature describing the heuristic design of PSA cycles (Jain et al., 2003) and works referring to carbon capture PSA processes (Liu et al., 2012, Wang et al.,2012, Shen et al.,2012) use blowdown step time ranging from 5 to 10% of the cycle time. In this thesis, the blowdown step time for the first stage is approximately 7 % of the total cycle time.

From the preliminary simulations that were carried out, four cases were selected to analyse the role of different operating conditions to meet the carbon capture targets with the lowest energy consumption. The first stage in all of the four investigated cases have CO_2 purity greater than 60% and more than 90.9% CO_2 recovery. The goal of these cases is to explore the influence of CO_2 recovery and purity in the first stage on the performance of the overall carbon capture unit. Furthermore these cases help identify whether the parameters that benefit the performance of the first stage are also beneficial for the second stage. **Table 6.6** shows the operating conditions for these four cases.

Table 6.6: Four configurations selected for the first stage

RUN	Purge Pressure (bar)	P/F (%)	t_{ads} (s)	t_{blow} (s)	Column diameter (m)	CO_2 recovery (%)	CO_2 purity (%)	Consumed power (kW)
1	0.25	10	240	38.5	2.42	97.88	72.26	130.3

2	0.30	10	240	38.5	2.42	95.68	72.63	116.4
3	0.4	10	240	38.5	2.44	92.48	72.42	95.71
4	0.40	17.5	300	38.5	2.40	97.16	63.27	107.00

It is important to underline that the PVSA unit is integrated into the CHP plant and consequently the total mass entering the unit in each cycle corresponds to the accumulated mass leaving the WGSR during the same time period. A lower feed flow during adsorption step time was used in the cases where more mass was used to pressurise the column (i.e., cases with lower purge pressure). The column diameter was adjusted for each case such that the superficial velocity in the adsorption step remains constant for all cases.

The first run achieves the largest recovery but also the largest energy consumption (**Table 6.6**, **6.7** and **6.8**). Runs 2 and 3 have different vacuum pressures but the same P/F ratio than Run 1 since they were intended to study the effects of increasing purge pressure on the CO_2 recovery. The results of this study are used for deciding the operating pressure for the second stage necessary to keep the carbon capture targets. Run 4 shows how the modification of the purge and feed ratio at the same pressure increases CO_2 recovery, but decreases purity. This is attributed to the purge step, which is performed with effluent nearly without any CO_2 content from the adsorption step, causing a dilution of the CO_2 in the column after the blowdown. Since the reduction in purity cannot be compensated by an increase in adsorption step times, the critical design criterion of the second stage for this run will be to reach the 95% CO_2 purity target.

For each of the selected runs on the first stage, different operating conditions for the second stage were studied. As shown in Eq. (6.5), the energy consumption in the vacuum pump is proportional to the ratio between the atmospheric and the purge pressure. For a fixed CO_2 recovery target, configurations involving higher purge pressure have lower energy consumption. As observed in the selection of the first stage operating conditions, the increase of the purge pressure reduces the CO_2 recovery; this is compensated for by increasing the P/F ratio. The increased P/F ratio decreases the CO_2 purity, thus requiring larger adsorption step times in order to avoid a reduction in purity. However, an increase of adsorption step times

reduces CO_2 recovery. **Table 6.7** presents the final configurations that meet the carbon capture targets and minimise the energy penalty (**Table 6.8**) associated with the carbon capture unit.

For Runs 1 and 2, it was possible to use a higher or equal purge pressure in the second stage since the CO_2 recovery in the first stage is greater than 95%, thus allowing a decrease in the energy consumption for the second stage (**Table 6.8**). For Runs 3 and 4, however, the purge pressure cannot exceed 0.20 bar since it would not be possible to reach the overall CO_2 recovery target of 90 % while keeping purities higher than 95 %.

Despite the efforts made to optimise the operating conditions, it can be seen (**Table 6.7** and **Table 6.8**) that the overall specific energy consumption is quite similar, at approximately 0.36 MW_e/kg of CO_2 for all cases. It was decided to explore the incorporation of pressure equalisation steps aimed to reduce the energy penalty associated with the carbon capture unit. The resulting CO_2 purity and recovery at the second stage of run 1_1PE are very similar to those of run 1 since the feed gas and the operating conditions of the two cases are almost identical. On the contrary, it is very interesting to observe that run 1_2PE achieved the targets with higher desorption pressure and higher P/F ratio than those of the run 1_1PE. Adding the PE steps increases the CO_2 purity to such a great extent that a higher P/F ratio can be used. Several simulations were carried out to achieve the targets run 1_2PE prior to finding the optimum operating conditions. In the first simulation, 0.40 bar of desorption pressure and a 0.46% P/F ratio are used; these are the same values as those of run 1_1PE and resulted in 96.5 % of CO_2 purity and 90.7 % of CO_2 recovery. It indicates that the use of PE steps contributed to the increase of the CO_2 purity while sacrificing CO_2 recovery. Since the CO_2 purity more than fulfils the target value while CO_2 recovery does not, the P/F ratio was increased from 0.46% to 1.15% in the second trial. The increase in the P/F ratio reduced the CO_2 purity to 95.8% but increased the CO_2 recovery to 94.1%. As the CO_2 recovery in this second trial approached the target value, the desorption pressure was increased to 0.45 bar in the third trial. This value satisfied the targets for CO_2 purity and recovery approaching the target values with a lower specific energy consumption of approximately 0.355 MW_e/kg of CO_2.

Figure 6.10 and **Figure 6.11** show the CO_2 mole fraction at the end of the adsorption step time for both stages. For the configurations analysed for the first stage, the CO_2 recovery decreases as the saturation of the bed increases, as expected. For the PVSA cycles for the second stage, the relationship between the CO_2 recovery and the CO_2 mole fraction profile is

less evident since the CO_2 mole fraction, the feed flow and the duration of the adsorption step time are not the same for all the runs. It can be seen, however, that Run 3 presents the lowest fraction of bed experiencing saturation since this configuration exhibits the highest value for the CO_2 recovery in the second stage.

Table 6.7: Operating conditions of two-stage PVSA units

	1st stage PVSA unit							2nd stage PVSA unit							Overall PVSA	
Runs	Desorp-tion Pressure [bar]	P/F ratio [%]	Column length [m]	Column radius [m]	$t_{FP}/t_{AD}/t_{DPE}/t_{BD}/t_{PP}/t_{PPE}$ (t_{cycle}) [s]	CO_2 purity [%]	CO_2 Rec. [%]	Desorp-tion pressure [bar]	P/F ratio [%]	Column length [m]	Column radius [m]	$t_{FP}/t_{AD}/t_{DPE}/t_{BD}/t_{PP}/t_{PPE}$ (t_{cycle}) [s]	CO_2 purity [%]	CO_2 Rec. [%]	CO_2 Rec. [%]	Carbon Rec. [%]
Run 1	0.25	10	3	1.21	38.5/240/0 /38.5/240/0 (557)	72.3	97.9	0.40	0.46	3	0.99	53.5/214/0 /53.5/214/0 (535)	95.0	91.8	89.8	87.8
Run 2	0.30	10	3	1.21	38.5/240/0 /38.5/240/0 (557)	72.6	95.7	0.30	0.41	3	1.05	60/240/0 /60/240/0 (600)	95.0	93.8	89.5	87.3
Run 3	0.40	10	3	1.22	38.5/240/0 /38.5/240/0 (557)	72.4	92.5	0.20	0.41	3	1.18	75/300/0 /75/300/0 (750)	95.2	96.8	89.3	87.4
Run 4	0.40	17.5	3	1.20	38.5/300/0 /38.5/300/0 (677)	63.3	97.1	0.25	0.41	3	1.09	80/320/0 /80/320/0 (800)	95.2	91.8	89.1	87.1
Run 1_1PE	0.25	10	3	1.22	19.25/240/19.25 /19.25/240/19.25 (557)	72.8	97.6	0.40	0.46	3	1.00	53.5/214/0 /53.5/214/0 (535)	95.1	91.2	88.9	87.0
Run 1_2PE	0.25	10	3	1.22	19.25/240/19.25 /19.25/240/19.25 (557)	72.8	97.6	0.45	1.15	3	1.00	27/214/27 /27/214/27 (536)	96.1	92.1	89.9	87.8

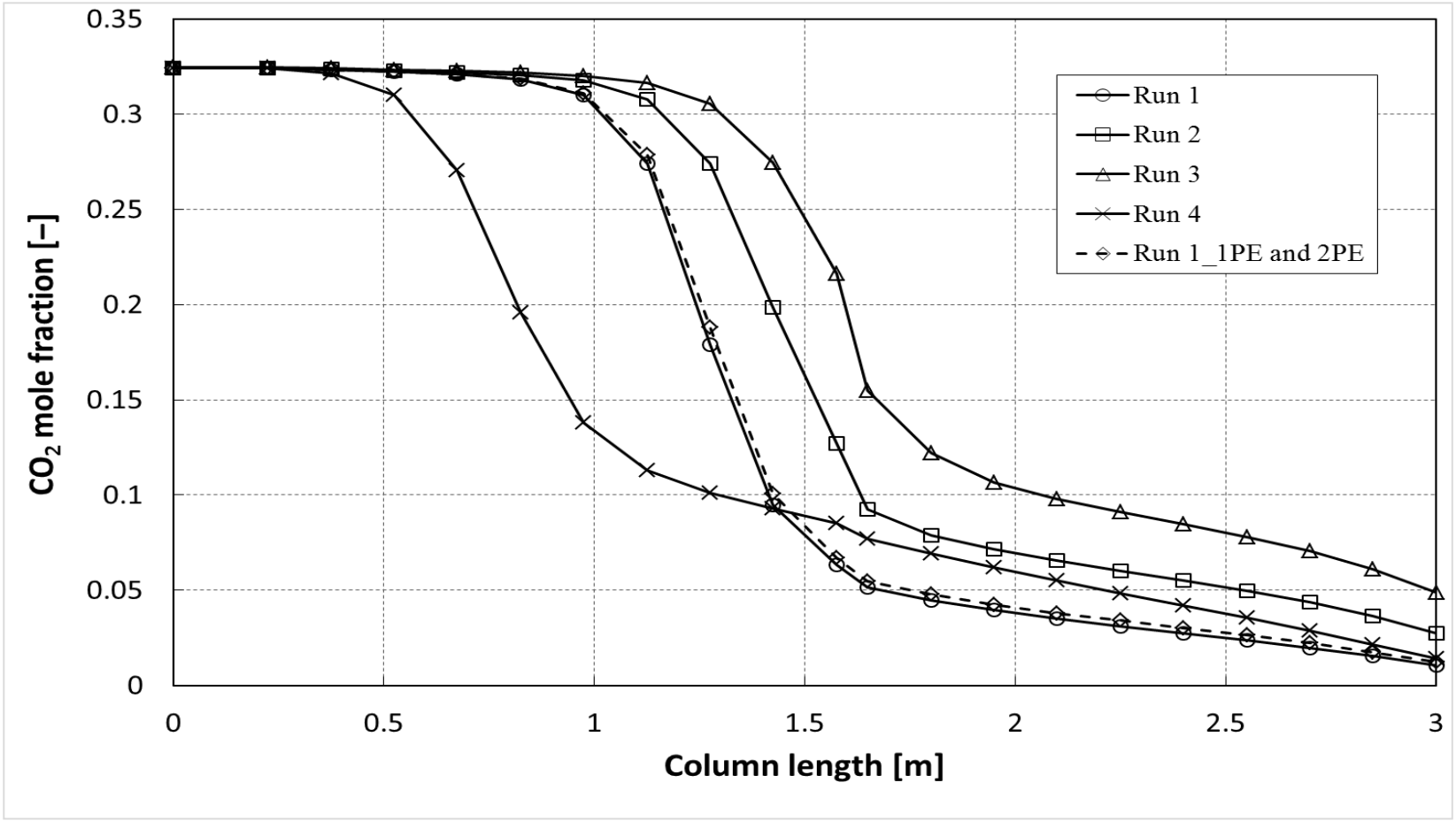

Figure 6.10: CO_2 mole fraction profile along the column at the end of adsorption step of the first stage PVSA unit

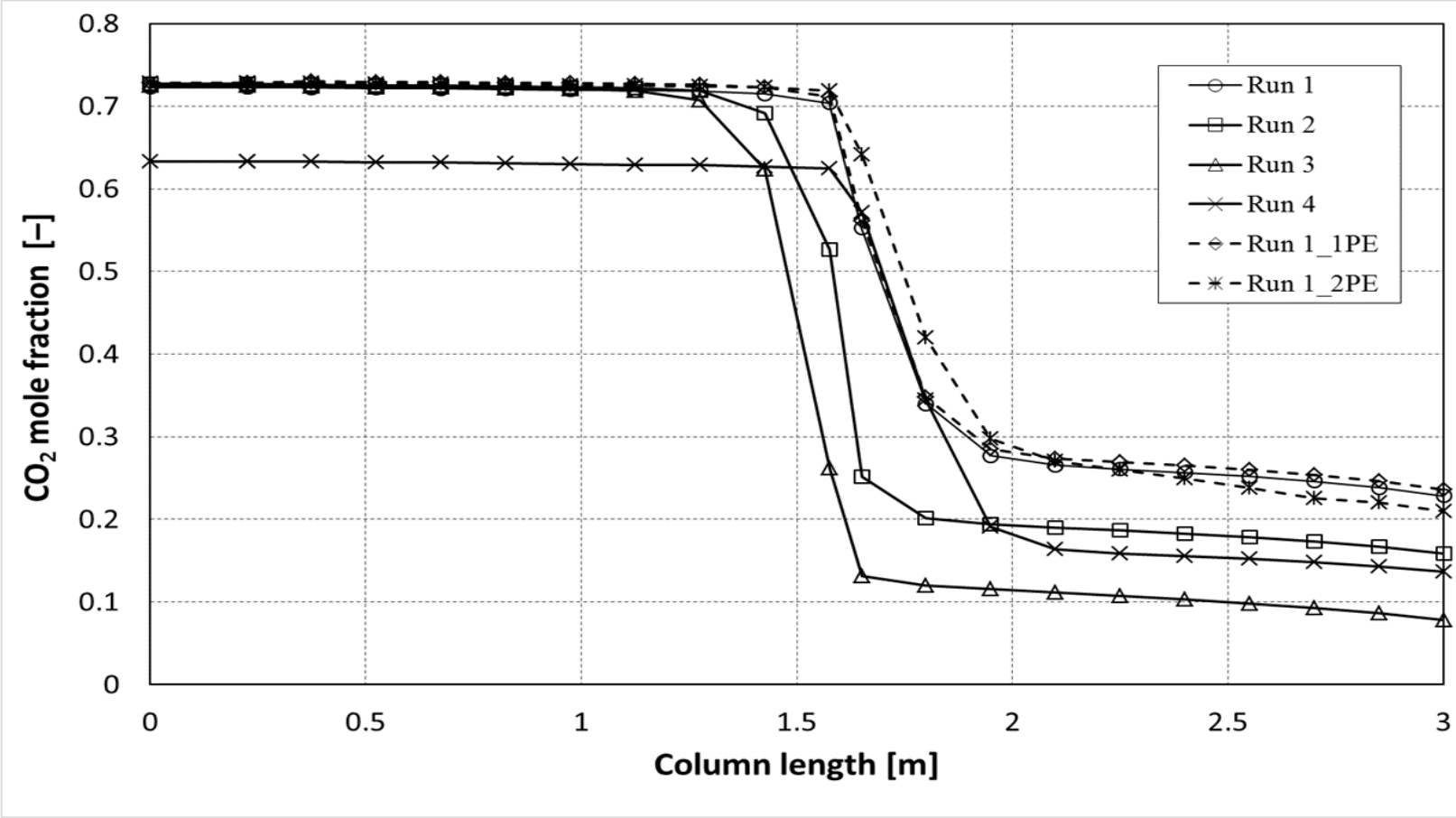

Figure 6.11: CO_2 mole fraction profile along the column at the end of adsorption step of the second stage PVSA unit

Table 6.8: Operating conditions of two-stage PVSA units

	1st stage PVSA unit			2nd stage PVSA unit			Overall	
Runs	Feed pressurisation (1.1 → 1.5 bar)	Evacuation (P_{des} → 1.1 bar)	Sub-total	Feed pressurisation (1.1 → 1.5 bar)	Evacuation (P_{des} → 1.1 bar)	Sub-total	Total	Specific power consumption [MWe/kg of CO_2]
Run 1	39.6	90.7	130.3	17.2	41.7	58.8	189.1	0.366
Run 2	39.6	76.8	116.4	16.8	54.6	71.4	187.9	0.366
Run 3	39.6	56.1	95.7	16.3	74.2	90.5	186.2	0.362
Run 4	39.6	67.4	107.0	19.6	62.6	82.2	189.2	0.370
Run 1_1PE	39.6	90.2	129.8	17.1	41.2	58.3	188.0	0.368
Run 1_2PE	39.6	90.2	129.8	17.1	36.2	53.2	183.0	0.355

6.3 Comparison with amine carbon capture processes

One of the purposes of this chapter is to compare the performance of an adsorptive pre combustion unit against currently employed CCS technologies. The conventional post combustion MEA configuration is the most mature carbon capture process at large scale (Kuramochi et al., 2011). Granted CCS demonstration projects in the UK are expected to employ this technology (Shell, 2015) and there are plants in England like the case of Ferrybridge in which 100 kt of CO_2/year are currently being captured (equivalent to 5 MW electricity. DECC,2013) using a post combustion MEA unit. If a plant were to be built in the near future, post-combustion using MEA would be the preferred option for carbon capture being as well the reference benchmarking technology when novel gas separation technologies are investigated. Research is currently being undertaken in the development of novel solvents that are expected to exhibit lower regeneration heat and therefore lower reboiler duties in the stripper. However, as explained in Chapter 1, these solvents are costly, mainly produced at lab scale and their potential application in post-combustion units at plant scale has only been studied in simulation-based studies. Given the fact that this thesis is scoped to compare the performance of PSA cycles with mature CCS technology (close to implementation), the comparison with novel solvents was not considered in this work opting for a MEA based process as a reference carbon capture technology for the comparison.

A conventional MEA process was designed to treat the effluent consisting of the mixture of the gas engine and the combustion zone flue gases. Since the temperature of the stream is approximately 160°C, conventional DeNOx and DeSOx treatments cannot be applied thus a larger MEA make up rates per unit of captured CO_2 (in comparison with conventional post combustion amine process for coal fired power plant) is predicted by the Unisim process design simulator make up estimations. The CO_2 composition (approximately 12-13%) considered in this work is quite similar to the feed considered in the study of a coal-based power plant published by Ahn (Ahn et al., 2013) therefore it was decided to design the process such that the reboiler duty is in the range of 3.5 MJ_{th}/kg of CO_2 as in the optimised version for the conventional amine configuration presented in the above mentioned article.

The amine process requires both heat and power for operation but most of the energy demand is heat (for the operation of the reboiler of the stripper), of which the temperature and

pressure is equivalent to LP steam as it was underlined in the previous paragraph. While PC-fired power plants or combined cycle power plants already have a steam cycle that can provide LP steam for the amine process, the biomass gasification CHP plant does not have any such steam cycle. Since the temperature of the resulting mixture of the gas engine flue gas and the effluent of the combustion zone is approximately 160°C, the maximum amount of steam produced at 1.9 bar is 214.4 kW[5] (the reboiler duty in the striper of the amine is 3400 kW). The maximum pressure at which steam can be produced at this temperature is 4.75 bar[6]. Consequently, neither the use of this stream as hot source for the steam production neither as hot source for a combined cycle (low pressure ratio) seems to be convenient. Extra district heat could be produced with the hot flue gas stream from the gas engine, although this would only increase the thermal efficiency of the plant by just 2 percentage points.

Taking into account what referred in the previous paragraph, there are two options to generate the required LP steam for the stripper of the reboiler: the first is to use the heat from the biomass gasification CHP plant to generate LP steam instead of producing hot water. In other words, a CO_2-laden solvent is regenerated at a steam stripper being driven by in-situ generated LP steam. Theoretically, this option is possible since the required heat duty for amine process is lower than the total heat recovered from hot water production. However, the amount of LP steam required is so huge that the heat recovered from the two hot streams originating from the gasification and combustion zones is not sufficient. The thermal recovery system must therefore be modified at the gas engine and at the gasification section to produce LP steam. As a result of these modifications, it is inevitable that the net thermal efficiency would be greatly reduced. Strictly speaking, the biomass CHP plant being integrated with the amine process in this way would no longer be regarded as a CHP plant; even though it could achieve 90% carbon capture, almost all of the heat produced would be consumed internally to generate LP steam for the stripper. If the carbon capture rate of the amine process is reduced by half (i.e., to a similar level as an adsorptive system, at 48.5%), the CHP plant may be able to produce a considerable amount of heat. However, it is not plausible that the power plant company would build an amine process achieving only 48.5% carbon capture rate instead of 90%; cost reductions resulting from the reduced amine process capacity would be relatively insignificant.

[5] Assuming a counter-current heat exchanger in which the hot fluid enters at 180°C and leaves at 130°C.

[6] Steam saturation pressure at 150 °C (assuming a temperature difference of 10°C in the counter-current heat exchanger)

The second option is to install a new biomass-fired boiler CHP plant with a much higher thermal efficiency than that of the biomass gasification CHP plant (50.1%). If the Rankine cycle is operated to produce steam at 370°C and 28 bara, the thermal efficiency (driven mainly by the heat recovered in the condenser of the cycle) is around 75% This option has a clear advantage over the first option in that there is no need to modify the original biomass CHP plant to generate steam. The superheated steam is used for extra power generation with a steam turbine and subsequently the exhaust steam needs to be conditioned to 134°C and 3 bara in a heat exchanger in order to make LP steam for the stripper reboiler (**Figure 6.12**). At the same time, some hot water is produced at the heat exchanger. Once the LP steam is condensed at the stripper reboiler, the condensed water is recycled to a deaerator. Then, the high pressure boiler feed water is pressurised and subsequently sent to the boiler to complete the steam cycle.

The heat required for MEA regeneration could alternatively be provided by an extra biomass boiler, which does not require the incorporation of an additional CHP combustion module. It must be noted, however, that the electricity generated in the addition combustion CHP plant (0.6 MWe) represents approximately 21% of the original plant production. The percentual increased CAPEX associated with the steam turbine and required piping is much lower than their contribution to the total electricity generation of the plant. According to an EPA cost survey for American biomass CHP plants (EPA, 2007), a steam turbine capable of producing electricity in the range of 0.5 MW_e costed USD 500 000 in 2007 while the total capital investment cost for the Gussing CHP plant in 2004 was approximately EUR 10 million (Simader, 2004). It must be noted that the condenser of the CHP combustion module is the reboiler of the amine and that if no electricity were produced, a boiler would also be required. The capital cost for a 4 MW boiler was around 2 million dollars in 2007 (EPA, 2007).

Table 6.9 displays the main operating conditions and energy consumption for three possible CHP plants: the base case presented in Chapter 5, a plant in which the amine process is incorporated as a carbon capture unit and another plant in which the PVSA unit has been designed to treat the effluent of the gasification zone (run 1_2PE from the previous section was chosen since it presented the lowest energy penalty)

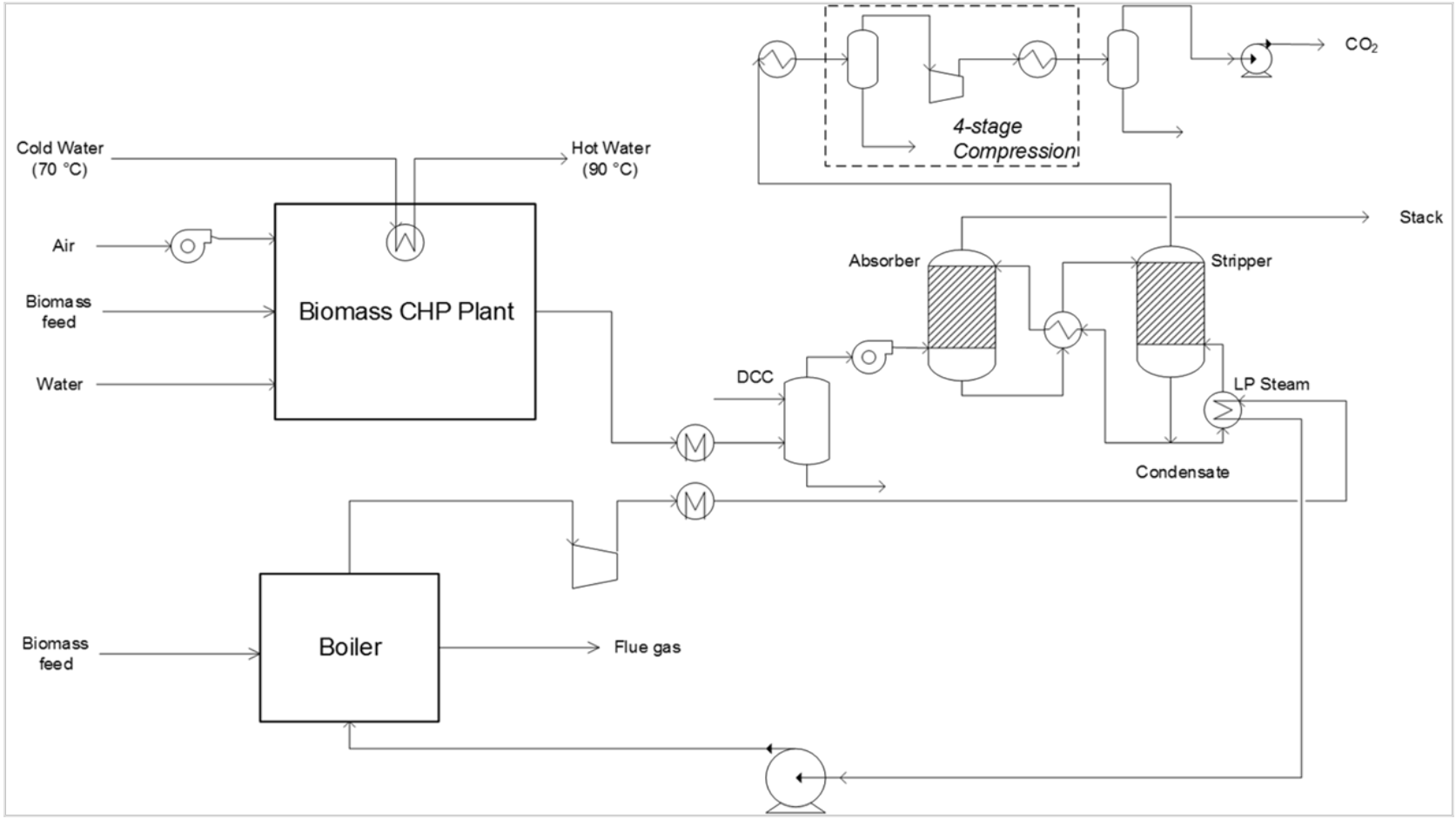

Figure 6. 12: Schematic diagram of a biomass CHP plant integrated with a MEA capture unit

Table 6.9: Comparison of the two amine configurations

	Base case	Case 1: WGSR+PVSA	Case 2: Biomass-fired boiler CHP + MEA
Biomass-fueled CHP plant			
Biomass heat input, LHV [MW_{th}]	10.07	10.07	10.07 (+4.49)
Syngas LHV [kJ/mol]	187.4	228.9 (shifted)	187.4
Syngas heat flow, LHV [MW_{th}]	6.91	6.37	6.91
Gas engine performance			
Electricity production [MW_e]	2.89	2.74	2.89
Power efficiency on the basis of biomass/syngas	0.287/ 0.419	0.278/ 0.439	0.287 / 0.419
Hot water production [MW_{th}]	3.03	2.80	3.03
Thermal efficiency on the basis of biomass/syngas	0.301 / 0.438	0.272 / 0.430	0.301/ 0.428
Hot water generation at gasification section [MW_{th}]	2.09	1.71	2.09
Power consumption at gasification section [MW_e]	0.09	0.09	0.09
Biomass-fired boiler CHP plant for steam generation			
Biomass heat input, LHV [MW_{th}]	–	–	4.49
Power generation at steam turbine [MW_e]	–	–	0.643
Steam pressure and temperature at the ' turbine inlet	–	–	28 bara, 370 °C
LP steam generation for amine process [MW_{th}] (efficiency)	–	–	3.34
Hot water generation [MW_{th}]			0.031
Heat-to-power conversion factor, –	–	–	0.162
Power consumption [MW_e]	–	–	0.021
Net power generation [MW_e] (efficiency)	–	–	0.622 (0.139)
Net thermal generation [MW_{th}] (efficiency)	–	–	3.37 (0.751)
Carbon capture unit			
Process		WGSR + PVSA + oxy-combustor	MEA

Power consumption [MW_e]	–	0.189	0.100
Heat consumption [MW_{th}]	–	–	3.34
Power consumption, CO_2 compression [MW_e]	–	0.184	0.297
Power consumption for oxygen production [MW_e]	–	0.008	–
Hot water generation at oxygen combustor [MW_{th}]	–	0.178	–
Hot water generation at WGSR [MW_{th}]		0.167	–
Carbon capture rate on biomass basis [%]	–	48.5% (87.3 % on the syngas basis)	58.4% (90.0% on the biomass-gasification CHP plant flue gas basis)
CO_2 avoided percentage per energy output base [%]		41.11%	43.80%
Specific power consumption per CO_2 captured (including CO_2 compression) [MJ_e/kg CO_2]	–	0.73 (1.03 including shift reaction)	1.08
Specific thermal consumption per CO_2 captured [MJ_{th}/kg CO_2]	–	0.510	2.332
Overall performance			
Net power generation [MW_e] (efficiency)	2.8 (0.278)	2.269(0.225)	3.02 (0.207)
Net hot water generation [MW_{th}] (efficiency)	5.12 (0.508)	4.86 (0.482)	5.15 (0.354)
Sum of the net power and thermal efficiencies	0.786	0.707	0.562
CO_2 emissions per unit of energy output [kg CO_2/MJ]	0.135	0.072	0.071
CO_2 avoided per unit of energy output [%]	-	46.7	47.4

To quantify the energy penalty involved in retrofitting the biomass gasification CHP plant with the capture process, two different indices reflecting the characteristics of the CHP are proposed in this study. These indices are the specific power consumption per captured CO_2 and the specific thermal consumption per captured CO_2. This is because, in the case of a biomass gasification CHP plant, the power being generated by running the gas engine cannot be converted into equivalent thermal energy production by reducing the hot water production. In other words, power and heat are not interchangeable in the CHP plant as is the case of power plants with a steam cycle.

The specific power consumption of unit CO_2 captured [MJ_e/kg] is calculated by

$$Specific\ Power\ Consumption_{(adsorption)} = \frac{P_{c,PVSA} + P_{c,CO2\ compression} + P_{c,O2\ production} + (P_{g,gas\ engine\_base} - P_{g,gas\ engine\_case\ 1})}{mass\ flowrate\ of\ captured\ CO_2} \quad (6.8)$$

$$Specific\ Power\ Consumption_{(Amine)} = \frac{P_{c,amine} + P_{c,CO2\ compression} + Heat\ input_{boiler\ CHP} \times \eta_{electrial\ at\ gasification\ CHP} - P_{g,boiler\ CHP}}{mass\ flowrate\ of\ captured\ CO_2} \quad (6.9)$$

The specific thermal consumption of unit CO_2 captured [MJ_{th}/kg] is estimated by Eq. (6.10) for the PSA and Eq. (6.11) for the amine process

$$Specific\ Thermal\ Consumption = \frac{H_{g,gas\ engine\_base} - H_{g,gas\ engine_{case}1} + H_{g,gasification\_base} - H_{g,gasification\_case\_1} - H_{g,WGSR} - H_{g,oxycombustor}}{mass\ flowrate\ of\ captured\ CO_2} \quad (6.10)$$

$$Specific\ Thermal\ Consumption = \frac{Heat\ input_{boiler\ CHP} \times \eta_{thermal\ at\ gasification\ CHP} - H_{g,boiler\ CHP}}{mass\ flowrate\ of\ captured\ CO_2} \quad (6.11)$$

As shown in **Table 6.9**, the specific power consumptions are very similar in both cases even though the amine process does not require as much power consumption as the adsorption process. This can be explained due to the fact that the index that was defined for the adsorption unit also accounts for a reduction in the power output of the gas engine associated with a lower

energy flow ($m_{syngas} * LHV$) to be processed in the device as consequence of the incorporation of the shift reactors (decarbonisation) and the PVSA cycles (lower mass flow). This decrease in electricity generation contributes to 0.73 MJ_e/kg CO_2 of the overall specific consumption of 1.73 MJ_e/kg CO_2 for the onfiguration with pre combustion PSA cycles.

A similar approach was employed for estimating the specific thermal consumption per captured CO_2. The thermal generation in the existing gasification CHP plant does not change in the amine case since the LP steam for amine process is entirely sourced from the new boiler CHP plant. As a result, the energy penalty can be estimated by calculating the expected thermal production at gasification CHP plant resulting from the additional biomass fed to the new boiler CHP ($Q_{boiler\ CHP} \times \eta_{th,gasification\ CHP}$). It should be noted that in **Table 6.9,** the specific thermal duty for the amine configuration (2.30 MJ_{th}/kg CO_2) is less than that of the stripper reboiler (3.5 MJ_{th}/kg CO_2). This difference occurs because in order to quantify the heat loss, the index reflects the thermal efficiency of the biomass gasification plant that is lower than the one related to the add- on combustion CHP plant.

On the basis of specific thermal and electrical consumption per unit of captured CO_2 and the consequent thermal and electrical efficiency once the configurations are implemented in the reference CHP plant (**Table 6.9**), it can be concluded that the pre-combustion adsorption capture unit performs better than the conventional MEA post-combustion process despite that the absorption unit exhibits a slightly higher percentage of CO_2 avoided emissions and 10 percent point higher overall carbon capture rate.

Conclusions

In this chapter, a two-stage two-bed PVSA Skarmstrom cycle was designed and simulated in the role of pre-combustion CO_2 capture unit at the biomass gasification CHP plant introduced in Chapter 5. The role of several operating conditions such as vacuum pressure, purge and feed ratio and adsorption step time was studied in order to optimise the energy consumption associated with the CO_2 capture process.

The performance of the pre-combustion adsorptive unit was compared against a conventional post-combustion amine configuration in term of carbon capture rate, specific

energy consumption and thermal and electrical efficiencies. Both units were designed for reaching approximately 90% CO_2 recovery from the feed inlet. The overall carbon capture rate in the PSA unit was around 48% while that of the plant with the adsorptive unit was close to 58%. The difference between the CO_2 recovery rates and the overall carbon capture value is a consequence of the CO_2 emissions from the combustion zone of the gasifier not being captured in the plant with the adsorptive unit. Conversely, for the CHP with amines, the high thermal consumption associated with the reboiler of the stripper requires a biomass-fuelled boiler to provide the required steam. The CO_2 emissions from the combustion flue gas are not being captured, resulting in a difference in CO_2 recovery rates and overall carbon capture.

It was successfully demonstrated that an adsorptive capture unit could be more efficient than conventional amine capture unit in all aspects despite the lower overall carbon capture rate. The novel process presents lower thermal and specific electricity consumption per unit of captured CO_2, leading to higher electrical and thermal efficiency for the CHP in comparison with the CHP in which the absorptive unit was incorporated. The adsorptive configuration also offers the advantage of requiring fewer modifications in the plant (i.e., no need of extra boiler or combustion CHP modules) thus lower investment costs would be expected for the small-medium scale of the plants under consideration.

It must be noted, however, that both configurations presented in this chapter do not reach the overall carbon capture rate of 90% for the energy plant. Possible future research work would involve designing configurations that allowed meeting this target as well as carrying out a cost assessment study as it will be discussed in the conclusion of this thesis.

References

Ahn H, Luberti M, Liu Z, Brandani S. Process configuration studies of the amine capture process for coal-fired power plants. Int. J. Greenh. Gas. Con. 2013; 16: 29-40.

CAESAR Project, FP7—ENERGY. European best practice guidelines for assessment of CO_2 capture technologies.2011

DEEC. UK Electricity Generation Costs Update. 2010.

DECC. Ferrybridge Carbon Capture Pilot (CCPilot100+). 2013

Dirar Q, Loughlin K. Intrinsic adsorption properties of CO_2 on 5A and 13X zeolite. Adsorption. 2013; 19: 1149-1163.

EPA. EPA Combined Heat and Power Partnership. Biomass CHP catalog. 2007.

Fiandaca G, Fraga E, Brandani S. A multi-objective genetic algorithm for the design of pressure swing adsorption. Eng. Optimiz. 2009; 41; Issue 9: 833-854.

Friedrich D, Ferrari M C , Brandani S. Efficient Simulation and Acceleration of Convergence for a Dual Piston Pressure Swing Adsorption System . Ind. Chem. Eng. Res. 2013; 52: 8897-8905.

Hu, X, Mangano, E, Friedrich, D, Ahn, H., Brandani, S. Diffusion mechanism of CO_2 in 13X zeolite beads. Adsorption. 2014; 20: 121–135

IPCC. Special Report on Carbon Dioxide Capture and Storage. 2005.

Jain S, Moharir A S, Li P, Woznny G. Heuristic design of pressure swing adsorption: a preliminary study. Sep. Purif.Technol. 2003; 33: 25-43.

Koryabkina N A., Phatak A A, Ruettinger W F., Farrautob R J, Ribeiro F H. Determination of kinetic parameters for the water–gas shift reaction on copper catalysts under realistic conditions for fuel cell applications. Journal of Catalysis. 2003; 217, Issue 1: 233-239.

Liu Z, Grande C, Li P, Yu J, Rodrigues A E. Adsorption and Desorption of Carbon Dioxide and Nitrogen on Zeolite 5A. Sep. Purif. Tecnol 2010; 46: 434-451.

Liu Z, Grande C, Li P, Yu J, Rodrigues AE. Multi-bed Vacuum Pressure Swing Adsorption for carbon dioxide capture from flue gas. Sep. Purif. Tecnol 2011; 81: 307-317.

Liu Z, Wang L, Kong X, Li P, Yu J, Rodrigues A.E. Onsite CO_2 capture from FlueGas by an Adsorption Process.Ind.Chem.Res 2012; 51: 7355-7363.

Mendes D, Mendes A, Madeira L M,. Iulianelli A, Sousa J M, Basile A. The water gas shift reaction from conventional catalytic systems to Pd based membrane reactors: a review. Asia Pac. J. Chem. Eng. 2009; 5, Issue 1: 111-137.

Meres J, Clausse M, Meunier F. Experimental investigation on CO2 postcombustion capture by indirect thermal swing adsorption using 13x and 5A zeolites. Ind. Eng.Chem Res. 2008; 47: 209-215.

NETL. Cost and Performance baseline for fossil energy plants , US Department of Energy 2007.

Park J, Beum H, Kim J, Cho SH. Numerical Analysis on the Power Consumption of the PSA Process for Recovering CO_2 from Flue Gas. Ind. Eng. Chem. Res. 2002; 41: 4122-4131.

Rao M B ,Sircar S. Thermodynamic Consistency for Binary Gas Adsorption Equilibria. Langmuir 1999; 15: 7258-7267.

Ruthven D M. Principles of Adsorption and Adsorption Processes . Brunswick : Wiley; 1984.

Saha D, Deng S. Adsorption equilibria and kinetics of carbon monoxide onzeolite 5A, 13X, MOF-5, and MOF-177.2009.. J. Chem. Eng. Data 54, 2245 – 2250.

Shen C, Liu Z, Li P, Yu J. Two-Stage VPSA Process for CO_2 Capture from Flue Gas Using Activated Carbon Beads. Ind. Eng. Chem. Res. 2012; 51: 7947-7955.

Shell. Peterhead CCS Project. 2014.www.shell.co.uk/energy-and-innovation/the-energy-future/peterhead-ccs-project.html

Skarstrom C W, Montvale N J. Method and Aparatus for Fractionating Gaseous Mixtures by Adsorption. Patent Number: 2944627, Unites State Patent Office ;1960.

Xiao P, Zhang J, Webley P, Li G, Singh R, Todd R. Capture of CO2 from flue gas streams with zeolite 13x by vacuum pressure swing adsorption. Adsorption. 2008; 14: 575-582.

Yang, R.T. Gas Separation by Adsorption Processes. Imperial College Press,Imperial College Press. 1997. London, UK.

Wang Y, Douglas Le Van M. Adsorption Equilibrium of Carbon Dioxide and Water Vapor on Zeolites 5A, 13X and Silica Gel: Pure Components. 2009; 54: 2839-2844.

Wang L, Yang Y, Shen W, Kong X, Li P, Yu J, Rodrigues AE. CO_2 capture from Flue Gas in an Existing Coal-Fired Power Plant by Two successive Pilot-Scale VPSA Units. Ind. Chem. Res. 2012; 52: 7947-7955.

Wang L, Yang Y, Shen W, Kong X, Li P, Yu J, Rodrigues AE. Experimental evaluation of adsorption technology for CO_2 capture from flue gas in an existing coal fired power plant. Chem. Eng.Sci. 2013; 10: 615-619.

Conclusions

Summary of the undertaken research and main findings

This work was intended to explore the feasibility of PSA cycles in the role of carbon capture technology in energy industries by simulating, designing and optimising PSA cycles to be integrated into an energy generation plant; quantifying as well the energy consumption associated with the required auxiliary unit operations and comparing the performance of the novel process against a conventional post combustion MEA configuration.

The design of PSA cycles requires robust simulation tools capable of predicting accurate results for the configurations employing the minimum amount of empirically determined parameters as input data and with a relatively simple and generic code that allows a fast modelling of a wide variety of adsorption systems enabling as well a fast convergence to cycle steady state (after a few cycles). The assumptions regarding the mass and energy transfer mechanisms between the gas and the solid phase strongly influence on the computational implementation of the solvers as well as on the type of input data that are necessary to perform the simulations. In the first part of this work, it was decided to explore the advantages and limitations of the Equilibrium Theory simplification when applied to the development of a generic PSA cycle simulator. The novel software introduced in this thesis (Esim) presents the next features:

- It can be used for stablishing the limiting efficiency that an adsorptive separation unit could reach (since kinetics and dispersive effects are not considered) and pre-selecting promising configurations for further investigation. The performance of these units will be further evaluated by employing full governing equations solvers that require diffusion coefficients as input data. The assumption of Equilibrium Theory reduces the number of diffusion coefficient determination experiments (especially in the case of novel sorbents) by just undertaking measures for the operating conditions for the chosen high performance configurations.
- A lower number of PDEs are needed to model the adsorption dynamics leading as well to fewer cycles to reach CSS condition.

- It allows the simulation of generic multi transition systems with a code implementation that can be employed without any relevant modification for the modelling of adsorption systems that obey any kind of equilibrium isotherm function.
- Its implementation has been validated against other PSA cycle solvers: Results for non-trace and non-isothermal adsorption breakthrough curves and CO_2 enriching cycles were compared against a gPROMS based code in which the adsorbed phase was simulated using the LDF model. Negligible differences were observed in cycle steady state separation performance indicators such as CO_2 recovery and CO_2 purity and in pressure and concentration profiles when modelling post combustion validation/ application equilibrium based system.

The second part of this thesis was focused on the design and the optimisation of PSA cycles to be incorporated in a low scale energy plant. Two stage two bed PSA cycles to be applied in the role of pre-combustion technology in a biomass gasification CHP plant was simulated. This type of energy plant was chosen since the University of Edinburgh is planning to build a bio fuelled CHP in one of its campus. The exemplary case that was modeled is based on the Gussing CHP plant that has been in operation since 2002.

The simulations for the pre-combustion PSA cycles were effectuated by using CySim. CySim is an in house software that allows the solution of the adsorption dynamics considering mass transfer resistances as described in Chapter 6. Esim was not employed for these simulations since the Equilibrium Theory simulator was still under development at the moment that this research started. As well, as it was previously described in Chapter 2, 4 and 6, results generated using Esim should be employed as a preliminary estimation; providing the thermodynamic limit for a given PSA cycle enabling as well the identification of a set of high separation efficiency configurations for being further studied with more accurate tools that require experimentally determined diffusion coefficients. For those systems in which kinetic or dispersive effects could be non-negligible on the separation under study and or strict purity requirements must be fulfilled (CO_2 adsorption on zeolite 13x for CCS applications), full governing equation solvers should be employed for simulating the cycles to be implemented as gas separation units meanwhile the Eq. Theory solver could be used

for a pre-selection of the configurations; reducing in this way the number of experiments to measure diffusion coefficients.

The influence of several operating conditions (eg.: vacuum pressure, purge and feed ratio and different time duration for the steps of the Skarmstrom cycle) was studied in order to optimise the energy consumption for a two stage two bed adsorption unit with pressure equalisations that once integrated to the CHP plant can be compared against a conventional post combustion plant in the next aspects:

- Both units are designed to capture approx.90 % of the CO_2 feed inlet reaching CO_2 purity higher than 95% however given the process configuration (explained in section 6.1 and section 6.3), the plant with pre combustion absorptive capture process presents an overall carbon capture rate of 49% while the CHP plant with absorptive configuration exhibits a carbon capture rate of 59%.
- The adsorptive unit presents lower specific electrical and thermal consumption per kilogram of captured CO_2 yielding to higher CHP efficiencies.
- Lower modifications are required for the CHP plant with pre combustion PSA cycles thus lower investment costs should be expected.

The results introduced in this thesis are pioneer as far as modelling, simulation and integration of pressure swing adsorption cycles in the role of carbon capture technology for power generation plants. Research carried out in this PhD shows that integrated PSA cycles can be a promising carbon capture process exhibiting lower energy consumption than post combustion MEA configuration, this is one of the few works in which adsorption units are completely integrated into an energy production plant and the selection of operating conditions and cycle configurations takes that into account. Energy penalty associated with auxiliary unit operation has also been quantified and considered when benchmarking the novel process against the conventional solvent based ones. Challenges related to the simulation of adsorption dynamics have also been critically analysed and the use of simplifications in the modelling of mass and energy transfer mechanism between the phases like the Equilibrium Theory assumption has enabled the development of a novel generic PSA cycle solver that is capable of selecting operating conditions and configuration for PSA cycles by just using the equilibrium isotherm function parameters as input data (preselecting promising configurations for further

detailed studies). It can then be concluded that the research objectives that were assigned for this PhD and that were mentioned in section 1.4 have been fulfilled with the research activities and the results presented in this thesis.

Limitations and future work

Possible improvements for the Equilibrium Theory solver would require to carry out research activities aimed to:

- Investigate and implement stability criteria that would enable to increase the time grid size thus to reduce the amount of evaluations of the updating formulas.
- Explore different and more optimised nonlinear root finding algorithms in order to reach cycle steady state with a lower execution time
- Modify the current code implementation to transform the software into a banded solver so that the evaluation of the updating routines are carried out just for those grids that present different values of the variable of interest than the ones for their neighbours. By acting this implementation, fewer evaluations will be necessary and consequently the required execution time will be lower.

Two main limitations that could be key driver for future work in the field of PSA cycle design, optimisation and integration of adsorptive units in energy plants are listed bellow:

- In this thesis, a technical feasibility and efficiency comparison between two carbon capture technologies has been presented however it would be also relevant to employ the presented results to carry out an economic study in order to compare the levelised cost of electricity (or heat) for both plants with CCS.
- The designed configurations, both for the CHP with adsorptive and absorptive carbon capture units have got a net carbon capture rate lower than 90% thus it would be useful to design CC configurations that met that target. Research to be undertaken to reach this objective would involve studyinyg and analysing the

optimal location for the PSA or amine based units in term of energy consumption, OPEX and CAPEX.

Finally, it can be said that the results presented in this work show that optimised PSA configurations can be a viable alternative carbon capture technology at low scale energy generation plant and that the outputs of this work and the suggested future research activities would enable to provide strong scientific arguments for the deployment of this technology as a tool for the decarbonisation of the energy matrix.

Annex I: Glossary and nomenclature

This section is intended to show the abbreviation for the main variables employed in tbalances for the adsorption bed

Abbreviation	Variable
A_c	Column area
$A_{c,a}$	Column axial surface area
$A_{c,l}$	Column lateral surface area
A_p	Pellet surface area
$b^0_{CO_2}$	Pre-exponential Arrhenius coefficient for Langmuir isotherm linear constant for CO_2
$b^0_{N_2}$	Pre-exponential Arrhenius coefficient for Langmuir isotherm linear constant for N_2
c_i	Concentration of component i in fluid phase
c_i^{feed}	Feed concentration for component i
$\widetilde{c_{P,ads}}$	Molar heat capacity at const pressure adsorbed phase
$\widetilde{c_{P,sol}}$	Specific heat capacity at const. pressure of the adsorbent
$\widetilde{c_P}$	Molar heat capacity at const. pressure
c_T	Total concentration in the fluid phase
c_T^m	Total concentration in the macropore
$\widetilde{c_V}$	Molar heat capacity at constant value
D_c	Column diameter
D_i^K	Knudsen diffusion coefficient for comp. i
D_i^L	Axial dispersion coefficient in the fluid phase for comp. i
D_i^m	Molecular diffusion coefficient for comp. i
D_i^μ	Micropore diffusion coefficient for comp. i
D_i^P	Macropore diffusion coefficient for comp.i
D_i^S	Surface diffusion coefficient for comp i
D_i^V	Pouiseuille diffusivity
ε	Bed porosity
ε_{cry}	Crystal void fraction
ε_p	Pellet void fraction
f	Conservative flux
f_i	Conservative flux for component balance equation
$F^n_{j-\frac{1}{2}}$	Numerical flux on the left border of the cell
$F^n_{j+\frac{1}{2}}$	Numerical flux on the right border of the cell
φ	Non-sphericality coecient
γ	First order moment
$(-\Delta\widetilde{H_{ads}})_{T_p}$	Total heat of adsorption per unit volume
$\widetilde{H_f}$	Enthalpy in the fluid phase per unit of volume

$\widetilde{H_f}$	Molar enthalpy in the fluid phase
$-\Delta\widetilde{H_i}$	Heat of adsorption comp i.
h_p	Heat transfer coefficient between the pellet and the bed
h_w	Heat transfer coefficient at wall
J_i	Diffusive flux of comp .i in the fluid phase
J_T	Thermal diffusive flux in the fluid phase
k_i^m	LDF mass transfer coefficient of comp. i in the macropore
k_i^μ	LDF mass transfer coefficient of comp. i in the micropore
k_i^p	LDF mass transfer coefficient of comp. i in the pellet
l_f^L	Axial thermal conductivity in the gas phase
l_p^L	Axial thermal conductivity in the pellet
l_p^R	Radial Thermal conductivity in the pellet
L_c	Column length
M	Molar mass
μ	Viscosity
P	Pressure
P^{feed}	Feed pressure
Pr_i	Prandlt Number
P_{ref}	Reference Pressure
$\widetilde{Q_i}$	Average concentration of comp i in the pellet
Q_i	Concentration of comp i in the pellet
q_i	Sorbate concentration of comp i
q_i^*	Sorbate concentration of comp i at equilibrium
q_T	Total sorbate concentration in the micropore
ρ_{bulk}	Bulk density
ρ_{cry}	Crystal density
ρ_p	Pellet density
$\rho_{skeletal}$	Skeletal density
r_p	Pore radius
R_p	Pellet radius
σ^2	Second order moment
τ	Tortuosity
t_{ads}	Adsorption step time
t_{blow}	Blowdown step time
t_{cycle}	Cycle time
t_{press}	Pressurisation step time
t_{purge}	Purge step time
T	Temperature
T_f	Fluid temperature
T_p	Pellet temperature
T_{ref}	Reference temperature
T_w	Wall temperature
U	External heat transfer coefficient
$\widetilde{U_{ads}}$	Internal energy in the adsorbed phase
U_f	Internal energy in the fluid phase
$\widetilde{U_f}$	Internal energy in the fluid phase per unit volume
$\widetilde{U_f}$	Molar Internal energy in the fluid phase

$\widetilde{U_p}$	Internal energy in the pellet per unit volume
$\widetilde{U_{p,f}}$	Internal energy in the macropore per unit volume
$\widetilde{U_{p,s}}$	Internal energy in the solid phase per unit volume
$\widetilde{U_{sol}}$	Internal energy in the adsorbent per unit volume
v	Interstitial flow velocity
v^{feed}	Interstitial flow velocity at feed conditions
V_c	Column volume
V_{cy}	Crystal Volume
V_p	Pellet Volume
W	Generic variable of interest
$\widetilde{W}$	Average value for the variable of interest
$y_{CO_2}^{feed}$	CO_2 feed molar fraction
$y_{N_2}^{feed}$	N_2 feed molar fraction